EFFECT OF TEMPERATURE ON THE DAMAGE OF HYBRID THICK COMPOSITES SUBJECT TO DROP-WEIGHT AND BALLISTIC IMPACTS

by

YOUGASHWAR BUDHOO

A dissertation submitted to the Graduate Faculty in Mechanical Engineering in partial fulfillment of the requirements for the degree of Doctor of Philosophy, The City University of New York

2011

This manuscript has been read and accepted for the
Graduate Faculty in Engineering in satisfaction of the
dissertation requirement for the degree of Doctor of Philosophy.

	Prof. Feridun Delale
Date	Chair of Examining Committee
	Prof. Mumtaz K. Kassir
Date	Executive Officer

Prof. Feridun Delale, Dept. of Mechanical Engineering, The City College of New York

Prof. Benjamin Liaw, Dept. of Mechanical Engineering, The City College of New York

Prof. Yiannis Andreopoulos , Dept. of Mechanical Engineering, The City College of New York

Prof. Jackie Li, Dept. of Mechanical Engineering, The City College of New York

Dr. Jerry Chung, Frontier Performance Polymer, Picatinny, New Jersey

Supervision Committee

THE CITY UNIVERSITY OF NEW YORK

ABSTRACT

EFFECT OF TEMPERATURE ON THE DAMAGE OF HYBRID THICK COMPOSITES SUBJECT TO DROP-WEIGHT AND BALLISTIC IMPACTS

by

Yougashwar Budhoo

Mentor: Professor Feridun Delale

Co-mentor: Professor Benjamin Liaw

ABSTRACT

The aim of this study is to investigate the low velocity and ballistic impact responses of thick-section hybrid fiber composites at various temperatures. Plain-woven S2-Glass and IM7 Graphite fabrics are chosen as fiber materials reinforcing the SC-79 epoxy. Four different types of composites consisting of alternating layers of glass and graphite woven fabric sheets are considered. The tensile tests were conducted following ASTM Standards D3039 (Standard Test Method for Tensile Properties of Polymer Matrix Composite Materials) and D3518 (Standard Test Method for In-Plane Shear Response of Polymer Matrix Composite Materials by Tensile Test of a ±45° Laminate) on hybrid and non-hybrid plain weave composite materials. Strips (6.35mm×25mm×250mm) of non-hybrid IM-7 Graphite/SC-79 epoxy denoted as GR for brevity, non-hybrid S-2 Glass/SC-79 epoxy called GL for short, hybrid GR/GL/GR and hybrid GL/GR/GL specimens were tensile tested. The tests were conducted at −60°C, −20°C, room temperature, 75°C and 125°C. Then the rule of mixtures was used to predict the Young's moduli of GL/GR/GL and GR/GL/GR using the experimental values obtained from the stress-strain curves of

the GL and GR specimens. The predicted Young's moduli of GL/GR/GL and GR/GL/GR were then compared to those obtained experimentally. It was found that the calculated Young's and shear moduli match closely (within 6 %) to those obtained experimentally. The Poisson's ratio was measured using strain gages. Classical lamination theory was used to calculate the thermal stresses developed in the hybrid woven composite, which were then compared to the maximum stress values obtained experimentally from the unidirectional tensile tests, to determine whether they were significant. It was determined that the calculated thermal stresses are negligible (in the order of 2.5%) compared to the failure stress of the composite, and thus will be neglected in impact modeling and computations.

Next, low-velocity impact tests were conducted using an Instron-Dynatup 8250 impact test machine equipped with an environmental chamber operable from -52 °C to 316 °C. Test temperatures were achieved in the same manner as in tensile testing. The impact tests were performed at an energy level of 30 Joules. Both destructive cross-sectional micrographs and nondestructive ultrasonic techniques used to evaluate the damage created by impact. Ultrasound C-scans were performed using a Physical Acoustics Corporation UltraPAC immersion ultrasonic imaging system.

The Finite Element code LS-DYNA was chosen to perform numerical simulations of low velocity and later ballistic impact on thick-section hybrid composites. The experimentally obtained force-time histories, strain-time histories and damage patterns of impacted composites are compared with Finite element results. Good agreement between experimental and FE results has been achieved when comparing dynamic force, contact stiffness, deflection, energy, strain histories and damage patterns from experimental

measurements and FE simulations. It was shown that the variation of results obtained from our low velocity impact experiments for the hybrid composite was very small (in the order of 8 %) when compared to those of the non- hybrid composite material. Also, when looking at the hybrid or non-hybrid composites, the effect of temperature at –60°C, –20°C was not significant, whereas at 75°C and 125°C was very significant.

The final portion of this research deals with ballistic impact experiments on the above mentioned composites and numerical modeling. Ballistic impact tests were performed using helium pressured high-speed gas-gun. In this case also, high and low temperatures were achieved in the same manner as those in the tensile testing. From experiments, it is concluded that GL has a better ballistic impact resistance compared to the other three composites layups. The ballistic limit of GL increases with an increase in test temperature, while GR is decreased. The ballistics limits for the hybrids were in between of those for GL and GR.

ACKNOWLEDGEMENTS

I would like to thank my mentor, Professor Feridun Delale, for his guidance throughout this study. I also want to thank my co-mentor Professor Benjamin Liaw for his priceless advices.

Special thanks to the supervising committee members and also Prof. Steven Cowin who was part of my supervising committee during my second exam.

I want to express my gratitude to those who has worked in the Material Processing and Solid Mechanics laboratory in The City College of New York during the period of my study, with special thanks to Ali Seyed Yaghoubi.

I would also like to express my thanks for funding from City University of New York through CUNY Collaborative Incentive Research Grants Program (80209-06 10) and CUNY Research Equipment Grant Competition (80212-12 04) for procuring part of the materials and equipment used in this research. This work is supported by U.S. ARMY-TARDEC under contract # W56HZV-09-C-0569

Finally, special thanks to my family who has been very supportive during the period of my study.

Yougashwar Budhoo

October 2010 in New York

TABLE OF CONTENTS

LIST OF TABLES

LIST OF FIGURES

Chapter 1

Introduction

The main idea of composite material is to combine different materials to produce a new material with performance unattainable by the individual constituents. It gives flexibility to the designer to tailor the new material with peak performance properties for a particular application. The essence of the concept of structural composites is this: the bulk phase carries the load over a large surface area, and transfers it to the reinforcement, which being stiffer and stronger, increases the strength and stiffness of the composite. The significance here lies in that there are numerous matrix materials and as many fiber types, which can be combined in countless ways to produce just the desired properties. As the demand for materials with higher stiffness to-weight ratio, higher strength to-weight ratio, tailoring ability, more resistant to harsh environment and damage tolerance arises, researchers and engineers seek to have a more profound understanding of the behavior and properties of different composites under various conditions.

1.1 Objective of this thesis

The objective of this research is to study the mechanical properties and behavior of woven hybrid composite materials at various temperatures under impact loading. This is accomplished in the following manner: First, by conducting unidirectional tensile testing at various temperatures(-60 °C, -20 °C, R.T, 75 °C and 125 °C), the mechanical properties of plain-woven S2-Glass and IM7 Graphite fabrics (fiber materials) reinforcing SC-79 epoxy (matrix material) are obtained and analyzed. Four different types of composites consisting of alternating layers of glass and graphite fabric sheets are considered in order to study the effect of hybridization at the different temperatures.

Second, the composite specimens are impacted at low energy level (30 J) and consequently low velocity at different temperature values (as given above) in order to study the impact properties. Third, the specimens undergo ballistic impact at various temperatures in order to determine the ballistic limit velocity (V_{50}). Fourth, the classical lamination theory is used to calculate the thermal stresses developed in the hybrid woven composite, and compared to the maximum stress values obtained experimentally. If the thermal stresses are large when compared to the maximum stress, then they are included in modeling, if not, they are neglected. Finally, a dynamic finite element model is developed to explain and simulate the experimental results obtained from low velocity and ballistic impact tests. The finite element model can then be used to study the behavior of other composites. This is very important since testing can be very time consuming and expensive.

1.2 Distinction of this thesis

To the best of our knowledge, the research topics listed below have not been studied previously:

a) Study of the effect of temperature on drop weight impact of hybrid and non hybrid woven composite materials
b) Study of the effect of temperature on ballistic impact of hybrid and non hybrid woven composite materials
c) Developing of testing methodologies for ballistic impact at high and low temperatures
d) Developing of a finite element model to predict the behavior of hybrid woven composites at high and low temperatures

Chapter 2

Literature Review

Since ancient times, steel has been used for its strength and reliability. In the 4th century BC steel weapons like the Falcata were produced in the Iberian Peninsula, while Noric steel was used by the Roman military. Steel and a few other metals have been the choice of material for engineers in engineering design.

It has been said that necessity is the mother of all inventions. With the need and demand for materials with better and higher specific mechanical properties, high stiffness to-weight ratio, high strength to-weight ratio, tailor ability and damage tolerance, the birth of advanced composites took place.

Since its birth in the 1960's, advanced composites have been used in various applications, many in the military field such as aircraft, tanks, bulletproof body armors, etc. Composites have also been used in civil aerospace applications, the automotive industry and transportation. Lately, many 'everyday' items are being made from composite materials. As examples, one may cite fishing rods, tennis rackets, etc.

Due to the large use of fiber-reinforced composites [1] in industry, tremendous research has been done to have a better understanding of the mechanical properties and behavior of these composites. Most research on engineering composite materials has been done after the 1950's.

With the motivation to reduce the cost of manufacturing, fibers in textile forms are being introduced for use in composites. In addition to lower the cost of manufacturing, textile composites offer better dimensional stability over a large range of temperatures, better

impact resistance and tolerance, subtle conformability and deep drawn moldability/shapeability [2].

The standard yarn/fiber material for textile composites was glass with polymer being the matrix material. However, lately graphite and aramid have also become popular yarn materials. In applications where stiffness-to-weight is important, graphite has become the dominant fiber. In applications where tensile strength-to-weight is the major consideration, aramid is preferred. However glass fiber is the most dependable material for many textile composites due to its lower cost [3].

Recently, there have been investigations of hybrid fiber composites, in which different types of fibers are incorporated into a single composite system. The mechanical properties of the hybrid composite will be somewhere between those for single fiber composites. Hybrid composites can be classified as one of four types [4]: Type A is made by intermingling different fibers in a common matrix (i.e., intermingled or intraply); Type B is formed by laminating layers with fibers of different types (i.e., interlaminated or interply); Type C is in a form of fiber skins with a fiber core; and Type D is constructed by fiber skins with a non-fiber core. In addition, if the reinforcements are fabric it is called interwoven and each fabric may contain more than one-type of fiber [5].

2.1. STUDIES ON THE MECHANICAL PROPERTIES OF HYBRID AND NON-HYBRID WOVEN COMPOSITES UNDER TENSILE LOADING.

a) Experimental studies

Tensile testing has been the most fundamental test in obtaining the mechanical properties of a particular material. The limitation of obtaining mechanical properties from tensile

testing using an MTS machine is that only low strain rates results can be obtained, therefore only material properties under quasi-static loading can be determined. Material properties under high strain rates require different types of tests such as tests using the Split Hopkinson Pressure Bar Test (SHPB) [6].

Researchers have looked at natural composites with a lot of emphasis on natural fibers instead of man made fibers. Natural fibers have shown to be suitable reinforcement materials for composites thanks to a combination of good mechanical properties and environmental advantages such as renewability and biodegradability. Jute, sisal, coir, pineapple leaf, banana, sun hemp, broom and wood are some of the natural fibers used in composites [7]. Despite their attractiveness, such as low-cost, light-weight, enhanced mechanical properties, natural fiber reinforced polymer matrix composites suffer from low modulus, lower strength and relatively poor moisture resistance. Hybridization of natural fibers with stronger and more corrosion-resistant synthetic fibers such as glass fiber and carbon fiber can improve the properties of the composite. Velmurugan [8] investigated the properties of (randomly mixed) palmyra fiber, glass fiber hybrid composites. The results show that the mechanical properties of the composites improved due to the addition of glass fiber along with palmyra fiber in the matrix. Paiva Júnior [9] investigated the tensile strength of plain weave hybrid ramie–cotton fabrics. Van de Velde [10] studied unidirectional (UD) and multidirectional (MD) flax/polypropylene composites. Arbelaiz [11] investigated the effect of fiber treatments and matrix modification on mechanical properties of flax fiber bundle/polypropylene composites. Some chemicals were used to improve the interfacial bonding between fibers and the

polymeric matrix. The results suggest that matrix modification led to better mechanical performance than fiber surface modification.

b) Theoretical studies

Several analytical models have been developed to predict the material properties and behavior of woven hybrid and non hybrid composites under tensile loading. Many of these models also incorporate the effect of moisture and temperature; however most of these models assume the properties of each individual constituent as being constant. For example, most of these models assume that the thermal expansion coefficient is temperature independent. Analytical models tend to provide a cost effective method to determine the effects of several parameters on the mechanical properties. These parameters include fabric weight, constituent volume fraction, yarn undulation, weave style and properties of the constituent materials. Several micro mechanical models based on the classical thin laminate theory have been developed. Scida [12] developed a model called MESOTEX to predict the elastic behavior of composites reinforced with hybrid and non-hybrid weaves.

A model which study the failure behavior of plain weave fabric laminates under on-axis uniaxial tensile loading was done by Naik and Ganish [13-15]

Ishakawa and Chou [16-20] have presented three models (mosaic, crimp and bridging) for the analytical and numerical prediction of the thermo-mechanical properties of woven composites (plain, twill and satin weaves). In the mosaic model, the fabric composite is idealized as an assemblage of (0/90) laminates in series. In the model the undulation of the fiber is not considered. The constants of the laminate are then determined by using

classical lamination theory where the assemblage of the [0/90] units can be defined from a series or parallel assumption that corresponds respectively to the upper and lower bound of the final stiffness. The crimp model was developed to take into account continuation and undulation of the fibers in the woven fiber composite. This model allows for determination of stress-strain beyond the elastic region. For satin composites, the interlaced region of the satin weave are separated from one another and are surrounded by straight tread region that act as the load carrying bridge between adjacent interlaced region. These repeating units have been represented by the bridging model. The prediction of elastic behavior by the mosaic model is in good agreement with experimental tests for satin fabric with high value of n_g, but not for plain weave fabric composites. The crimp model is more appropriate for the case of plain weave composite but is inadequate for evaluating the behavior of satin weave composites with high n_g. The bridging model gives good results but due to its idealization, is limited to satin weave with $n_g \geq 4$. Peng and Cao [21] developed a non-orthogonal constitutive model to characterize the anisotropic material behavior of woven composite fabrics under large deformation. Huang [22, 23] developed a unified approach based on bridging the micromechanics model to the simulation of inelastic and strength properties of textile (woven, braided, and knitted) fabric reinforced composite laminates. Yu [24] developed a new constitutive model based on a homogenization method by considering the microstructure of composites including both the mechanical and structural properties of fabric reinforcement.

c) Numerical Models

Finite element method is a powerful tool that can be used to model the mechanical behavior of materials. E.J. Barbero, P. Lonetti, and K.K. Sikkil used a a meso-level damage model implemented into ANSYS as a user-defined material model to predict the non-linear behavior of plain-weave reinforced laminates under tensile loading[25]. Tabiei and associates [26-29] developed micromechanical models for woven composites using the method of cells and the four-cell method, to predict their properties. Most of the commercially available finite element software such as ABAQUS, LS-DYNA do not have user-defined material model to introduce nonlinear stress-strain behavior into the system. However these finite element software packages allow users to create user-defined interfaces to simulate the actual behavior of the material. Thus, Tabiei and associates successfully implemented nonlinearity into the finite element codes.

2.2. STUDIES ON THE LOW VELOCITY IMPACT RESPONSE OF HYBRID AND NON-HYBRID PLAIN WEAVE WOVEN COMPOSITES

An impact event is considered to be a low velocity impact if the contact period of impactor with the target is longer than the period of the lowest vibrational mode. For low velocity impact, the support conditions are crucial since the stress waves propagating outward from the impact point have time to reach the edges of the structural element, causing its full-vibrational response. On the other hand, in high velocity or ballistic impact, the response of the structural element is governed by the ‘local’ behavior of the material in the neighborhood of the impacted zone, the impact response of the element being generally independent of its support conditions. The contact period of the impactor

is much smaller than the period of lowest vibrational mode of the structure. Hyper velocity impact involves projectiles moving at extremely high velocities such that the local target materials behave like fluids and the stress induced by the impact is many times the material strength [30]. Some researchers [31] have classified impact loads depending on the velocity of the impact. Low velocity impact, in the order of 1 m/s, represents a tool dropped on a composite structure. Intermediate velocities, in the range of 10-100 m/s, represent runway debris striking an airplane. Ballistic impacts, in the velocity range of 100-1000 m/s, represent the impact of bullets, fragment and other low-mass projectiles on composite and textile protective armors or structures.

a) Experimental Studies

Many low velocity impact experiments have been conducted on woven composites where the material response, damage patterns and damage mechanisms have been studied. A large number of these composites used glass [32-33] or carbon [34] as the reinforcement. It was found that they have excellent impact resistance compared to FRPs (fiber reinforced plastics), FMLs (fiber metal laminates) [35]. Sevkat and etal. [36] studied the effect of repeated impact on hybrid composites and found that hybridization increases the impact resistance of plain weave graphite composites when they are sandwiched between layers of glass composites. Sevkat also looked at the effect of different impactors and found that they had little effect on the damage pattern and response of woven composite specimens. He also did extensive work on the effect of energy and velocity on the impact response of hybrid and non-hybrid plain weave composites. To date most of the research on low velocity impact in composites has mainly focused on impacting unstressed specimens. However this does not adequately reflect the real multidirectional complex

loading states that the materials experience during their service life. Limited research [37-38] has been done to evaluate the low impact response of composites under pre-stress condition. For example Whittingham [39] studied the effect of an initial pre-stress on the response of carbon-fiber/epoxy laminated plates subjected to low velocity impact. Prior to being impacted, the samples were loaded either uniaxially or biaxially using a specially designed test rig. It was concluded that pre-stress does not significantly affect the response of the composite.

b) Analytical Models

There are many models developed to predict the low velocity impact response of composites, such as the spring-mass, energy-balance, complete and semi-analytical models, etc.

1. Spring-mass model

In the spring-mass model, the impactor and the plate are represented by two masses connected to each other with a Hertzian spring which represents the force-indentation relationship of contact. The plate is attached to the fixed boundary through other springs which represent the bending, shear and membrane stiffnesses. Khalili [40] developed a model for a sandwich panel and derived closed-form solutions for the contact force, displacements of the impactor and the panel in the transverse direction. His model uses discrete three-degrees-of-freedom dynamic system with equivalent masses and springs.

2. The Energy balance model

Shivakumar [41] developed a simple energy-balance model, which is based on the principle of conservation of total energy of the plate-impactor system. Assuming the whole system behaves quasi-statically; It was assumed that all the initial kinetic energy of

the impactor was used to deform the plate when the plate reaches its maximum deflection.

3. Complete models

The impact information predicted from simple models is limited and not very accurate. Hence, complete models, in which the whole impact system is fully modeled, are developed and accurate solutions can be obtained [42-43].

4. Semi analytical models

Some models make use of experimental data to complement the analysis in predicting the response of the composite. Jimenez [44] proposed a model which has two systems set up in a serial arrangement. The first one is a spring-dashpot and the second is a hertzian spring-dashpot that simulates the indentation. Since the differential equation that describes this system does not have an analytical solution, a 4th order Runge–Kutta algorithm was used. The overall energy loss was calculated by means of the restitution coefficient, which was measured experimentally; these results were compared with those obtained solving the differential equation.

5. Other Models

Malekzadeh [45] proposed a new three-degrees-of-freedom (TDOF) springs–masses–damper (SMD) model to predict the contact force history of composite sandwich panels with transversely flexible core. Chun [46] in his study assumed the contact area between the striker and plate very small, and used the Hertzian contact law to evaluate the contact force. Guinarda [47] studied the 3D damage analysis of low-velocity impacts on laminated composites.

c) Numerical Models

Numerical models such as the finite element method (FEM) are quite useful and cost effective since experiments can be quite expensive and time consuming while closed form analytical solutions are limited to linear solutions (with many simplifying assumptions) of stress states, for specific geometries, lay-ups, loads, and boundary conditions. Li [48-49] developed a numerical model, based on the Mindlin [50] plate element to directly and completely simulate the low-velocity impact-induced damages in laminated plates which can describe the various damages and their mutual effects. Besant [51] further modified the existing finite element code FE77 for analysis of impact of composites. The sandwich panels were modeled using 8 noded shell elements for skin and two layers of 20 noded brick elements for core. Elder [52] reviewed the damage mechanics and fracture methods available in the literature for predicting delamination under impact. He concluded that the linear elastic fracture mechanics method has been used extensively where the shape of the delamination front can be predicted and a suitably shaped mesh can be provided. However, as impact events produce irregular shaped delamination fronts, this method requires an adaptive mesh approach that is not yet available in any of the major analysis codes. The cohesive fracture model solves some of the limitation of the linear elastic fracture mechanics method; however a definitive study of its abilities has yet to be found in the literature. The delamination threshold load method is an extremely simple method and provides surprisingly good results. The review concludes that additional development of current techniques is required before a definitive predictive delamination method is available. Hou [53] implemented an

improved delamination criterion for laminated composite structures into LS-DYNA3D to take into consideration the out-of-plane stresses for damage initiation. The new delamination criterion was verified by experimental results for low-velocity impact.

Naik [54], in another study, simulated the behavior of woven-fabric laminated composite plates under transverse central low-velocity point impact by using a modified Hertz law and a 3D transient finite-element analysis code. The in-plane failure behavior of the composites was evaluated by means of a failure function based on the Tsai-Hill quadratic failure criterion. Lee [55] predicted the low velocity impact response of hybrid laminated composite plates (graphite/epoxy-glass/epoxy and graphite/epoxy-kevlar/epoxy) using the finite element method, and compared the results with those of a single laminated composite plate (graphite/epoxy) impacted at the center of the plate with velocity v. The modified contact law suggested by Yang and Sun [56] was used for calculating the contact force. Sevkat and others [36] used the 3-D dynamic nonlinear finite element (FE) software, LS-DYNA, by incorporating a user-defined damage-induced nonlinear orthotropic model to simulate the experimental results of drop-weight tests. Good agreement between experimental and FE results was achieved when comparing dynamic force, strain histories and damage patterns from experimental measurements with FE simulations.

2.3 BALLISTIC IMPACT RESPONSE OF HYBRID AND NON-HYBRID, PLAIN WEAVE WOVEN COMPOSITES

a) Experimental Studies

Almost all researchers have used the same experimental procedures in conducting ballistic impact tests and analysis on composite specimens. Basically, the different kinds of plates are impacted at different velocities and post-impact data is evaluated using different techniques.

Ballistic response of fabric-reinforced composites has also been studied by few researchers [57-60]. Cheeseman [61] has reviewed a number of studies on the ballistic performance of textiles. He concluded that material properties, projectile geometry, impact velocity and multiple plies have a profound influence on performance. However the effect of other factors such as fabric structure, far field boundary conditions and friction are not as apparent. Czarnecki [62] developed a semi empirical method to estimate V_{50} of composite laminates.

b) Analytical models

Naik [63-65] has a number of publications especially on the analytical modeling of woven composites. His models are based on various energy absorbing mechanisms. These are: cone formation on the back face of the target, tensile failure of primary yarns, deformation of secondary yarns, delamination, matrix cracking, shear plugging and friction during penetration. Classification that was made for low-impact analytical models is also valid for ballistic impact models. Some models were proposed for calculating force, displacement and velocity in ballistic impact of woven fabrics [66-69].

Puente [70] developed an analytical model to study the impact process of a spherical projectile penetrating at high velocity into a carbon/ epoxy plain woven laminate. The model is based on energy balance, where the kinetic energy of the projectile is absorbed by the laminate by three different mechanisms: laminate crushing, linear momentum transfer and tensile fiber failure. Morye [71] developed a simple model for calculating the energy absorption of polymer composites upon ballistic impact.

c) Numerical Models

Although quite a few software are available to analyze impact problems, most people tend to use LS-DYNA for ballistic problems since it explicit solver deals quite well with impact problems. Numerical modeling is very handy in analyzing ballistic impact, since parameters can be easily varied. Sevkat etal. [72] used a combined experimental and 3D dynamic nonlinear finite element (FE) approach to study damage in composite beams subject to ballistic impact using a high-speed gas gun. Self-designed FEM models are also employed for ballistic-impact problems [73-74].

2.4 COMMON STUDIES ON TENSILE, LOW VELOCITY AND BALLISTIC-IMPACT RESPONSE OF COMPOSITES: TEMPERATURE EFFECT

In addition to mechanical loading, composite materials are also exposed to other types of agents that affect the behavior of the material and which can lead to failure. Maybe the most common agent other then force that may adversely affect composites is temperature. Some research has been done to study the effect of temperature on composite materials. High-performance thermo-plastic matrices used in composite materials need to be

processed at high temperatures; therefore, thermal residual stresses arise due to the mismatch of thermal expansion coefficients of the fibers and the thermoplastic matrix. Since residual stresses are inherently present in virtually all composite materials and influence the properties of the composite structure, it is important to take them into consideration in the event that they are significant. Parlevliet, Bersee and Beukers [75-77] did a study of the literature focusing on the formation of residual stresses due to manufacturing, experimental techniques in quantifying these residual stresses and also the effect of these residual stresses. They classify the residual stresses into three categories, micromechanical or intra-laminar residual stresses which arise from mismatch expansion coefficients of matrix and fiber materials, macro mechanical or inter-laminar stresses which arises from difference in properties between laminae and finally, global stresses (skin-core stresses) which arise from the gradient of cooling rate between the surface of the material and the core. These stresses can lead to waviness of the fibers, transverse cracking of the composite, often referred to as micro cracking, delamination, warpage of the laminates, etc. In this research, it is assumed that there are no thermal stresses in the composite material due to manufacturing or that they are not significant.

The environmental loading conditions that a composite is subjected to play a key role in determining its impact failure process. Thus, heat resistance of composites to low and high temperatures has to be studied carefully. However, the fracture behavior and failure mechanisms of laminated composites at low and high temperature levels are complicated when compared with those at room temperature. In the aeronautics and aerospace industries the specific behavior of the composite material at very low temperatures is extremely important. CFRP structural components can suffer high velocity impact at

cryogenic temperatures. Such is the case for high-flying aircrafts (–60 °C) and spacecraft orbiting around the Earth (–150 °C when not directly exposed to solar radiation). Combat aircraft may suffer ballistic impact; spacecraft may be impacted by space debris. In addition to these examples, cryogenic composite tanks can suffer low velocity impact during maintenance operations.

The first step of this research was to determine the mechanical properties of the composite material by tensile testing at room, high and low temperatures. These properties will be very important since they will serve as the base data for further modeling and analyzing the behavior of the material under different loading conditions. To the best of our knowledge limited research had been done to study the effect of temperature on the mechanical properties of composites, especially woven composites. Bosze [78] investigated the effect of temperature on the tensile strength of the pultruded rods of unidirectional hybrid glass/carbon-epoxy composites core and proposed a convenient method to predict the temperature dependence of strength for similar unidirectional composites with the following formula:

$$\sigma_s(T) = \sigma_{To}[E'(T)\frac{1}{E'(T_o)}] \qquad (1.1)$$

where $\sigma_s(T)$ is the strength at temperature T, σ_{To} is the strength at the reference temperature (room temperature), $E'(T)$ is the storage modulus at temperature T, and $E'(T_o)$ is the storage modulus at the reference temperature. Dlouhy [79] studied the thermal aging of a glass matrix composite reinforced by short carbon fibers as well as by ZrO2 particles (hybrid composite) at temperatures in the range of 500–700 °C for exposure durations of 24 hours in air. It was reported that the fracture toughness and flaw

tolerance resistance decreased with increasing temperature. Schmitt-Thomas [80] investigated the effect of changing temperature on the strength performance and failure behavior of hybrid short-fiber-reinforced thermoplastic composites. He concluded that the micro-failure behavior of the composite is closely related to temperature. Lipetzky [81] examined the mechanical behavior of a 2D woven, 0-90 SiC fiber-reinforced SiC matrix composite at room temperature, 850, 1000 and 1200 °C

Liaw et al. [82] discussed the tension-induced damages of S2 glass/toughened epoxy composites at room and elevated temperatures. They also provided an experimental technique for in situ tensile testing of ceramic matrix composites at elevated temperatures within a scanning electron microscope.

Temperature effect on low velocity impact of hybrid composites exhibits more complexity due to the difference in thermal expansion coefficients of fibers and resin. Hirai [83] studied the temperature effect on the low-velocity impact response of vinyl-ester-matrix composites reinforced with woven E-glass fabric. He found that the damage and the residual properties of the laminates vary with fiber surface treatment and impact test temperature. The damage area increases with increasing temperature and impact energy. In another study, Levin [84] reported a decrease in delamination area with increase in temperature in the range between -40 ^{o}C and 70 ^{o}C for a carbon–fiber composite laminate subjected to high-energy impact. Salehi-Khojin [85] studied low velocity impact behavior of fiberglass and Kevlar composite at temperatures ranging from -50 to 120 ^{o}C in an attempt to better characterize the impact properties of laminated composites. The focus of his study was to show the effect of temperature on the impacted composites. Compression tests were conducted to determine the remaining compressive

strength after impact. It was found that at low impact energy, the amount of maximum absorbed energy is almost constant and independent of temperature. With increasing energy level, absorbed energy becomes more and more dependent on temperature. At each of the impact energies, maximum deflection is a function of impact energy and temperature such that maximum deflection increases with a corresponding increase in impact energy or temperature. Gomez [86-88] summarized the results of low velocity impact tests carried out at different temperatures ranging from 20 ^{o}C to –150 ^{o}C on CFRP laminates. It was shown that damage induced in CFRP laminates by low velocity impact loads (when no perforation occurs) increases with impact energy. The experimental results obtained in this work showed that cooling the laminate before impact has an effect on damage similar to that of increasing the impact energy. Khojin [89] has studied the temperature effect on carbon fiber sandwich composite plates with three layers carbon and a layer of Kevlar or hybrid layer at energy levels of 15, 25 and 45 J at different temperatures ranging from -50 ^{o}C to 120 ^{o}C. Temperature was found to have significant effect on the impact behavior of graphite and combinations of graphite with hybrid and Kevlar. Schultz [90] studied the effect of temperature and strain rate on the strength of PET/glass fiber composites. Dutta [91] analyzed the energy absorption of graphite/epoxy plates under low velocity impact using a Split Hopkinson pressure bar, and found a small dependence on temperature.

Since the majority of applications of thick-section composites are for military use, temperature in armor-grade hybrid fiber composites during ballistic impact and projectile penetration should also be carefully study. The literature available on this particular subject for thick-section hybrid composites is very limited. It practically does not exist

for thick-section interwoven hybrid composites; however, there are some work done on the temperature effect on ballistic impact of composites. Kwang-Hee et al. [92] studied the effect of temperature variation (-30 to 120 ^{o}C) on damage of orthotropic CFRP laminates at non-penetrating impact velocities (up to 100 m/s). They observed a linear relationship between the impact energy and the delaminated area, as well as an increase in the damaged area as the temperature decreased.

In a similar high velocity impact study on cross ply laminates of polyethylene fiber/epoxy matrix system [93], it was found that the damage initiation energy doubled when the temperature was increased from -50^{o} to 100 ^{o}C. In contrast, laminates containing plain-weave fabrics showed very little influence of temperature on the total impact energy required for complete penetration of the specimen. Lo´pez-Puente et al. [94] extended this analysis down to -150^{o}C. Both of them focused their work on high velocity perforating impacts (from 100 to 500 m/s), far away from the threshold impact energy.

2.5 Major contribution of this research

Based on literature review it was found that limited research and in some cases no research has been done on the temperature effect on the behavior of hybrid composites; specifically the temperature effect on the low velocity impact response and on the ballistic resistance or ballistic limit. The goals of this thesis are listed below:

a) Study of the effect of temperature on drop weight impact of hybrid and non hybrid woven composite materials
b) Study of the effect of temperature on ballistic impact of hybrid and non hybrid woven composite materials

c) Developing of testing methodologies for ballistic impact at high and low temperatures

d) Developing a finite element model to predict the behavior of hybrid woven composites at high and low temperatures

Chapter 3

Experimental set-up and the materials

3.1 The materials and the specimens

The individual constituent materials combined to form the composite material used in this research are, IM-7 graphite (IM7-GP 6000) and S2-glass (S2-4533 6000) woven fabrics placed in SC-79 toughened epoxy resin matrix. The IM-7 graphite woven fabric and SC-79 epoxy matrix form the non-hybrid composite called GR. The S2-Glass woven fabric and SC-79 epoxy matrix form the non-hybrid laminate called GL. A GL laminate will be sandwiched between two GR layers to form the hybrid laminate called GR/GL/GR. Finally the fourth layup is formed by a GR layer sandwiched between two GL layers to form the second hybrid laminate called GL/GR/GL. S2-glass fabrics and IM7-graphite fabrics were supplied by the Hexcel Corporation. The matrix, SC-79 toughened epoxy resin, which has Part A (Batch number: SC79A012307) and Part B (Batch number: SC79B012507), was supplied by Applied Poleramic Inc. The manufacturing of the composite was done by EDO Fiber Innovations. The vacuum assisted resin transfer molding (VARTM) technique was used to stack the plain woven fabrics together (Fig.3.11). The specimens were cured at 177^0 C. Fiber volume fraction for all types was 55%. The final thickness of the specimens was 6.35 mm.

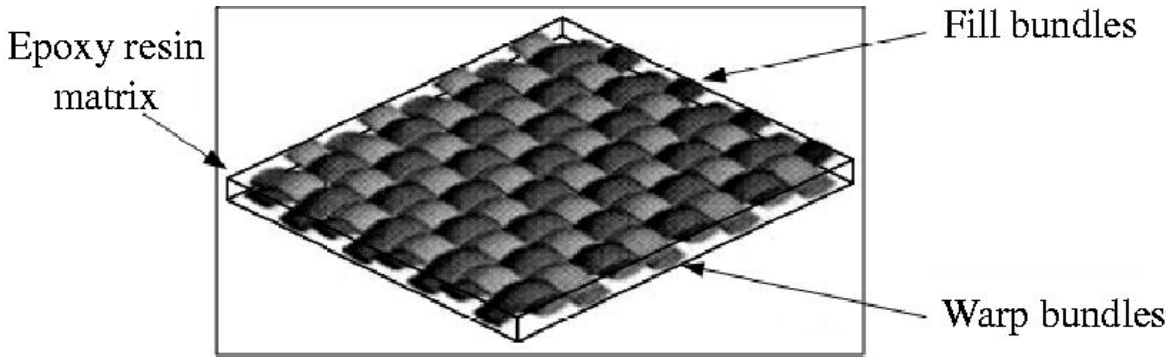

Figure 3.1 Plain-woven fabrics

The four different stacking sequences that were used consist of the following number of layers. GL specimens contain 37 layers of glass fabrics (Fig. 3.2.a). For the GL/GR/GL specimen, the glass outer skins contain 9 layers of glass fabric on each side. The graphite core contains 16 layers of graphite fabrics (Fig 3.2.b**).**

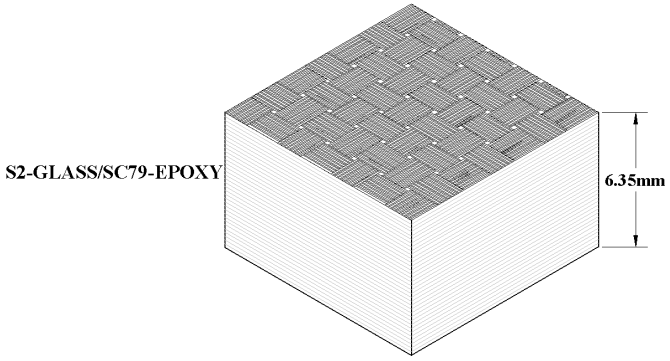

Figure 3.2 a) Woven S2-glass/ SC79 Epoxy composite

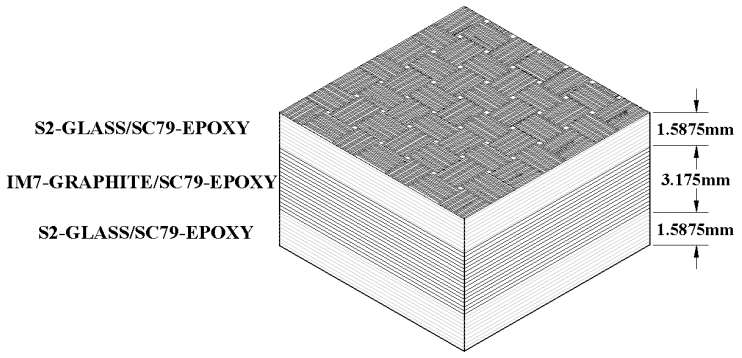

Figure 3.2 (b) Woven S2-glass, IM7-graphite/ SC79 Epoxy hybrid composite

The GR/GL/GR specimens contain 8 layers of graphite fabric skin on each side, while the glass core has 16 layers of glass fabric (Fig. 3.2**.c).** The GR specimens contain 28 layers of graphite fabrics (Fig. 3.2.d). Although the thickness was constant for all types, the number of the fabric layers used in each composite varies due to the different thickness of graphite and glass fabric layers.

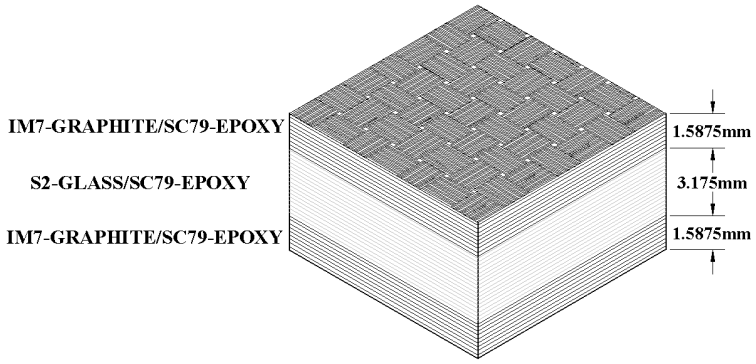

Figure 3.2 (c) Woven IM7-graphite, S2-glass / SC79 Epoxy hybrid composite.

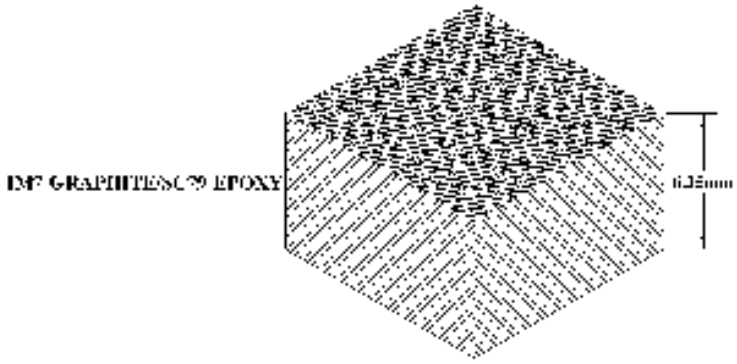

Figure 3.2 (d) Woven IM7-graphite/ SC79 Epoxy composite

All of the tensile tests were conducted using strip specimens (Fig.3.3.a). All drop-impact tests were conducted on square specimens (Fig.3.3.b).Rectangular specimens will be used for ballistic tests (Fig.3.3.c).

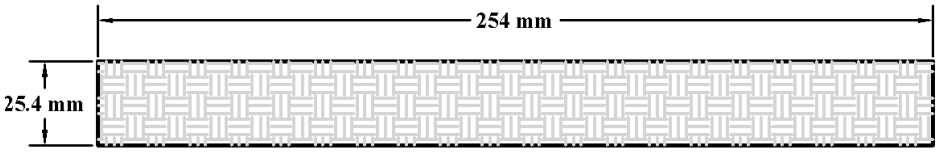

Figure 3.3 (a) Tensile test specimen dimensions

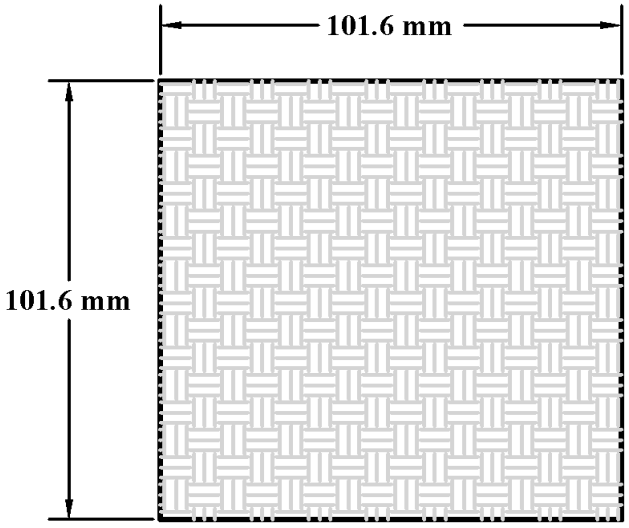

Figure 3.3 (b) Low velocity impact test specimen dimensions.

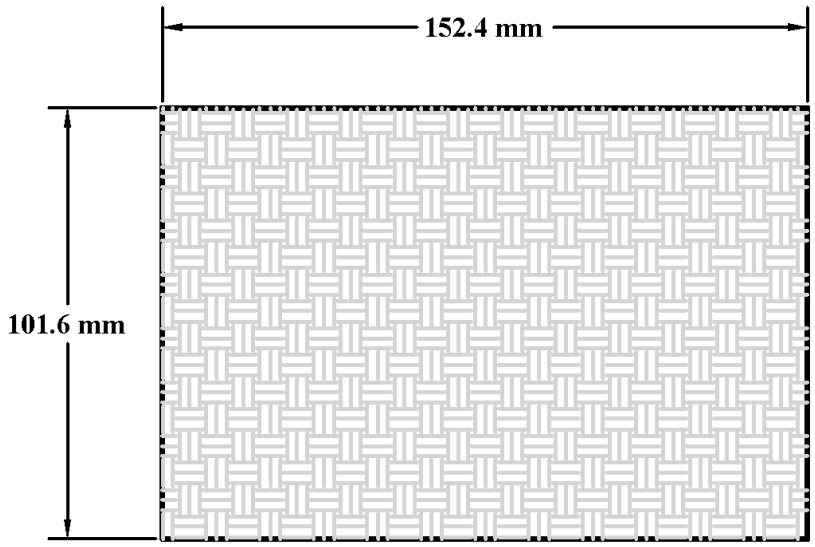

Figure 3.3 (c) Ballistic impact test specimen dimensions.

(Figures 3.2 (a) through 3.3 (c) were taken from [45, 81])

3.2 Tensile test set-up

In the tensile testing portion of this research all specimens were tested under uniaxial tension in an environmental chamber of a 22-kip MTS servo-hydraulic universal testing machine (MTS 810) at −60°C, −20°C, room temperature, 75°C, and 125°C. Although there could be a choice between force control, displacement control and strain control, all of the tensile tests in this study were displacement controlled. The different types of grips with the option to vary the gripping pressure give the user choice in selecting the best type of grip along with grip pressure that is most suitable for the testing condition. This is very important for low temperature tests where slippage between grip and specimen can easily occur due to ice formation on the specimen. The user also has the choice of force cartridge and displacement cartridge in operating the MTS machine. The choice of

cartridge is based on knowing the maximum force required to fracture the specimen and also its total elongation.

In the high temperature tensile tests, the temperatures were achieved by using an internal heater that was built into the chamber. The low temperatures were obtained using liquid nitrogen. Both loading and elongation histories were recorded in volts through a National Instruments (NI)-DAQ based Lab View data acquisition system. Simple conversions were made from voltage to displacement and force to obtain force-time and displacement-time histories.

Figure 3.4 MTS machine with environmental chamber and liquid nitrogen tank

3.3 Drop-weight impact tester

The low velocity impact (drop weight) study investigated the effect of temperature on hybrid and non-hybrid woven composite panels (100mm×100mm×6.35mm). A drop-weight impacted the specimen at five different temperatures: –60°C, –20°C, room temperature, 75°C and 125°C. All the impact tests are performed using Instron-Dynatup 8250 impact test machine, a typical drop-weight impact tester (Fig. 3.5).The impact energy was fixed at 30 Joules for all the tests which corresponds to an impact velocity of 3.12 m/s. The shape of impactor nose can be different; however in this study all tests were performed using a hemispherical impactor with a diameter of 16 mm.

Figure 3.5 Instron Dynatup impact machine with environmental chamber.

With the attached environmental chamber, an open coil heater provided the high temperatures, while the low temperatures were achieved through the use of liquid nitrogen. Specimens were clamped circumferentially with a 76 mm diameter fixture,

where the clamp was considered to be a fixed-fixed support. Using Dynatup 930-I data acquisition system, the time histories of impact loads were measured and recorded using a load cell located just above the impact nose and the impact velocity was also measured by one pair of photoelectric-diode system attached to the base of the test machine. With Dynatup 930-I data acquisition system, only load (the resistive force of the specimen) vs. time and initial impact velocity (just prior to impact) can be measured directly. Using the equations of motion, energy absorbed by the specimen, the velocity of impactor and deflection at the impact center can be derived and recorded into file. The equations used are as follows (assuming data collection starts at t = 0):

Table 3.1 Notations used in drop impact tests

Notation	
v_i	Impact velocity measured by photodiodes.
$p(t)$	Load value measured by 930-I at time t.
m	Total mass of impactor (impact tower and nose)
g	Acceleration of gravity
$f(t)$	Total force acting on the impactor at time t.
$a(t)$	Resultant acceleration of the impactor at time t.
$v(t)$	Velocity of the impactor at time t.
$x(t)$	Deflection (position) of the impactor at time t.
$K(t)$	Kinetic energy of the impactor at time t.
$V(t)$	Potential energy of the impactor at time t.
$E_a(t)$	Energy absorbed by the specimen at time t.
$E(t)$	Total energy of the impactor /specimen system at time t.

$$f(t) = mg - p(t) \tag{3-1}$$

$$a(t) = \frac{f(t)}{m} = g - \frac{p(t)}{m} \tag{3-2}$$

$$v(t) = v_i + \int_0^t a(t)dt = v_i + gt - \frac{1}{m}\int_0^t p(t)dt \tag{3-3}$$

$$x(t) = \int_0^t v(t)dt = v_i t + \frac{1}{2} g t^2 - \tfrac{1}{m} \int_0^t (\int_0^t p(\tau) d\tau) dt \qquad (3\text{-}4)$$

$$E(t) = K(t) + V(t) + E_a(t) = K(0) \qquad (3\text{-}5)$$

where $K(0) = \frac{1}{2} m v_i^2$ and since the displacement is small the potential energy can be neglected. Thus, the energy absorbed by the specimen can be computed as:

$$E_a(t) = K(0) - K(t) = \tfrac{1}{2} m \{v_i^2 - [v(t)]^2\} \qquad (3\text{-}6)$$

3.4 Ballistic impact tester

The ballistic impact tests were performed using an in house designed gas-gun setup equipped with an environmental chamber. Inside the chamber is a fixture which holds the specimen to be impacted. A 22 caliber copper bullet fitted in to a plastic sabot was used as the projectile. The sabot is very important and provides a tight fit of the projectile in the gun barrel. The gun consists of helium tank, temporary gas storage vessel, solenoid valve and stainless-steel barrel.

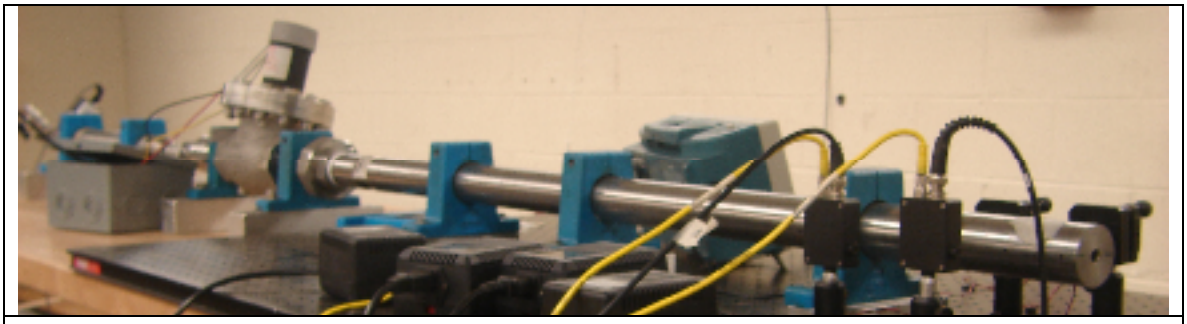

Figure 3.6 Ballistic gas gun

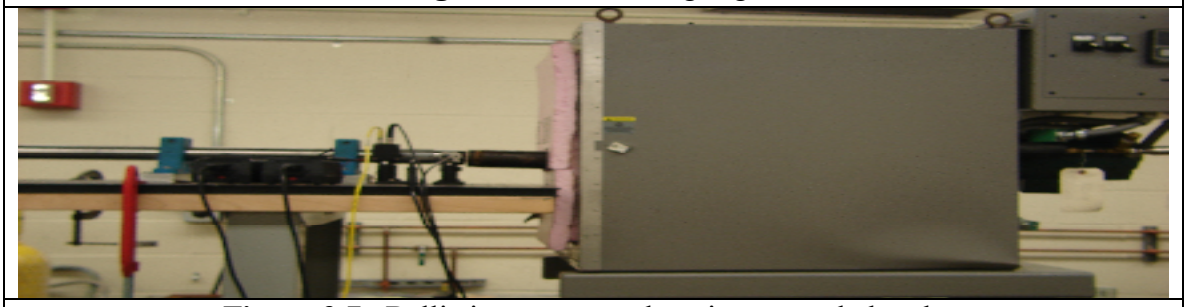

Figure 3.7 Ballistic gas gun and environmental chamber

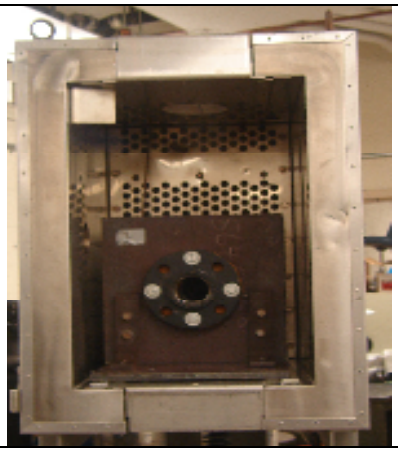

Figure 3.8 Fixture

Figure 3.9 Sabot and bullet

The figures above show the gas gun with the environmental chamber fixture and bullet with sabot. Figure 3.10 shows the dimensions and clamped areas of the specimen to be impacted. The boundary conditions of the clamped sides are assumed to be fixed-fixed.

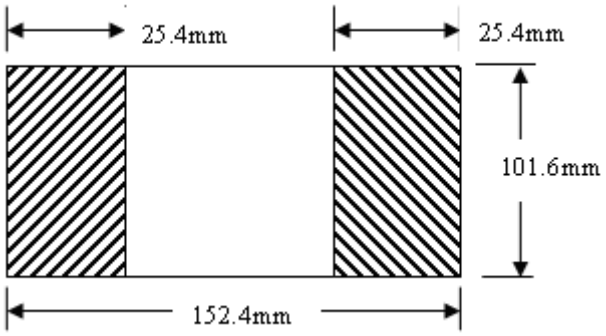

Figure 3.10 Ballistic impact test specimen

Compressed helium was used to launch the projectile. The velocity of the projectile can be varied by changing the pressure used to launch the projectile or by changing the location of the bullet in the gun barrel. Placing the bullet closer to the exit of the gun barrel lowers the velocity of the bullet since the pressure used to launch the bullet will be smaller as compared to when the bullet is placed further away from the exit. The velocity of the bullet is measured as follows: two holes are drilled in the barrel where two laser

beams continuously feed two optical sensors. When the projectile passes through the holes, it blocks the lasers, the sensors sense the change in intensity of light and an oscilloscope captures the voltage change. The velocity of the projectile is then calculated from the distance between the two sensors divided by the time that projectile spends traveling between the two holes. As the bullet exits the gun barrel it strikes the specimen that is in the environmental chamber at the specific test temperature. The specimens were impacted at five different temperatures: –60°C, –20°C, room temperature, 75°C and 125°C. The specimens were first soaked at the desired test temperature for thirty minutes before impact. This is done to eliminate any temperature gradient in the test specimens.

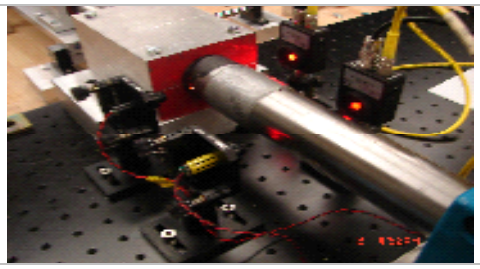

3.11.(a) Lasers and optical sensors

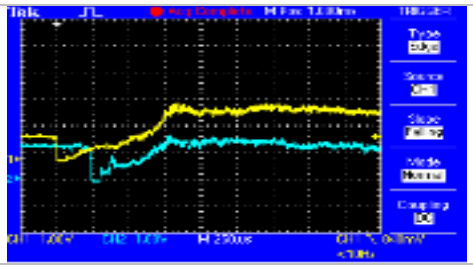

3.11. (b) Voltage-time histories

Figure 3.11 Setup to measurement velocity during ballistic impact

The force-time histories and the deflection-time histories can not be measured with our set-up. However, two strain gages placed one inch away from the impact point, one in the radial direction and the other in the hoop direction, measure the dynamic strain histories of the specimen during impact.

3.5 Ultrasonic Damage Evaluation System

Ultra PAC, an advanced, modular and expandable ultrasonic system (Fig. 3.12) was used to scan and conduct the damage evaluation for the impacted specimens. Scanning was done using the through-transmission techniques. Figure 3.13 shows an illustration of the through-transmission setup. Flat and focused transducers (0.25 inch in diameter) of various frequencies (5 to 25 MHz) can be chosen for different specimens. Lower frequency transducers give better result when scanning thick specimens, therefore in this research, the 5MHz transducer was used.

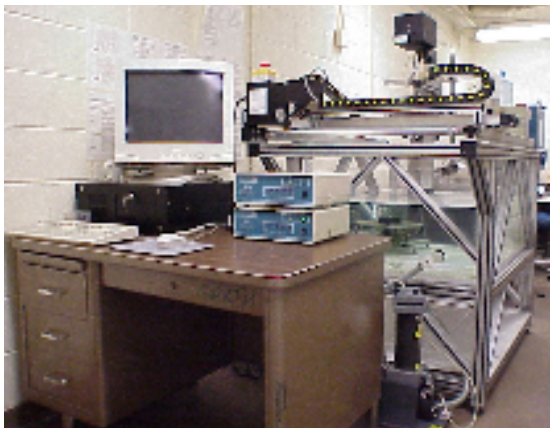

Figure 3.12 The UltraPAC system

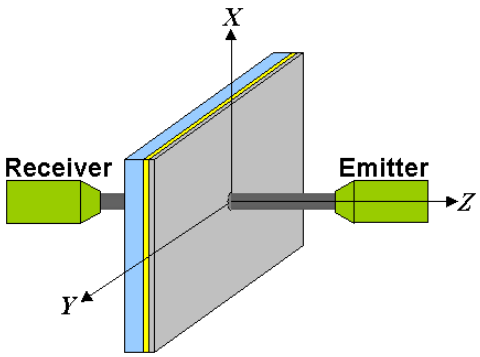

Figure 3.13 Through-transmission technique

Chapter 4

Tensile tests on woven hybrid composites

4.1 Experimental studies

Strip specimens of dimensions 6.35mm×25.4mm×254mm with four different lay-ups were tested under uniaxial tension at 125 °C, 75 °C, room temperature (R.T), –20 °C and –60 °C. The desired temperatures were achieved using an environmental chamber, where each specimen was allowed to soak at the required temperature for thirty minutes before testing. During this soaking period, one end of the specimen was clamped while the other end was free; this was done in order to allow the specimen to elongate freely. The tests were conducted using a universal testing machine also known as MTS while specimens were still in the environmental chamber. Both loading and elongation histories were recorded using a National Instruments (NI)-DAQ based Lab View data acquisition system. The longitudinal and shear modulus of each specimen were calculated from the acquired data. Due to the woven fiber structure, the transverse (in-plane) modulus of the composites was assumed to be the same as the longitudinal (in-plane) modulus. Thus, tensile tests for transverse direction were not carried out. For each lay-up configuration a minimum of three tests were conducted. Strain gages were also mounted on the specimens to record the output strain. The output data obtained from the stain gages were then used to calculate the Poisson's ration of each specimen. In addition, a digital camera was used to capture the surface strain progression.

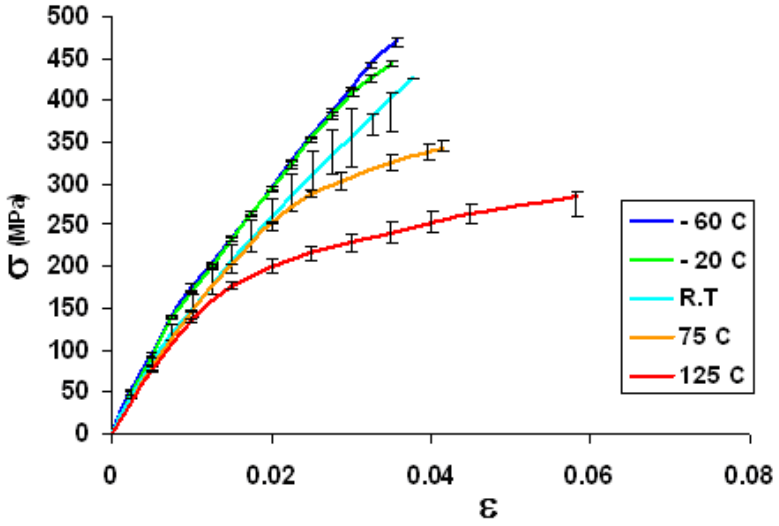

Figure 4.1 Longitudinal and transverse stress-strain curves for GL specimens at 125 °C, 75 °C, R.T, –20 °C and –60 °C

In Figure 4-1 the longitudinal stress-strain curves of GL are shown at the five different temperatures. Each specimen in the tests didn't exhibit the identical stress-strain relationship; however the curves were very close to each other especially in the elastic range. In order to avoid clustering of data, only a representative curve is plotted along with an error bar which represents the range of results obtained from the tests.

It is seen that at low temperatures the effect of temperature is less pronounced than at higher temperatures. At high temperatures, the stress-strain curves become more non linear. Figure 4.2 shows the stress-strain curves for GL specimens with ± 45 fiber orientation. The results indicate that temperature has a significant effect on the shear properties of GL specimens.

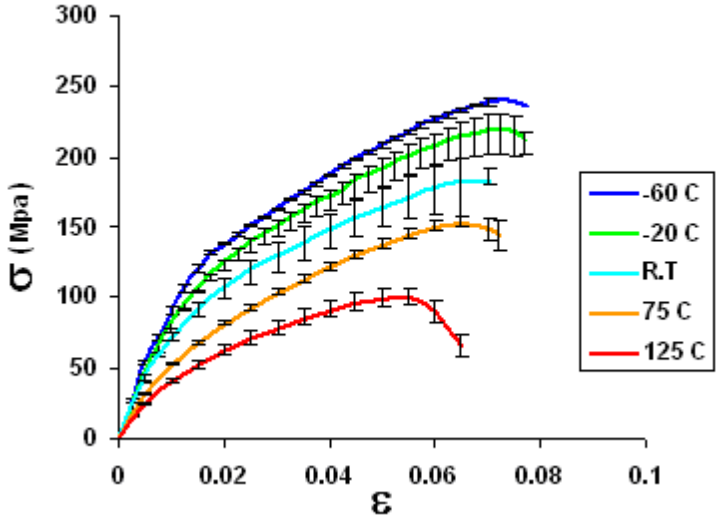

Figure 4.2 Stress-strain relations for ± 45 GL specimens at 125 °C, 75 °C, R.T, –20 °C and –60 °C

Figure 4.3 shows the longitudinal stress-strain curves for hybrid GR/GL/GR specimens. The curves can be divided into three portions. The first portion is almost linear at all test temperatures followed by a mostly nonlinear portion. Then the material had a sudden drop in stress due to the fracture of the graphite part of the hybrid specimen. However, the glass part in the hybrid composite was still undamaged, providing some strength which constitutes the third portion of the curve.

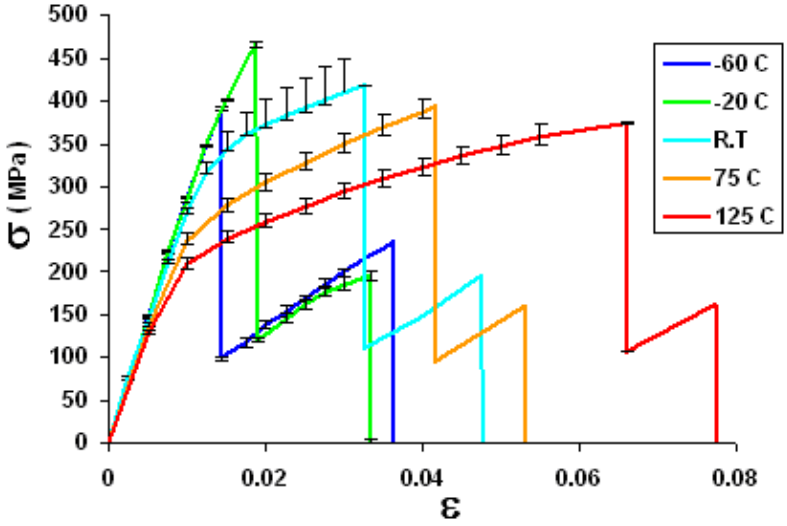

Figure 4.3 Longitudinal and transverse stress-strain curves for GR/GL/GR specimens at 125 °C, 75 °C, R.T, –20 °C and –60 °C.

Figure 4.4 shows the stress strain curves of the GR/GL/GR specimen with ± 45° fiber orientation. Here, there is no drop before failure. This is due to the fact that the graphite and glass layers failed together. It is observed that all the curves are non-linear. Also at higher temperatures the specimens did not totally fracture.

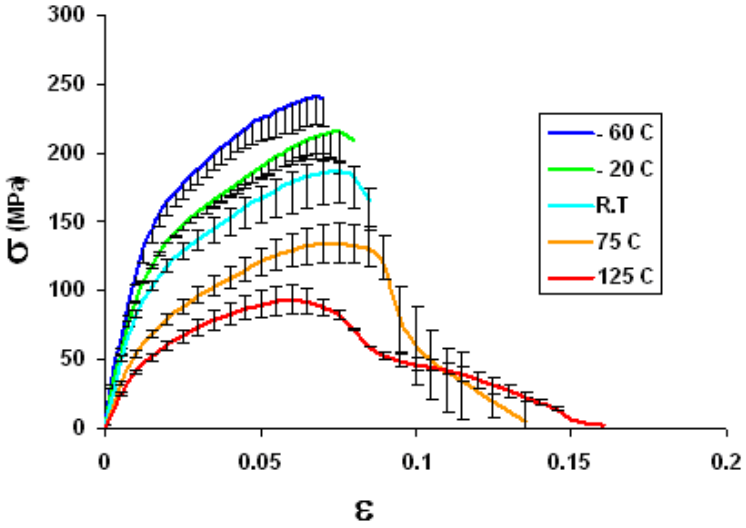

Figure 4.4 Stress-strain relations for ± 45 GR/GL/GR specimens at 125 °C, 75 °C, R.T, –20 °C and –60 °C

In Figures 4.5 and 4.6, the stress strain behavior of hybrid GL/GR/GL specimens is seen to be similar to that of the hybrid GR/GL/GR specimens described above.

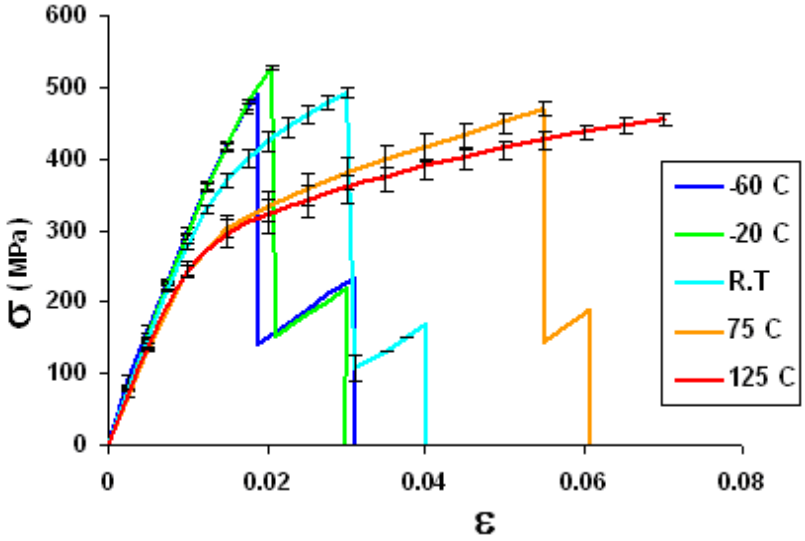

Figure 4.5 Longitudinal and transverse stress-strain curve for GL/GR/GL specimens at 125 °C, 75 °C, R.T, –20 °C and –60 °C.

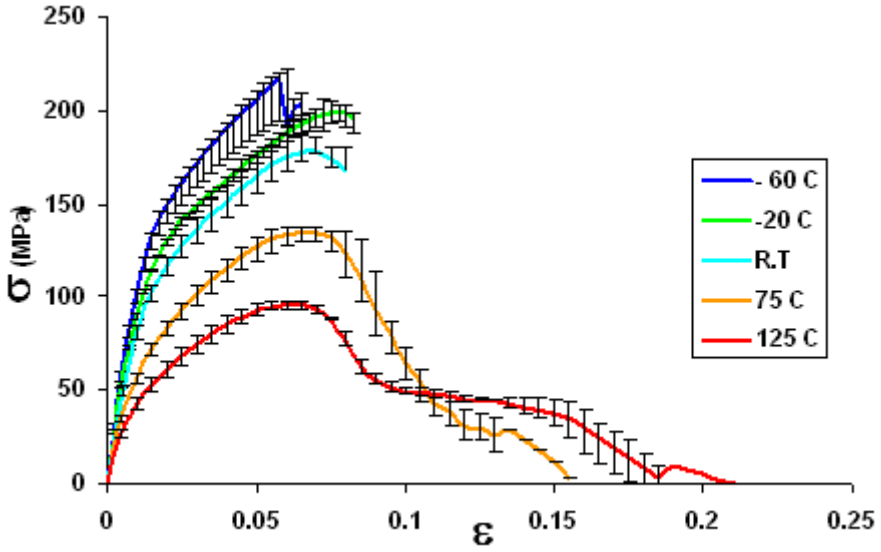

Figure 4.6 Stress-strain curve for ± 45 GL/GR/GL specimens at 125 °C, 75 °C, R.T, –20 °C and –60 °C

Figure 4.7 shows the longitudinal stress-strain relation of the GR composite specimens. Tests conducted at each test temperature were very consistent with each other.

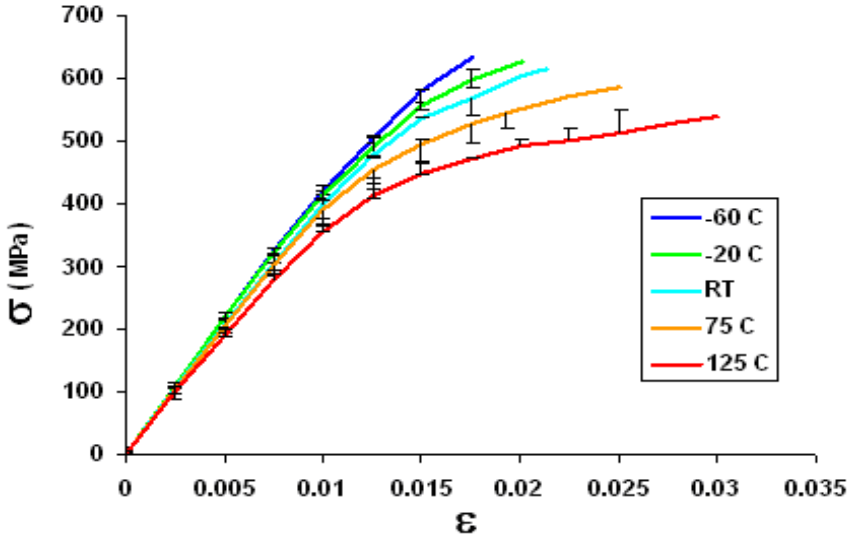

Figure 4.7 Longitudinal and transverse stress-strain curves for GR specimens125 °C, 75 °C, R.T, –20 °C and –60 °C

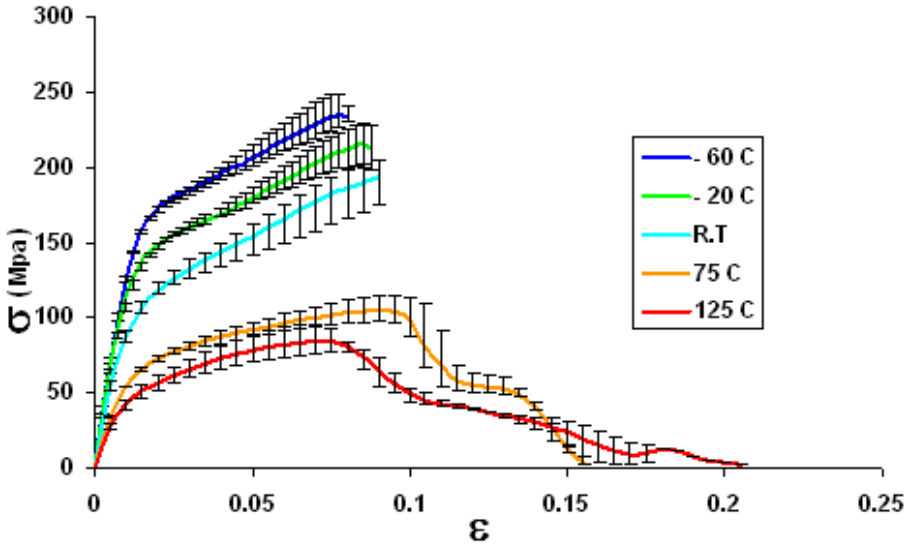

Figure 4.8 Stress-strain curves for ± 45 for GR specimens 125 °C, 75 °C, R.T, –20 °C and –60 °C

The GR specimens are shown to have higher failure strength than all the other specimens at a given test temperature. The stress-strain relations for ± 45° GR specimens are shown in Figure 4.8. All the specimens exhibit a linear behavior followed by a non-linear portion. At higher temperatures again the specimens did not fracture completely.

Tables 4.1 and 4.2 show the summary of material properties obtained from the uniaxial tension tests. GR at –60 °C has the highest Young's modulus (43.8 GPa) and ultimate stress (633 MPa) compared to all specimens at all temperature values. Overall it is also seen that GR exhibits the highest stiffness and strength while GL exhibits the lowest. The hybrid specimens have material properties which are intermediate between those of GR and GL. It can also be seen that as the temperature increases the stiffness of the material decreases.

Figure 4.9 shows the longitudinal stress strain curves for all layups at room temperature. It can be seen that the curves for the hybrids are somewhere in between those of the two non-hybrid. This trend is similar for all the test temperatures.

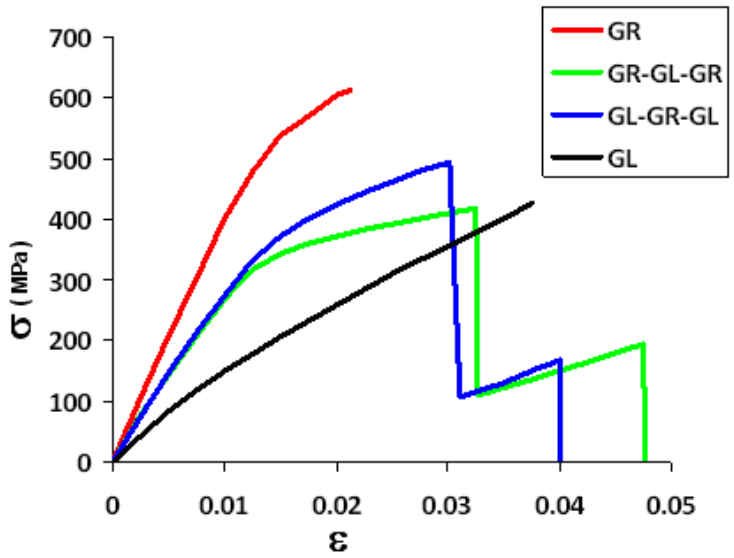

Figure 4.9 Longitudinal stress-strain curves for all layups at R.T

Table 4.1 Material properties for 0°/90° plain weave composites

Composite	Test Temperature	$E_1=E_2$ (GPa)	σ_{max} (MPa)	ε_{max} (%)
Non-Hybrid GL	−60 °C (−76 °F)	19.395	469	3.56
	−20 °C (−4 °F)	18.927	443	3.46
	R T (R T)	17.047	427	3.76
	75 °C (167 °F)	16.139	342	4.13
	125 °C (257 °F)	15.038	286	5.81
Hybrid GL/GR/GL	−60 °C (−76 °F)	31.985	489	1.90
	−20 °C (−4 °F)	30.285	529	2.05
	R T (R T)	29.036	493	3.08
	75 °C (167 °F)	27.102	470	5.50
	125 °C (257 °F)	26.894	459	8.10
Hybrid GR/GL/GR	−60 °C (−76 °F)	31.460	388	1.43
	−20 °C (−4 °F)	30.725	466	1.87
	R T (R T)	30.305	418	3.26
	75 °C (167 °F)	27.208	393	4.15
	125 °C (257 °F)	25.912	374	6.59
Non-Hybrid GR	−60 °C (−76 °F)	43.820	633	1.76
	−20 °C (−4 °F)	43.715	628	2.01
	R T (R T)	42.559	614	2.13
	75 °C (167 °F)	41.497	586	2.54
	125 °C (257 °F)	40.392	544	3.60

Table 4.2 Material properties for ±45° plain weave composites

Composite	Test Temperature	E_{xy} (GPa)	σ_{max} (MPa)	ε_{max} (%)
Non- Hybrid GL	–60 °C (–76 °F)	10.118	239.50	7.8
	–20 °C (–4 °F)	9.474	219.34	7.7
	R T (R T)	8.667	182.43	7.0
	75 °C (167 °F)	6.288	152.12	7.2
	125 °C (257 °F)	4.940	100.27	6.5
Hybrid GL/GR/GL	–60 °C (–76 °F)	12.117	216.05	5.9
	–20 °C (–4 °F)	10.872	198.62	8.3
	R T (R T)	9.794	178.41	8.0
	75 °C (167 °F)	6.571	135.03	8.0
	125 °C (257 °F)	5.275	95.67	7.8
Hybrid GR/GL/GR	–60 °C (–76 °F)	12.782	240.70	7.0
	–20 °C (–4 °F)	11.177	214.57	8.1
	R T (R T)	9.939	186.38	8.5
	75 °C (167 °F)	6.604	133.44	9.0
	125 °C (257 °F)	5.070	92.89	9.2
Non- Hybrid GR	–60 °C (–76 °F)	13.96	233.41	8.0
	–20 °C (–4 °F)	12.906	213.20	8.7
	R T (R T)	10.739	193.05	9.0
	75 °C (167 °F)	6.765	104.86	10.3
	125 °C (257 °F)	5.481	49.40	11.0

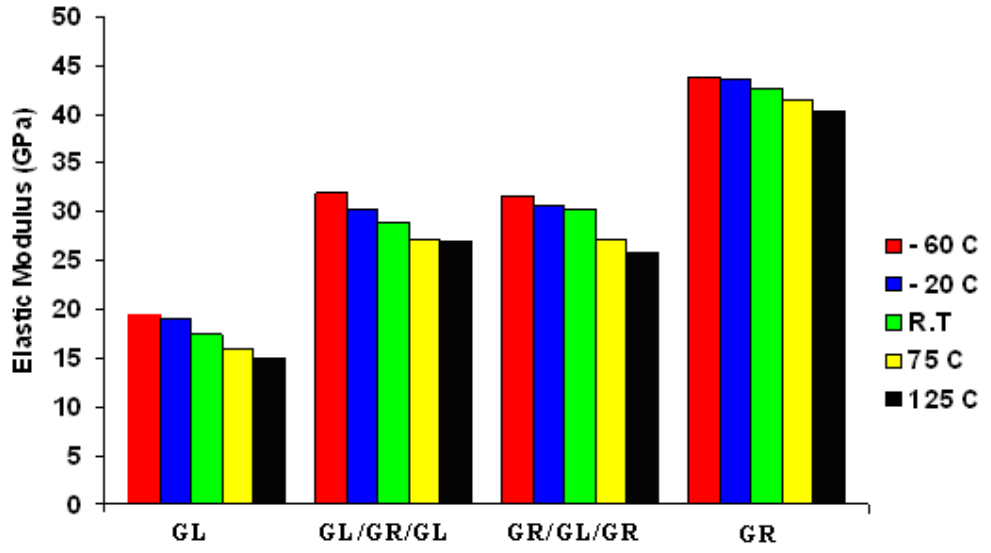

Figure 4.10 Elastic Moduli of all layups at different test temperatures

Figure 4.10 shows the change in elastic moduli as the test temperature changes for all layups. It is a summary of table 4.1 for the variation of elastic moduli.

4.2 Using the Rule of Mixtures to determine the Young's Modulus of Hybrid Composites

Using the rule of mixtures (RoM), the Young's moduli for the hybrid composites were calculated and then compared with those obtained experimentally from the uniaxial tensile tests. The rule of mixtures for fiber reinforced composites can be written as:

$$E_c = V_f E_f + V_m E_m$$

where E_c, E_f, E_m are the Young's moduli of the composite, fiber, and matrix, respectively, and Vf, Vm are the fiber and matrix volume fractions. To obtain the Young's modulus of the hybrid composite, the formula was applied to the laminae,

$$E_c = V_{GR/E} E_{GR/E} + V_{GL/E} E_{GL/E}$$

where $V_{GR/E}$, $V_{GL/E}$ are the volume fractions of the GR and GL laminae of the hybrid GR/GL/GR and GL/GR/GL laminates, and $E_{GR/E}$, $E_{GL/E}$ are the Young's moduli of the GR and GL specimens respectively, obtained from the tensile tests.

Table 4.3 Material properties for 0°/90° composites from experiments and applying RoM

Composite	Test Temperature	Young' Modulus from Experiment	Young's Modulus from RoM
Hybrid GL/GR/GL	–60 °C (–76 °F)	31.985	31.61
	–20 °C (–4 °F)	30.285	31.32
	R T (R T)	29.036	29.80
	75 °C (167 °F)	27.102	28.82
	125 °C (257 °F)	26.894	27.71
Hybrid GR/GL/GR	–60 °C (–76 °F)	31.460	31.61
	–20 °C (–4 °F)	30.725	31.32
	R T (R T)	30.305	29.80
	75 °C (167 °F)	27.208	28.82
	125 °C (257 °F)	25.912	27.71

Table 4.4 Material properties for ±45° composites from experiment and applying RoM

Composite	Test Temperature	Young' Modulus From Experiment	Young' Modulus from RoM
Hybrid GL/GR/GL	–60 °C (–76 °F)	12.117	12.04
	–20 °C (–4 °F)	10.872	11.19
	R T (R T)	9.794	9.70
	75 °C (167 °F)	6.571	6.53
	125 °C (257 °F)	5.275	5.21
Hybrid GR/GL/GR	–60 °C (–76 °F)	12.782	12.04
	–20 °C (–4 °F)	11.177	11.19
	R T (R T)	9.939	9.70
	75 °C (167 °F)	6.604	6.53
	125 °C (257 °F)	5.070	5.21

From Tables 4.3 and 4.4 it can be seen that there is good correlation between experimental results and those obtained using RoM. The RoM provides a better prediction for the Young's modulus of the ±45° laminates than of 0°/90° composite specimens.

4.3 Determination of material properties for numerical simulation

In this research the 3-D dynamic finite element (FE) software LS-DYNA, with Chang-Chang composite damage material model was used to simulate the experimental results of the drop-weight and ballistic tests. In this model, nine constants are required to define the composite material. These constants are: Young's modulus in longitudinal direction (E_1), transverse Young's modulus (E_2), Young's modulus in thickness direction (E_3), shear moduli in three planes (G_{12}, G_{13}, G_{23}) and the generalized Poisson's ratios (v_{12}, v_{13}, v_{23}). E_1 and E_2 were assumed to be same due to the woven structure of the composites and

were obtained from tensile tests. The out-of-plane Young's modulus (E_3) at R.T was computed using the formula derived for the transverse modulus: $E_3 = \frac{E_m E_{f,t}}{v_f E_m + (1 - v_f) E_{f,t}}$

Here V_f is the fiber volume fraction and E_m and $E_{f,t}$ are the Young's moduli of the matrix and the fiber along the transverse directions, respectively. In this study, the following values were used: V_f = 55%, E_m (SC-79) = 3.06 GPa [95], $E_{f,t}$ (S2-glass) = 85 GPa [96], $E_{f,t}$ (IM7-graphite) = 12 GPa [97] which resulted in: E_3 (S2-glass) = 6.5 GPa and E_3 (IM7-graphite) = 5.2 GPa.

Since equipment was not available to conduct compression tests at various temperatures, the out-of-plane Young's modulus (E_3) was obtained as follow: Strain gages were placed on the GL and GR specimens in the thickness direction and the corresponding mechanical strain was recorded during unidirectional tensile testing at various temperatures, i.e. ε(T) and ε(R.T)

Here, ε(T) = strain as a function of test temperature and ε(R.T) is the strain at room temperature. For loading in the fill direction (longitudinal direction), where $\sigma = \sigma_1$, we define $f(t) = \frac{E_1(T)}{E_1(R.T)}$

where $E_1(T)$ and $E_1(R.T)$ are the Young's moduli in the longitudinal direction at temperature (T) and room temperature (R.T) respectively.

We can assume that the same strain relationship holds in the 3-direction,

Therefore, $\varepsilon_3(T) = \varepsilon_3(R.T) f(T)$ (1)

Here $f(t)$ is obtained by plotting $\frac{\varepsilon_1(T)}{\varepsilon_1(R.T)}$ vs. temperature.

Using eq. (1), and the relations $\varepsilon_3(T) = \frac{\sigma_3}{E_3(T)}$ and $\varepsilon_3(R.T) = \frac{\sigma_3}{E_3(R.T)}$ we obtain

$$E_3(T) = \frac{E_3(R.T)}{f(T)} \tag{2}$$

where $E_3(T)$ and $E_3(R.T)$ are the Young's moduli in the thickness direction at temperature (T) and room temperature (R.T) respectively.

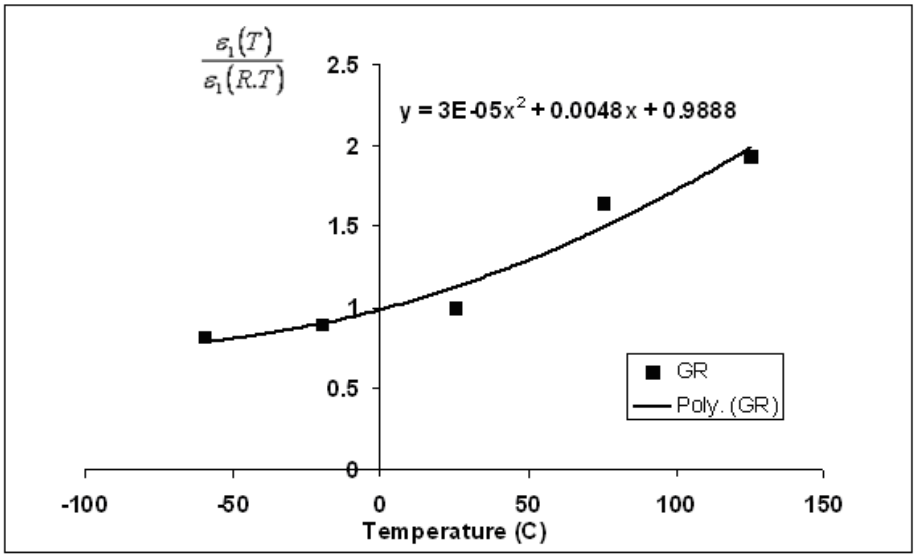

(a) $f(T) = 3*10^{-5}(T)^2 + 0.0048(T) + 0.9888$

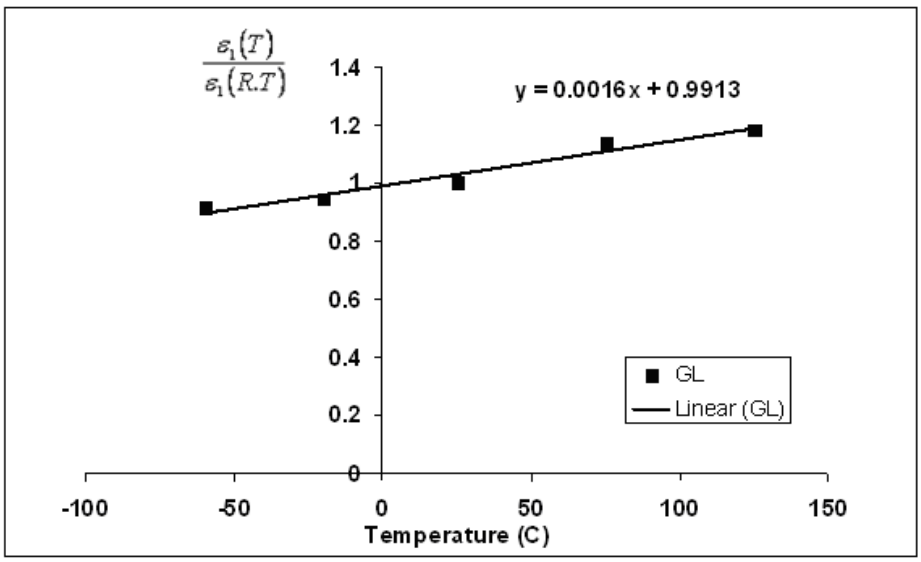

(b) $f(T) = 0.0016(T) + 0.9913$

Figure 4.11 Ratio of strain in thickness direction vs. temperature to obtain *f (T)*

Since *E3 (R.T)* is measured, then using eq. (2), one can estimate E_3 *(T)*.

Following the ASTM Standard D-3518, the corresponding shear stress, shear strain and in-plane shear modulus were calculated using the relations: $\tau_{12} = \frac{\sigma_x}{2}$, $\gamma_{12} = \varepsilon_x - \varepsilon_y$, and $G_{12} = \frac{E_x}{2(1+\nu_{xy})}$, respectively. Here $\sigma_x = \left(\frac{P}{A}\right)$ is the axial stress, ε_x and ε_y are the axial and transverse strains, respectively ($\varepsilon_y < 0$) and $\nu_{xy} = -\frac{\varepsilon_y}{\varepsilon_x}$ is the associated Poisson's ratio obtained in the ASTM D-3518 ±45° laminate tensile test while E_x is the initial slope of the stress-strain curve obtained from that test. As verification G_{12} was also calculated by taking the initial slope of the τ_{12} vs. γ_{12} curve, where the results closely match those obtained using the ASTM D-3518 standard. The shear moduli in the remaining two planes were obtained through the relations $G_{13} = G_{23} = \frac{E_z}{2(1+\nu_{xz})}$

Figs. 4.12 and 4.13 depict the temperature-dependent shear stress-shear strain curves of the GL and GR composites, respectively, from high to low temperatures. The slopes of these curves give the shear moduli of the material. The nonlinear behavior of the curves is due to damage as well as temperature effect.

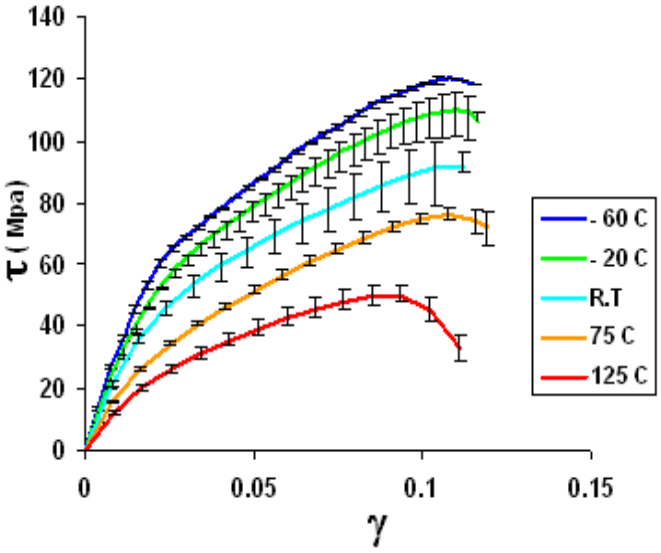

Figure 4.12 In-plane shear stress-strain curves with their slopes representing shear moduli for GL at 125 °C, 75 °C, R.T, –20 °C and –60 °C

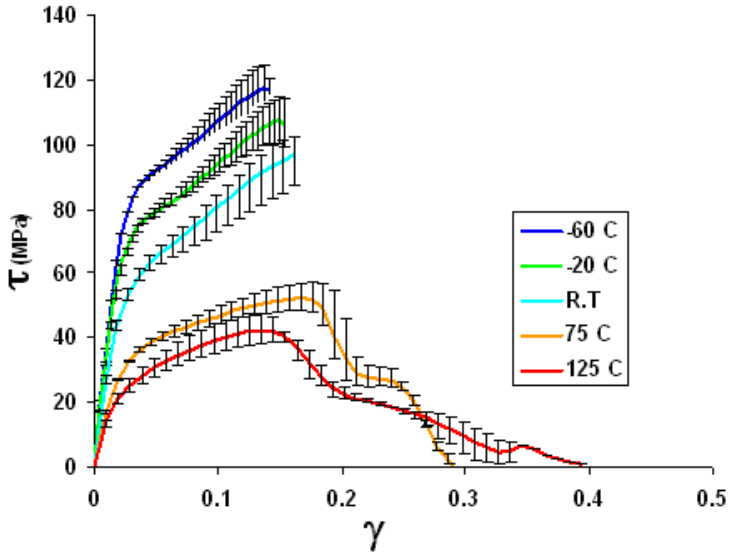

Figure 4.13 In-plane shear stress-strain curves with their slopes representing shear moduli for GR at 125 °C, 75 °C, R.T, –20 °C and –60 °C

The Poisson's ratios ν_{12} and $\nu_{13}=\nu_{23}$ were obtained from three strain-gages mounted on woven glass (Fig. 4.14.a) and woven graphite (Fig. 4.14.b) composite specimens for the tensile tests.

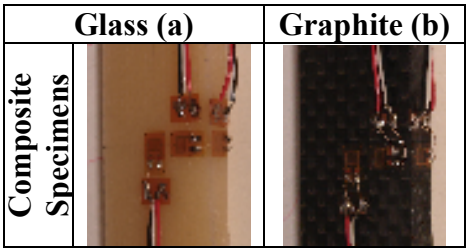

Figure 4.14 Location of strain gages to measure the Poisson's ratio of woven glass and woven graphite toughened epoxy composites

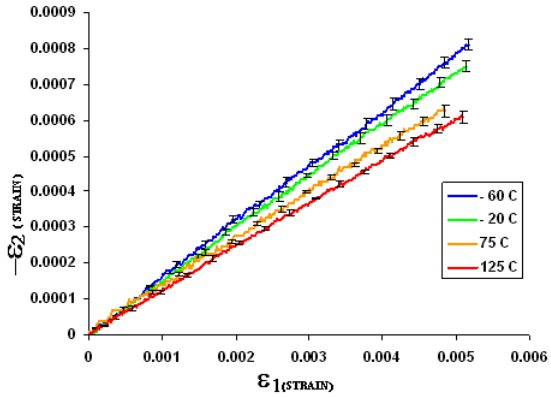

Figure 4.15 Poisson ratio ν_{12} of woven GL

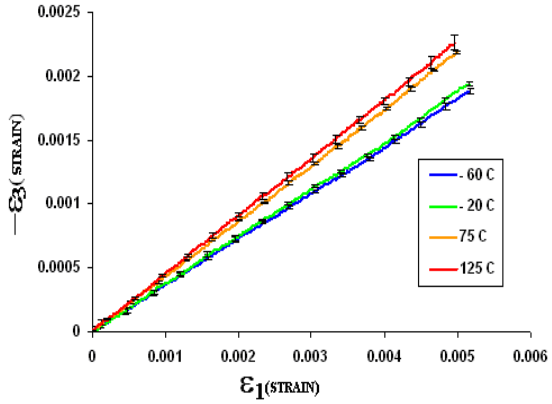

Figure 4.16 Poisson ratio ν_{13} of woven GL

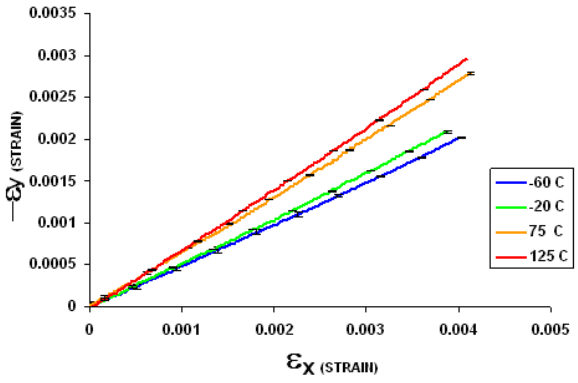

Figure 4.17 Poisson ratio ν_{XY} of woven GL

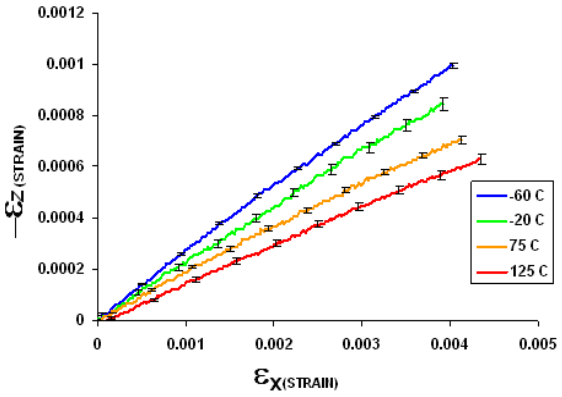

Figure 4.18 Poisson ratio ν_{XZ} of woven GL

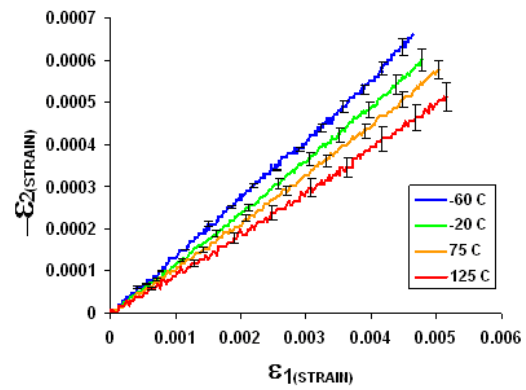

Figure 4.19 Poisson ratio ν_{12} of woven GR

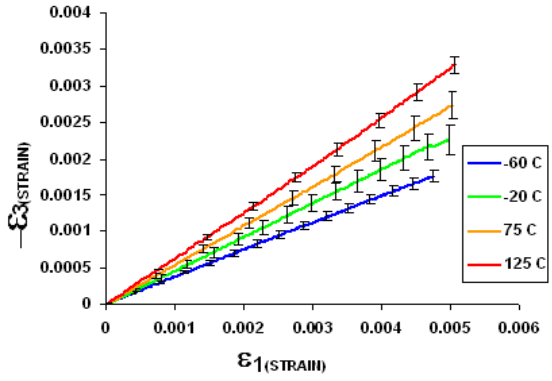

Figure 4.20 Poisson ratio ν_{13} of woven GR

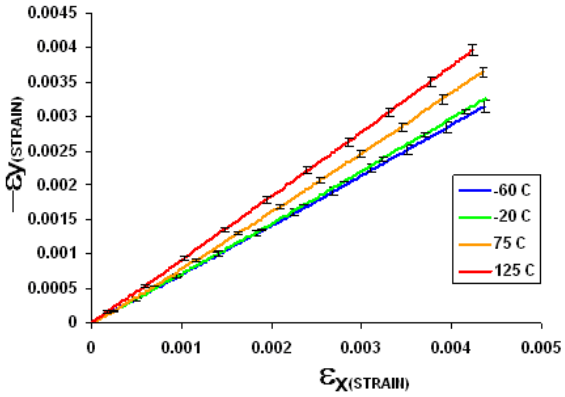

Figure 4.21 Poisson ratio ν_{XY} of woven GR

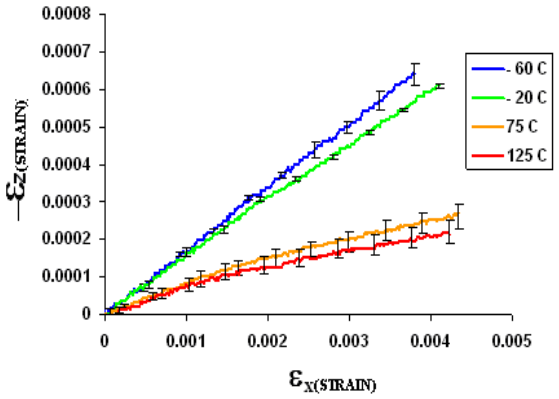

Figure 4.22 Poisson ratio ν_{XZ} of woven GR

Figures 4.15 to 4.18 show the ε_1 vs. ε_2, ε_1 vs.ε_3, ε_x vs. ε_y and ε_x vs. ε_z curves respectively, for GL specimen at various temperatures from which $\nu_{12}, \nu_{13} = \nu_{23}$, ν_{XY} and $\nu_{XZ} = \nu_{YX}$ of GL are determined. Figures 4.19 to 4.22 shows the ε_1 vs. ε_2, ε_1 vs.ε_3, ε_x vs. ε_y and ε_x vs. ε_z curves respectively, for GR specimens at various temperatures from which $\nu_{12}, \nu_{13} = \nu_{23}$, ν_{XY} and $\nu_{XZ} = \nu_{YX}$ of GR are determined. Table 4.5 below shows the Poisson's ratios obtained from the above graphs for the GL and GR specimens respectively.

Table 4.5 Poisson's ratio of woven glass and graphite fibers-reinforced toughened epoxy

Composite	Test Temperature	ν_{12}	$\nu_{13}=\nu_{23}$	ν_{xy}	$\nu_{xz}=\nu_{yz}$
Non- Hybrid Glass	–60 °C (–76 °F)	0.152	0.370	0.487	0.246
	–20 °C (–4 °F)	0.145	0.361	0.515	0.214
	R T (R T)	0.13	0.41	0.578	0.184
	75 °C (167 °F)	0.128	0.436	0.656	0.153
	125 °C (257 °F)	0.121	0.453	0.702	0.147
Non- Hybrid Graphite	–60 °C (–76 °F)	0.140	0.382	0.726	0.170
	–20 °C (–4 °F)	0.129	0.462	0.754	0.162
	R T (R T)	0.121	0.427	0.794	0.102
	75 °C (167 °F)	0.116	0.627	0.846	0.085
	125 °C (257 °F)	0.099	0.649	0.921	0.081

As seen in table 4.5, the Poisson's ratio appears to be a function of temperature. As the temperature increases the Poisson's ratios ν_{12} and $\nu_{xz}= \nu_{yz}$ decrease for both GR and GL specimens while the Poisson's ratios $\nu_{13}=\nu_{23}$ and $\nu_{xz} = \nu_{yz}$ increase. The Poisson's ratio ν_{13} tends to increase with an increase in temperature.

Table 4.6 summarizes all the material properties that will be used in the finite element simulation at each test temperature.

Table 4.6 Mechanical properties of woven GL and GR composites

		$E_1=E_2$ (GPa)	E_3 (GPa)	G_{12} (GPa)	$G_{13}=G_{23}$ (GPa)	ν_{12}	$\nu_{13}=\nu_{23}$	ρ (kg/m^3)
Glass	–60 °C	19.39	7.26	2.98	2.65	0.152	0.370	1766
	–20 °C	18.92	6.78	2.78	2.49	0.145	0.361	1761
	R .T	17.04	6.50	2.74	2.30	0.130	0.410	1755
	75 °C	16.13	5.85	1.89	2.03	0.128	0.436	1750
	125 °C	15.03	5.46	1.44	1.87	0.121	0.453	1744
Graphite	–60 °C	43.82	6.43	3.97	2.32	0.140	0.382	1392
	–20 °C	43.71	5.75	3.93	1.96	0.129	0.462	1387
	R .T	42.55	5.20	3.08	1.81	0.121	0.427	1381
	75 °C	41.49	3.43	1.99	1.05	0.116	0.627	1375
	125 °C	40.39	2.53	1.67	0.76	0.099	0.649	1370

4.4 Conclusion from tensile test results

a) As the test temperature increases, the elastic modulus of the material tends to decrease. It can also be seen that the modulus of toughness (This may be calculated as the entire area under the stress-strain curve from the origin to rupture.) of the material increases with an increase in temperature.

b) As the test temperature increases, the Poisson's ratio ν_{12}, decreases where as $\nu_{13}=\nu_{23}$ increases.

c) The over-all mechanical properties of hybrid composites were between those of GL and GR composites.

d) The rule of mixture can be used successfully to predict the elastic and shear moduli of hybrid composites.

Chapter 5

Measurement of Thermal Expansion Coefficient Using Strain Gages

In this study it was important to obtain the thermal expansion coefficients of the composites GL and GR. The thermal expansion coefficients are used in determining the thermal stresses developed in the specimen while soaking them to the desired test temperature before testing begins. While analytical methods are available to determine the thermal expansion coefficients [99], it was more convenient to determine the expansion coefficients experimentally using strain gages. The guidelines used to measure the expansion coefficients were closely governed by those given in [100].

5.1 Formulation of equations used in the experiment

When resistance strain gages are installed on any stress-free test specimen and the temperature is changed, the output of the gage changes correspondingly. This effect is referred to as thermal output. It is caused by a combination of two factors. First, the resistivity of the grid material is changed as temperature changes and second, resistance occurs because the thermal expansion coefficient of the grid alloy is usually different from the test material to which it is bonded. Thus, with temperature change, the grid is mechanically strained by an amount equal to the difference in expansion coefficients. The net resistance change can be expressed as the sum of the resistivity and of the differential expansion effects as:

$$\frac{\Delta R}{R} = \left[\beta_G + (\alpha_s - \alpha_G)F_G\right]\Delta T \qquad (1)$$

where $\frac{\Delta R}{R}$ = unit resistance change in grid material

β_G = thermal coefficient of resistivity of grid material

$\alpha_s - \alpha_G$ = difference between coefficients of thermal expansion of specimen and grid respectively

F_G = gage factor of the strain gage

ΔT = temperature change from initial reference temperature

The indicated strain due to a resistance change in the gage is given as:

$$\varepsilon_i = \frac{\Delta R / R}{F_I},$$

where F_I is the instrument gage setting

The thermal output in strain units can then be expressed as follow,

$$\varepsilon_{T/O(G/S)} = \frac{[\beta_G + (\alpha_s - \alpha_G)F_G]\Delta T}{F_I}$$

where $\varepsilon_{T/O(G/S)}$ is the thermal output of grid alloy G on specimen S.

Usually, the instrument gage factor is set equal to that of the strain gage, so F_I=F_G and

$$\varepsilon_{T/O(G/S)} = \left[\frac{\beta_G}{F_G} + (\alpha_s - \alpha_G)\right]\Delta T \qquad (2)$$

It was shown experimentally [100] that the difference in thermal output for two different materials is due only to the difference in thermal expansion properties of the two materials. Following this idea, the thermal expansion coefficient of an unknown material can be obtained as follows:

Rewriting equation (2) twice, once with the gage installed on a material of unknown expansion coefficients α_s and again for the same type of gage installed on a standard reference material with known expansion coefficient α_R we obtain:

$$\varepsilon_{T/O(G/S)} = \left[\frac{\beta_G}{F_G} + (\alpha_s - \alpha_G)\right]\Delta T \qquad (3a)$$

$$\varepsilon_{T/O(G/R)} = \left[\frac{\beta_G}{F_G} + (\alpha_R - \alpha_G)\right]\Delta T \quad (3b)$$

Subtracting equation (3b) from (3a), and rearranging, we get:

$$\alpha_S - \alpha_R = \frac{(\varepsilon_{T/O(G/S)} - \varepsilon_{T/O(G/R)})}{\Delta T} \quad (4)$$

Thus, the difference in expansion coefficients, referred to a particular temperature range, is equal to the unit difference in thermal output for the same change in temperature.

5.2 Procedure used to obtain the thermal expansion coefficient for Plain-Weave GL and GR composite material

(1) Identical strain gages (CEA-13-062UW-350) were mounted on a reference material with known thermal expansion (Aluminum 6061-T6 with α_R = 23.6 μm/m-°C or 13.1 μin/in-°F) and on the composite specimen.

(2) Both specimens were placed in an environmental chamber where the temperature was raised to a specific value and the specimens were allowed to soak for 30 minutes. The strain gages were attached to a strain indicator and recorder. At the end of thirty minutes, the strain output was read and recorded.

(3) Tests were done at 45 ºC, 55 ºC, 65 ºC, 75 ºC and 85 ºC taking into account the change in gage factor of the strain gage with temperature [100].

(4) Strain outputs were then substituted into equation (4) to calculate the thermal expansion coefficients for the composite GL and GR specimens.

(5) Finally, the average of the thermal expansion coefficients was calculated using the results from various temperatures (since all values were close to each other).

Table 5.1 Thermal expansion coefficients of GL and GR composites

Composite	Test Temperature	$\alpha_1 = \alpha_2$ (°C)$^{-1}$	α_3 (°C)$^{-1}$
Non- Hybrid Glass	45 °C (113 °F)	6.8×10^{-6}	8.01×10^{-5}
	55 °C (131 °F)	7.2×10^{-6}	8.21×10^{-5}
	65 °C (149 °F)	7.1×10^{-6}	8.18×10^{-5}
	75 °C (167 °F)	7.3×10^{-6}	8.25×10^{-5}
	85 °C (185 °F)	7.4×10^{-6}	8.26×10^{-5}
Average α		**7.1×10^{-6}**	**8.18×10^{-5}**
Non- Hybrid Graphite	45 °C (113 °F)	3.14×10^{-6}	7.73×10^{-5}
	55 °C (131 °F)	3.33×10^{-6}	7.64×10^{-5}
	65 °C (149 °F)	3.33×10^{-6}	7.72×10^{-5}
	75 °C (167 °F)	3.56×10^{-6}	7.81×10^{-5}
	85 °C (185 °F)	3.59×10^{-6}	7.82×10^{-5}
Average α		**3.38×10^{-6}**	**7.74×10^{-5}**

5.3 Conclusion

From Table 5.1 it can be seen that as the temperature increases the thermal expansion coefficients tends to increase but the increase is very small. Since our study is only focused on a temperature range of –60 °C to 125 °C, it will be assumed that the change in thermal expansion coefficient over this temperature range is negligible; hence the average thermal expansion coefficients will be used.

Chapter 6

Low velocity impact tests on woven composites

In this thesis, low velocity (drop weight) impact studies were carried out at a fixed energy level and velocity but with a variation in temperature. The low velocity impact tests were carried out on non hybrid GL and GR specimens and also hybrid GL/GR/GL and GR/GL/GR specimens. All specimens had dimensions of 101.6mm × 101.6mm × 6.35mm. Tests were carried out using an Instron-Dynatup 8520 instrumented drop-weight impact tester. Figure 6.1 shows the schematics of the experimental set-up for the low-velocity impact tests.

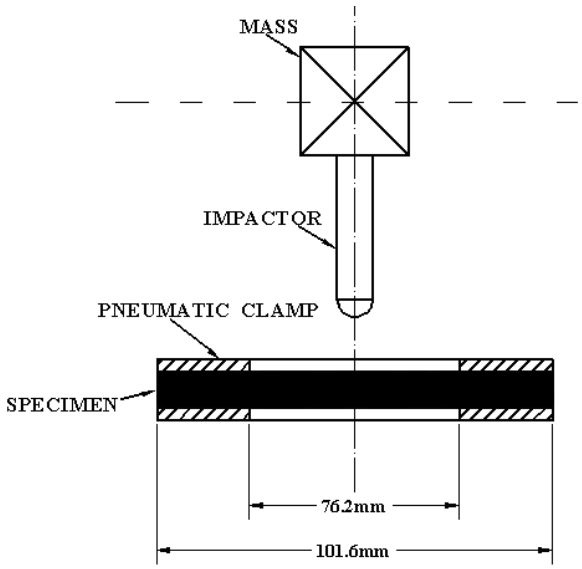

Figure 6.1 Schematic of the drop-weight impact test set-up.

6.1 Effect of temperature on the low-velocity impact response of composites

During all the impact tests, a 5.1 kg weight was attached to the steel impactor with a hemispherical tup of 16 mm diameter for a total of 6.15 kg. The mass was placed at a height of 49.7 cm above the specimen and released to free fall on the specimen.

The free fall due to gravity resulted in an impact velocity of 3.12 m/s and an impact energy of 30J.

Two strain gages were mounted on the impact side of each specimen. They were mounted at a distance of 25.4 mm from the center of the specimen. These strain gages measured the dynamic strain resulting from the impactor striking the specimen. From SG-1 the radial strain was obtained while from SG-2 the hoop strain was obtained. Figure 6.2 shows a schematic of the orientation of the strain gages and their location on the specimen. Each specimen was clamped circumferentially along a diameter of 76.2 mm in a pneumatic-actuated clamping fixture. Each of the four layups of composite specimens was tested at −60°C, −20°C, R.T, 75°C, 125°C. To achieve these temperatures, the specimens were placed in an environmental chamber attached to the instrumented drop-weight impact tester and allowed to soak to the desired temperature for thirty (30) minutes before testing. During this soaking period, the specimens were not clamped but allowed to expand and shrink under the desired high and low test temperatures respectively.

During the test, the time histories of impact force, velocity, deflection, energy and the ensuing dynamic strains were recorded. For post-mortem observation, optical pictures of the front and back surface of the damaged composites were first taken. The impacted specimens were then scanned using an immersion ultrasonic system. The through transmission technique using a pair of 5 MHz focused and flat transducers was employed to detect the internal delamination in the damaged composite panel. Finally, the specimens were machined carefully into two halves along a central line to reveal the internal damage.

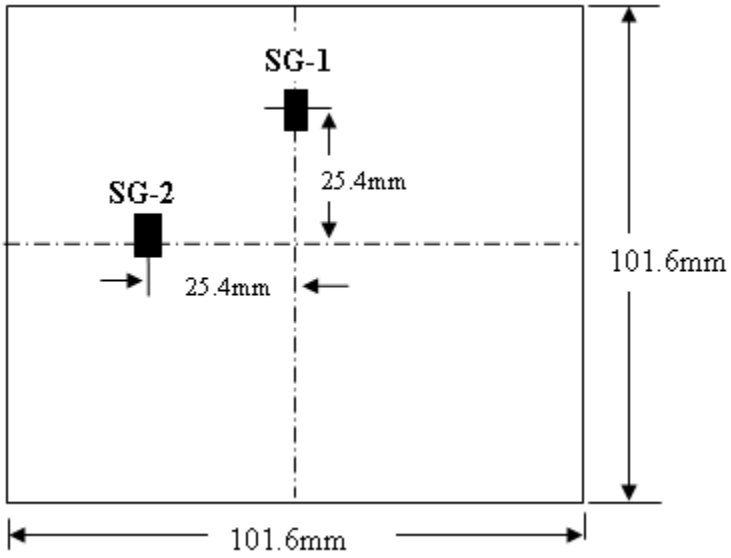

Figure 6.2 The location of strain-gages on composite specimen to be drop-weight impact tested

(a) Experimental results

Reviewing the literature, it was found that many different factors tend to affect the damage mechanisms and damage patterns in composite materials. Some of these factors include lay-up configuration, laminate thickness, impactor size and shape, constituent properties, temperature, impact velocity and energy, etc. To the authors' knowledge, no studies have been carried out on the effect of temperature on the impact response of thick section non hybrid GL, GR or hybrid GL/GR/GL and GR/GL/GR composites. Visual inspection showed that the GL specimens were the most resistant to impact damage.

As shown in Figure 6.3, for the highest test temperature, i.e. 125 °C, horizontal and vertical front surface cracks were created in GL specimens. This is often referred to as micro-buckling, where the fibers on the top surface buckle due to compression on the upper surface. As the temperature decreases, it can be seen that the severity of micro

buckling decreases i.e. the length of the front surface crack decreases with decreasing temperature. For all the test temperatures it can be seen that no back surface splitting occurred. From the C-scan images, it can also be seen that the damaged area slightly decreases with a decreasing test temperature.

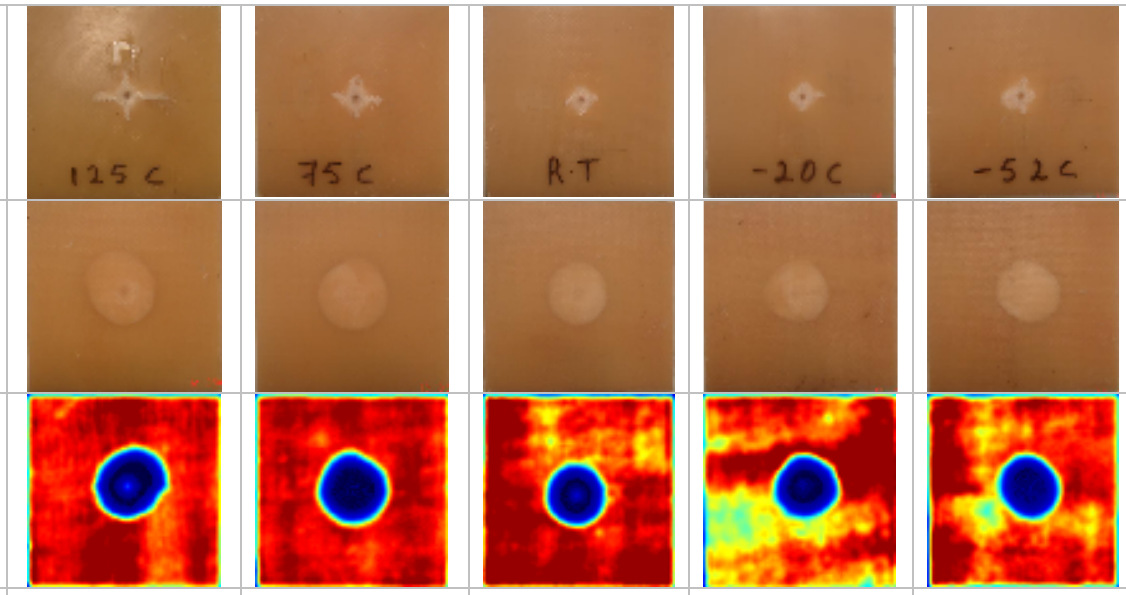

Figure 6.3 Optical fractographs and C-scan of non-hybrid GL composite specimens after a 30J energy level drop-weight impact at various temperatures

Impact tests were conducted on two groups of hybrid composites. The first, called GL/GR/GL has two glass layers as the outer skins and a graphite layer as the inner core; whereas the second called GR/GL/GR consists of graphite layers as the face sheets and a glass layer as the core material. As shown in Fig.6.4, horizontal and vertical front surface cracks tend to decrease as the test temperature decreases from125 °C to –20 °C and then changes direction and start to increase as the test temperatures keeps decreasing. Upon carefully examination of the specimens, it was seen that there was no back splitting on any of the samples after testing.

In Fig. 6.5, drop-weight tests conducted on the second hybrid composite group, i.e. the GR/GL/GR specimens, showed horizontal and vertical front surface cracks for all specimens tested. The size of cracks decreased with decreasing temperature from 125 °C

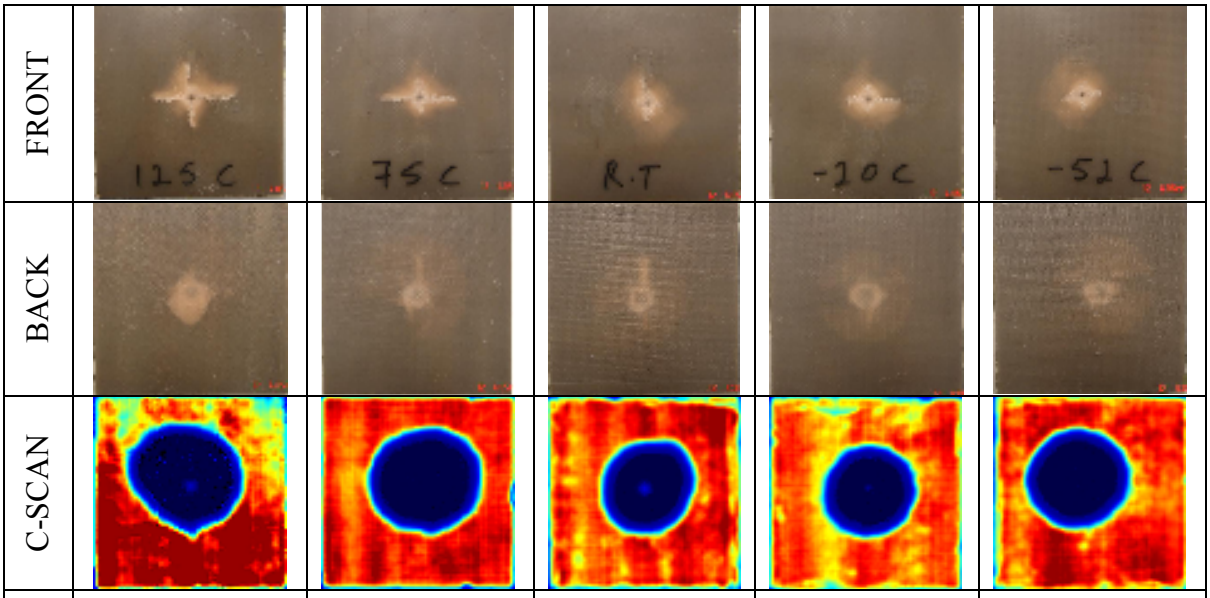

Figure 6.4 Optical fractographs and C-scan of hybrid GL/GR/GL composite specimens after a 30J energy level drop-weight impact at various temperatures

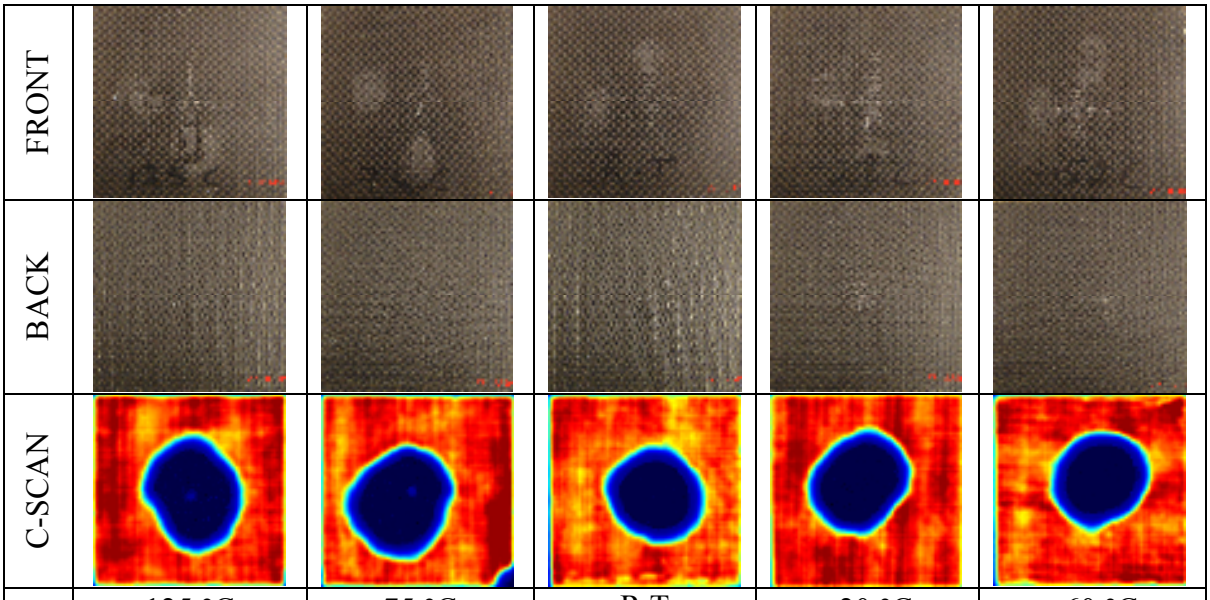

Figure 6.5 Optical fractographs and C-scan of hybrid GR/GL/GR composite specimens after a 30J energy level drop-weight impact at various temperatures

to R.T, but it was difficult to determine a proper trend of horizontal or vertical front surface cracks at the cryogenic temperatures i.e. –20°C and –60°C. Back surface splitting was not severe but can be seen only for R.T, –20°C and –60°C. Although drop-weight impact tests on both groups of hybrid composites were performed under similar conditions. The difference in stacking sequence results in some differences in the size of the generated horizontal and vertical front surface cracks as well as the severity of penetration and back surface splitting. Finally, as shown in Fig. 6.6, the GR non-hybrid composite was tested. At all test temperatures there was back surface splitting. When the horizontal and vertical front surface cracks were studied after impact, it was observed that the size of the cracks was very similar to those observed for GR/GL/GR hybrid composites.

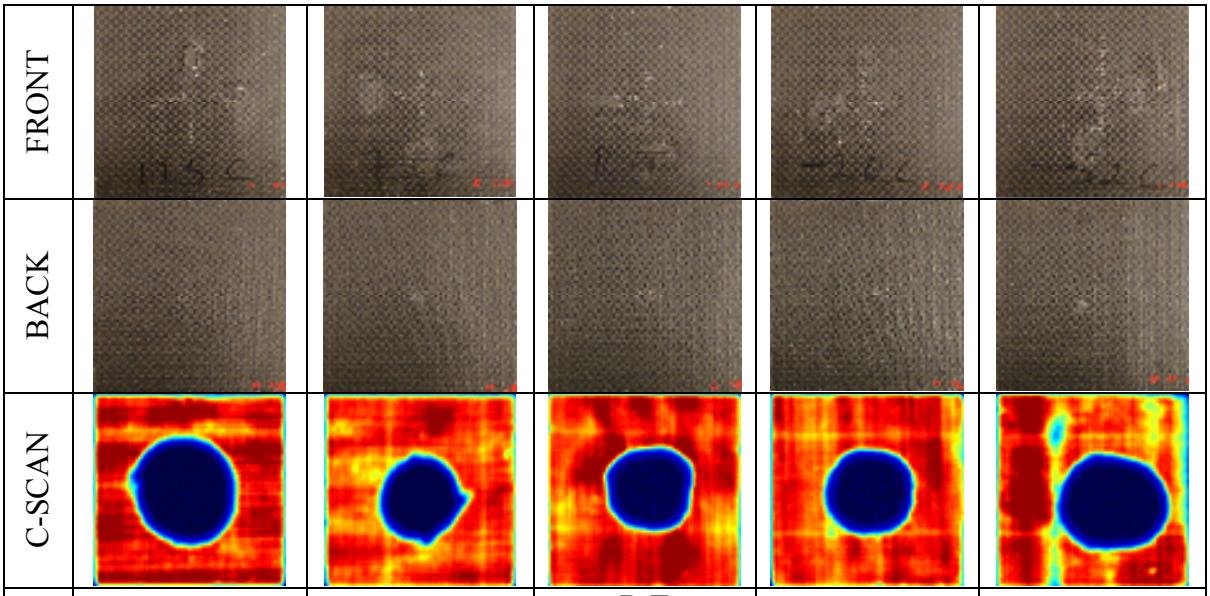

Figure 6.6 Optical fractographs and C-scan of non-hybrid GR composite specimens after a 30J energy level drop-weight impact at various temperatures

Due to the color of the GR specimen the fractographs couldn't properly capture the front surface cracks clearly; however they tend to decrease with a decrease in temperature from 125 °C to R.T and start increasing again from R.T to −60 °C. From all the images it can be seen that for the hybrid specimens the C-scan reveals the damage to be more asymmetric and larger while that of the non hybrids is smaller and more symmetric.

(b) Impact force

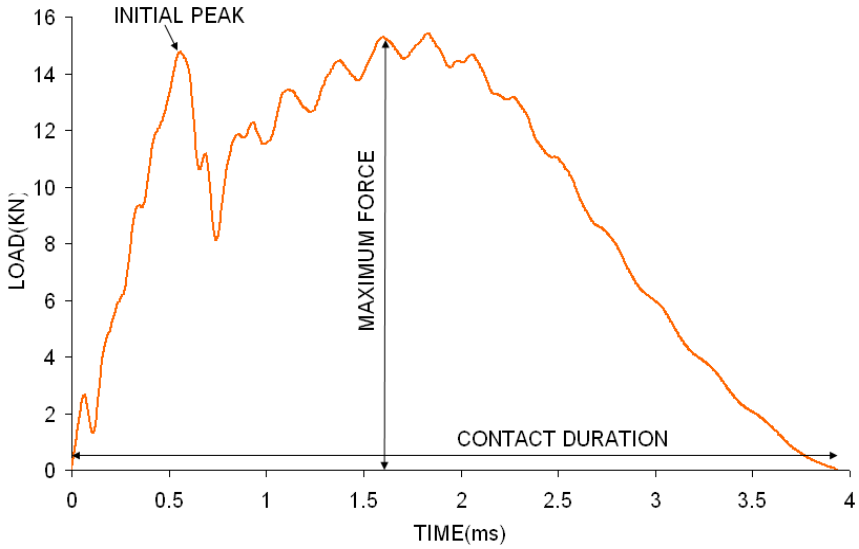

Figure 6.7 Representative force-time history curve from drop-weight impact test

The Dynatup 930-I data acquisition system measures only the initial velocity of the impactor and force *vs*. time directly. The remaining parameters, such as absorbed energy, velocity of impactor and deflection, are calculated using equations of motion. Important damage mechanisms can be studied by understanding the force time history curve from an impact test. Fig 6.7 shows a representative force-time history curve from a drop weight impact test. The initial peak on the curve represents the initiation of delamination.

If the impact force is less than the initial peak value, then there will be no damage or delamination of the material and the response will be elastic, i.e. the force time history curve will almost be sinusoidal. In the event that the maximum force of impact is greater than the load bearing capabilities of the material, there will be fiber shear-out. In other words, the commencement of fiber shear-out indicates that the load bearing capacity of the laminate is reached, hence little resistance will be provided against higher impact energies.

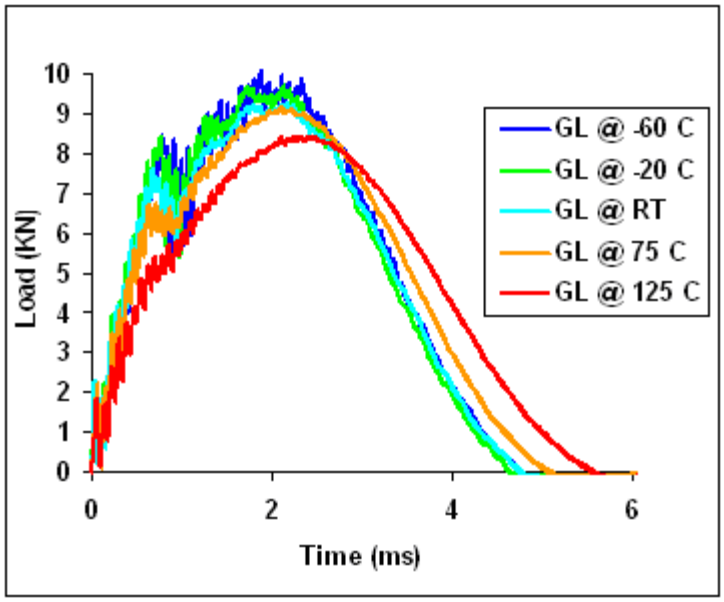

Figure 6.8 Time histories of the impact forces of non-hybrid GL composites at –60°C, –20°C, R.T, 75°C, 125°C.

In Figure 6.8 it can be seen that as temperature decreases, the initial peak of the time histories of impact force increases. This indicates that the force required to create a delamination increases with a decrease in temperature. The time it takes to reach this initial peak also increases with a reduction in test temperature. Also the maximum force increases as temperature decreases. Since the impact force is the force measured by the impactor, it is the resistance the impactor experiences when it is in contact with the

specimen. Therefore, at low temperatures, the GL specimen is more resistant to damage and is therefore tougher.

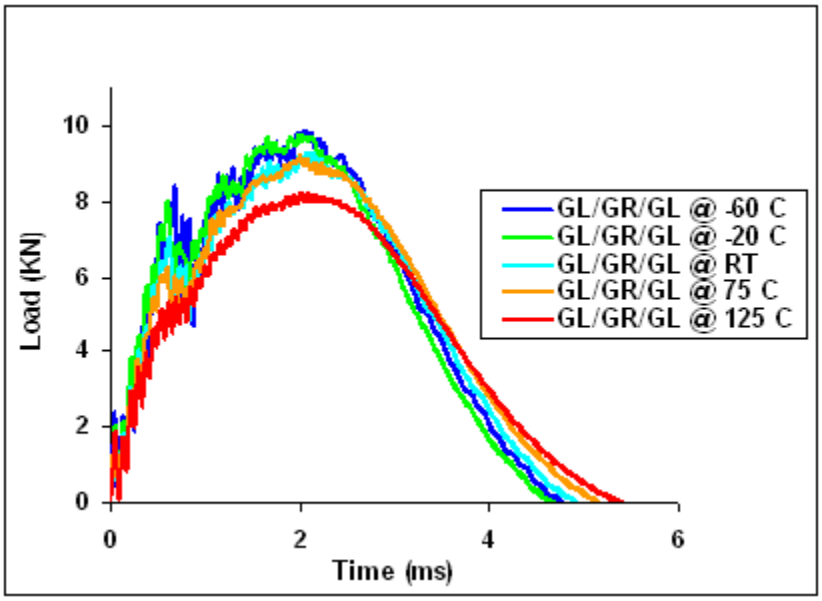

Figure 6.9 Impact force-time histories of hybrid GL/GR/GL composites at –60°C, –20°C, R.T, 75°C, 125°C.

In Figure 6.9 a similar trend of response is found to that as GL. One may notice that after the initial peak, the drop in force is quite significant at low temperatures and as the temperature increases the drop becomes negligible. Figure 6.10 shows the impact force time history of the second hybrid composite specimen, i.e. GR/GL/GR. For both hybrids, it can be seen that although the maximum force is almost the same at R.T and 75°C, their initial peaks are more distinct. At –60°C, –20°C, R.T for hybrid GR/GL/GR, not only is there a drop after the initial peak but a few other drops along the impact force history curve. It was realized that these were the specimens that had back splitting after impact.

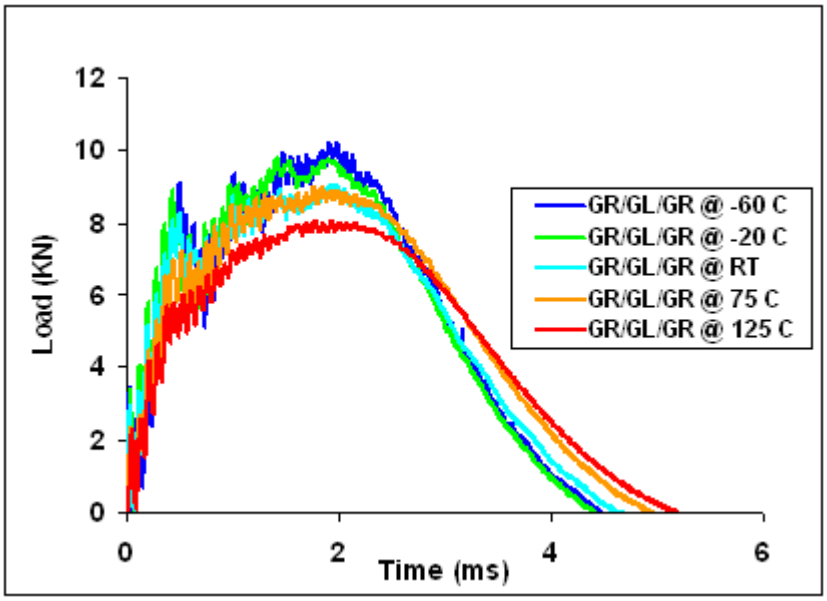

Figure 6.10 Impact force-time histories of hybrid GR/GL/GR composites at –60°C, –20°C, R.T, 75°C, 125°C.

During all tests conducted on the non-hybrid GR specimens, a sudden drops right after the linear increase was observed (Fig. 6.11).

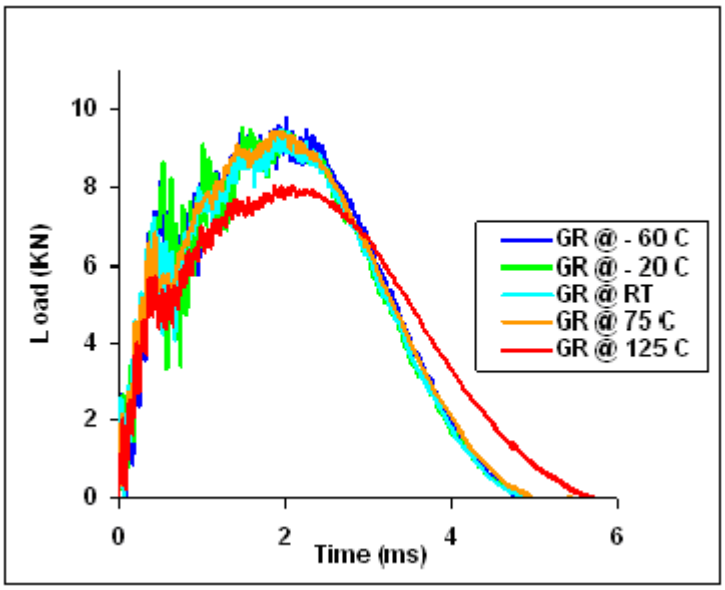

Figure 6.11 Time histories of the impact forces of non-hybrid GR composites at –60°C, –20°C, R.T, 75°C, 125°C.

In these tests, the observed increase in force oscillation after the initial drop was similar to those observed during the tests at –60°C, –20°C, R.T for hybrid GR/GL/GR. On inspection, it was seen that all the specimens had back splitting. Drops in the force-time histories happened earlier than those for the other three types of composite tested. The maximum force values were also low compared to those observed during the impact of the other three composite types. Once the force-time histories of the drop impact tests and optical pictures of the impacted composites were examined, it was concluded that impact tests which created back surface splitting, exhibited sudden drops at their force-time histories (making a simple comparison among the force time history for the four types of composite at 125 °C) with a combination of oscillation of the force-time curve. It was also evident that the only specimens with back splitting were those with GR on the outside of the sandwich or the GR specimens. It can also be concluded that the impact force is mostly affected by tests conducted at 125 °C.

For comparison, the maximum forces created during impact tests are plotted in Fig. 6.12. Although the forces are quite close to each other, it can be said that while GL sustained the highest force, GR composite resisted the lowest. Hybrid composites have a maximum force that is a little higher than that of GR composite while the maximum force produced by these composites was a little less than that of the GL composite. The maximum force is seen to increase with a decrease in test temperature. This is due to the fact that at high temperature, the material is softer and hence more compliant to the advancing impactor.

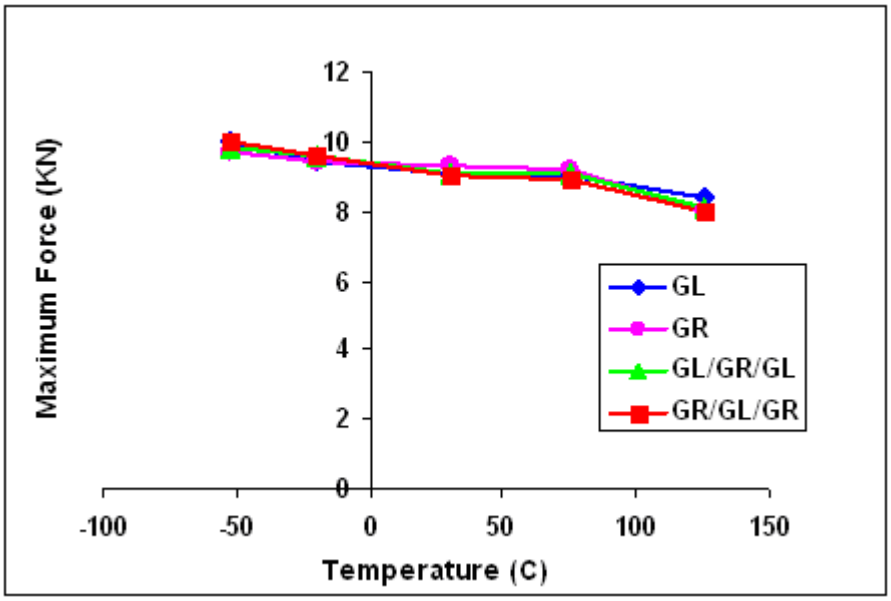

Figure 6.12 Comparison of the variation of maximum impact forces with temperature.

Figure 6.13 shows the initial peak force plotted against test temperature. The initial peak value of the impact force is a representation of the starting point of the delamination or damage in composite material. Drop-weight impact tests conducted on the hybrid GR/GL/GR specimens show the highest initial peak force compared to the other three composites, followed by GR, GL and then GL/GR/GL with the smallest initial peak. It can also be seen that the initial peak force tends to decrease for all four types of composites with an increase in temperature.

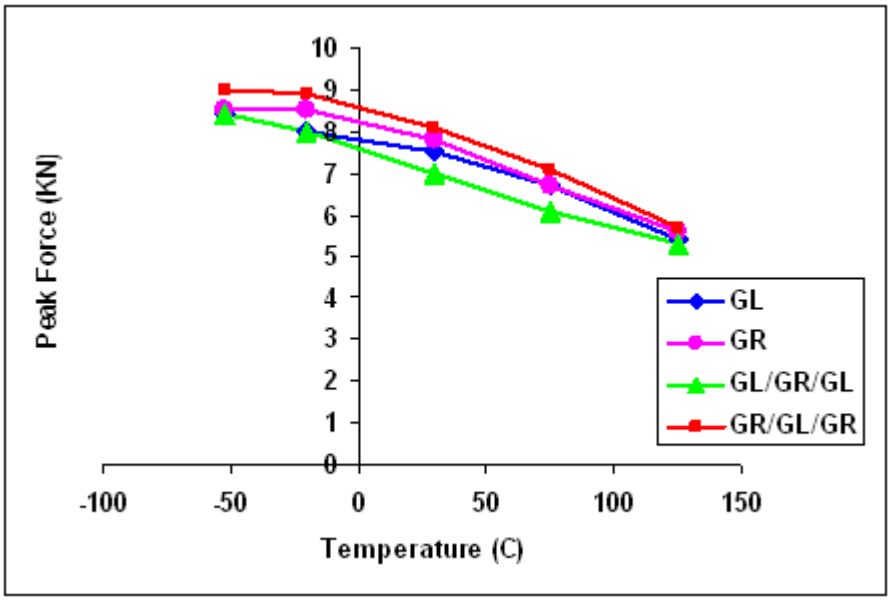

Figure 6.13 Comparison of the variation of initial peak forces for composites impacted at various test temperatures

(c) Contact duration

Fig.6.14 shows the comparison of contact durations against temperature for the four different layups of composite specimens. It can be seen that the contact duration tend to increase slightly with an increase in temperature for all layups. As the temperature increases, the specimens becomes more ductile, hence, there is more deformation of the impacted specimen. In the event that the impactor penetrates the composite, contact duration is mainly governed by the friction between impactor and composite. During penetration, fibers and matrix materials are either pushed to the sides or pushed ahead at the tip of the impactor. After damaging the composite, not much resistance comes from composite.

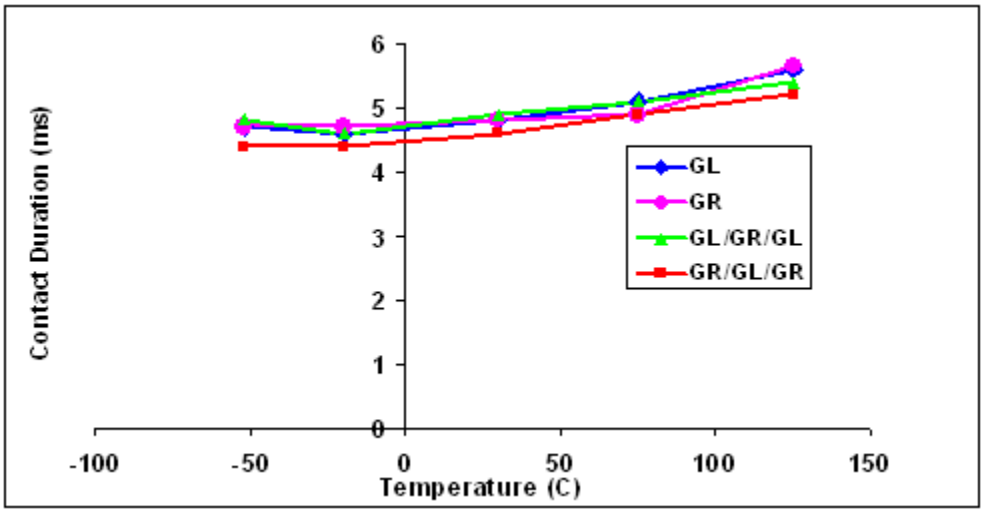

Figure 6.14 Comparison of contact durations for composites impacted at various temperatures

However impactor still cannot easily moves forward due to the friction forces. Energy spent for friction in unit time can be less than energy spent for damaging the composite and that may cause some increase in contact duration. GR/GL/GR has the shortest contact time while GR has the longest contact time, in four out of the five test temperatures. Each layup of composite material is consistent in terms of contact time with respect to temperature, but inconsistent in contact time with respect to the others. One possible explanation is that during manufacturing of the composite specimens, residual stresses may have developed in the material. During soaking of specimen for testing, this stress becomes larger or smaller, therefore the total residual stress in each specimen with respect to each other is different at each test temperature, and hence, the behavior is slightly different. Rebound of the impactor was observed for all the composites. Since the deformation of the composite is not severe, the impactor travels until its entire energy is

spent and then it bounces back. Increasing velocity would increase the energy of the impactor and thus the impactor will have to travel more to spend the extra energy.

(d) Dynamic strain histories

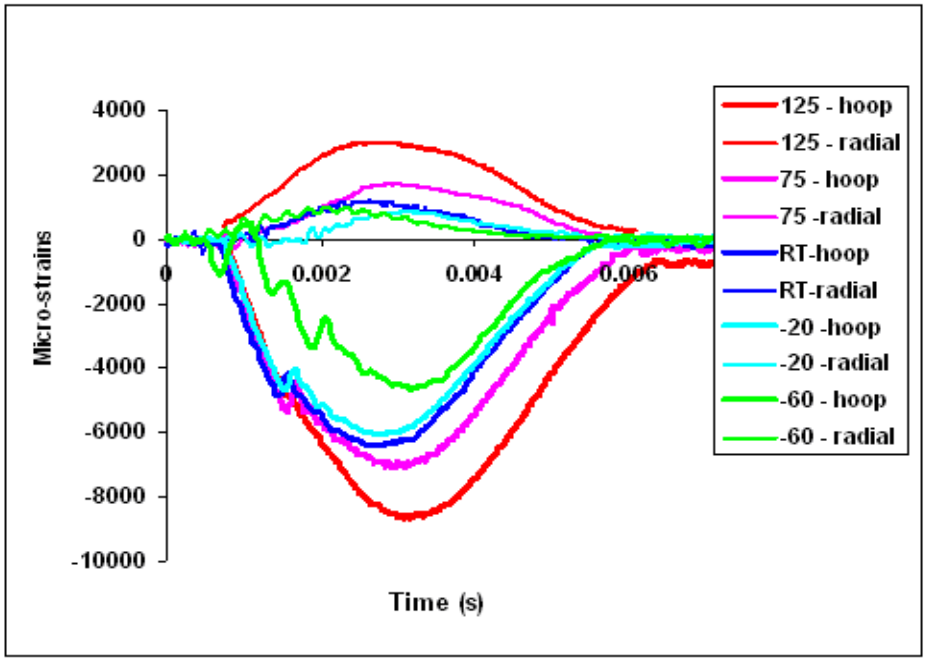

Figure 6.15 Dynamic strain histories for GL impacted at various temperatures

Figure 6.15 shows the strains obtained from two strain gages placed on a GL specimen impacted at the five test temperatures. Strains above the time axis are the radial strains while those below the time axis are the hoop strains. Strain gages were placed one inch away from the point of impact. In the figure, it can be seen that the absolute value of the hoop strains is higher than that for the radial strain at each temperature. Figures 6.16 and 6.17 show the strain histories for the hybrid composites. The absolute value of strain tends to increase with an increase in temperature. One reason for this is that as the temperature increases, its stiffness decreases, hence the material deforms more.

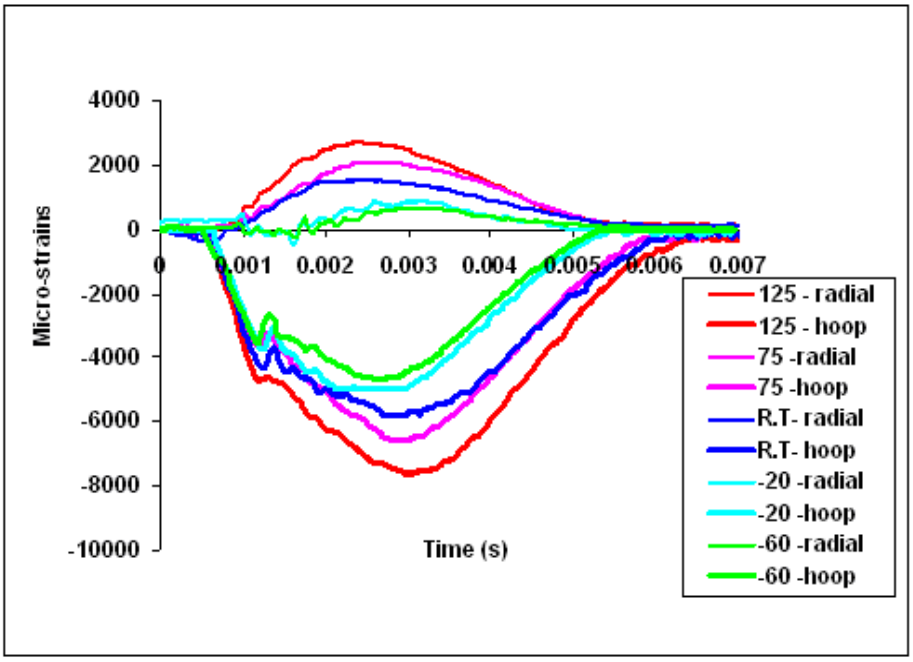

Figure 6.16 Dynamic strain histories for GL/GR/GL impacted at various temperatures

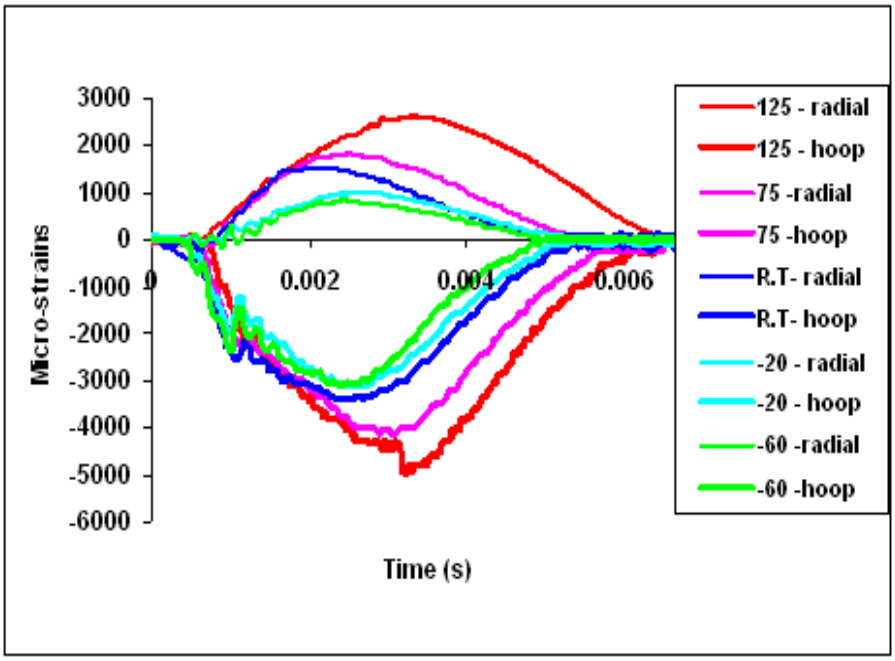

Figure 6.17 Dynamic strain histories for GR/GL/GR impacted at various temperatures

This was evident from the tensile testing. It can also be seen that as the temperature increases, the initial slope of the strain history tends to get steeper or in other words, the strain rate increases with an increase in temperature. This can also be explained by the reduction in stiffness in the material with an increase in temperature. Due to reduction in stiffness, and increase in ductility, the material exhibits larger deformation at a fixed time as compared to a material with a higher stiffness.

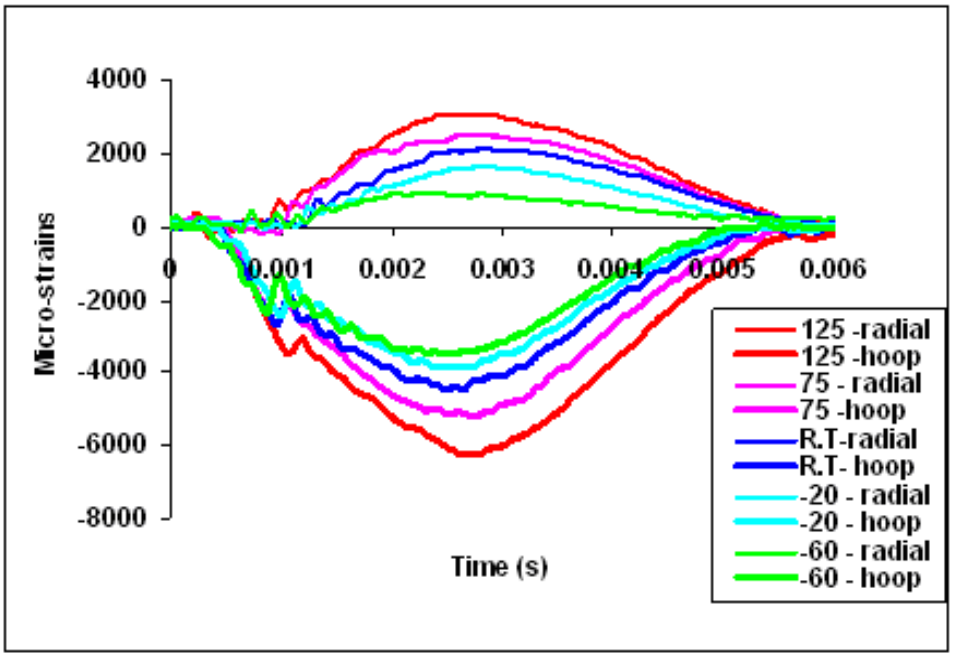

Figure 6.18 Dynamic strain histories for GR impacted at various temperatures

In Figure 6.18 the strain history of GR is shown. The trend of strain history is similar to that of the other three composites. It can be seen that for the GR and the GR/GL/GR specimens, the strain values at a given temperature are smaller than those for GL and

GL/GR/GL specimens. This could be due to the fact that GR is more brittle and has a smaller failure strain than GL.

(e) Impact energy

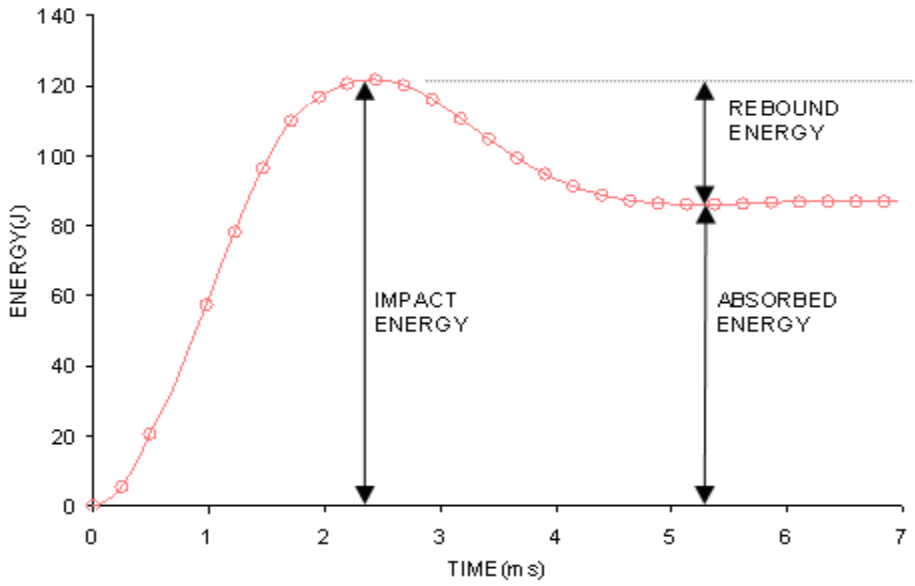

Figure 6.19 A typical energy history curve for drop-weight impact test when the impactor rebound occurs.

Composite materials use various mechanisms to absorb energy when they are impacted. It is believed that the three major method of energy absorption by composites are delamination, fiber shear out and fiber breakage. When an impactor drops from a certain height, its potential energy is converted to kinetic energy. At the time of impact, this kinetic energy goes into deforming the specimen (elastically and plastically) while some of it gets dissipated by the internal mechanisms of the composite. There are also other ways in which this energy gets dissipated, such as friction, etc. At the time of maximum

penetration or when the velocity of the impactor is zero, the corresponding energy is referred to as the impact energy. If the energy absorbed by the composite specimen is small, usually the impactor bounces back with a rebound energy.

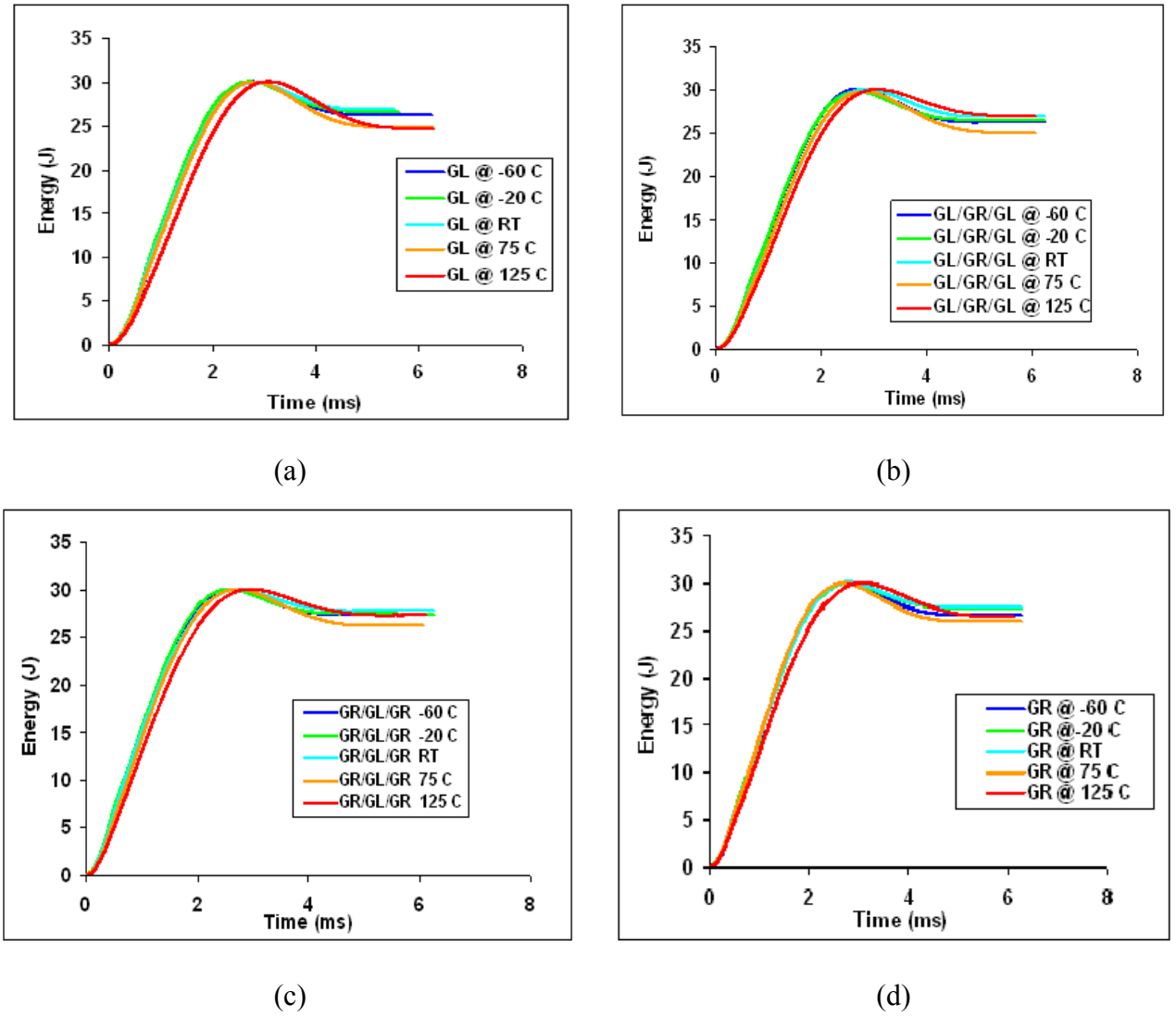

Figure 6.20 Energy-time histories of (a) GL, (b) GL/GR/GL, (c) GR/GL/GR and (d) GR for the impact tests conducted at –60°C, –20°C, R.T, 75°C, 125°C

Figure 6.19 shows a typical energy history curve in the case where the impactor bounces back. In the event that all the impacted energy is absorbed by the specimen, then the

impactor will not rebound. In this case sometimes, perforation of the specimen can be observed. In Figure 6.20, the energy history of all four layups of composites is shown at all the test temperatures. It can be seen that up to the point where the energy curve reaches its maximum peak, all the composite layups with the exception of GR follow a general trend. As the temperature decreases, the slope of the energy history curve tends to increase. Looking only at the curves for high temperatures i.e. 75°C, 125°C, it can be seen that the absorbed energy for the 125°C test is more that that for 75°C. In all cases the absorbed energy for –60°C, –20°C, R.T did not vary significant and was more than that for high temperatures, except for that of GL/GR/GL.

(f) Contact force vs. deflection

In Figure 6.21 the contact force vs. deflection of the composite plate is plotted. This is sometimes referred to as the stiffness. During the loading portion, it can be seen that the material has a highly oscillating behavior. Also the initial peak of the force-deflection curve tends to decrease with an increase in temperature. This peak represents the beginning of delamination**.** It can also be seen that the initial slope of curve tend to decrease with an increase in temperature. We can therefore conclude by looking at Figure 6.21 that the stiffness of the material tends to increase as the test temperature decreases, and the maximum force increases with a decrease in temperature.

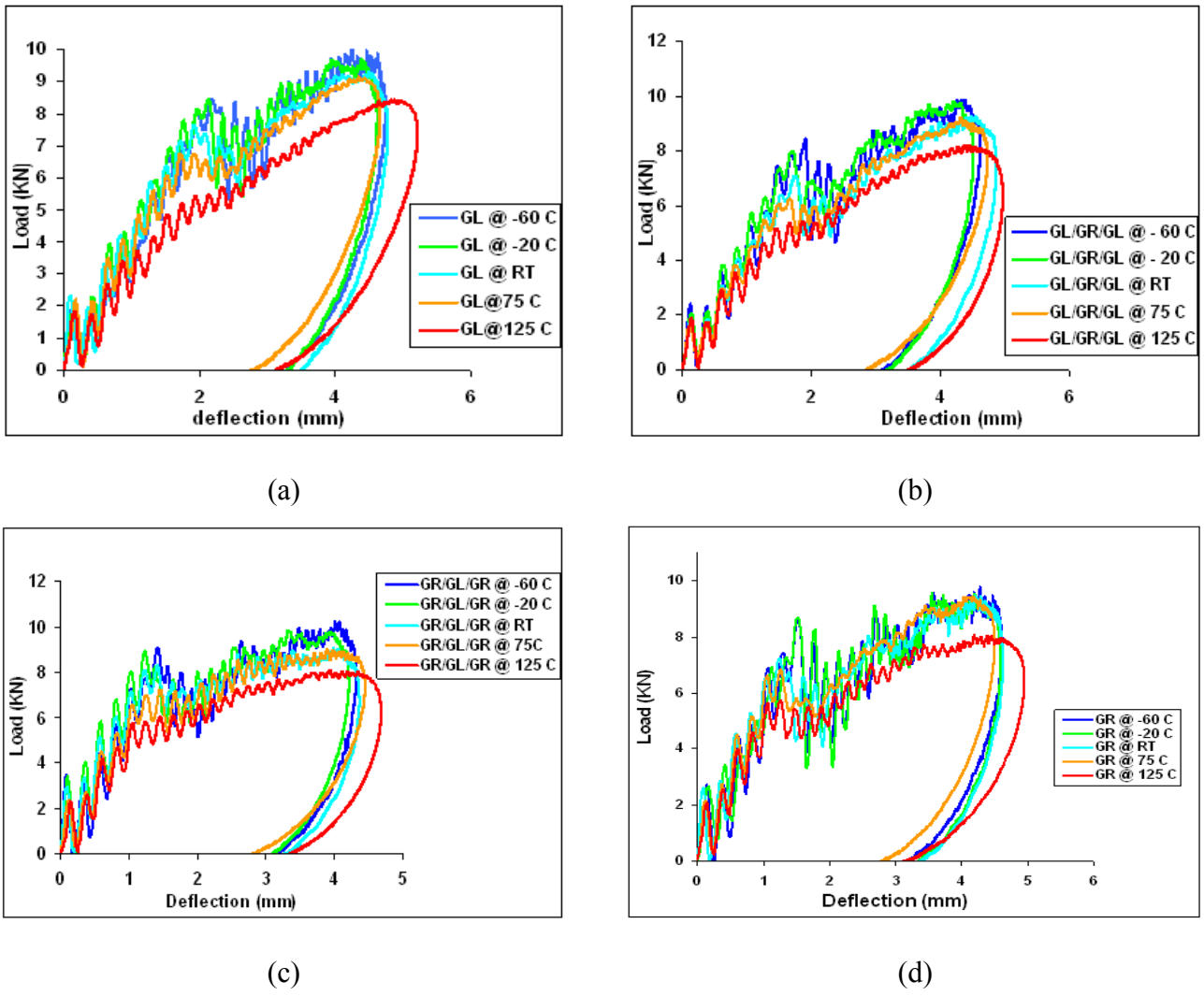

Figure 6.21 Contact force vs. deflection of (a) GL, (b) GL/GR/GL, (c) GR/GL/GR and (d) GR for the impact tests conducted at –60°C, –20°C, R.T, 75°C, 125°C

(g) Delamination

In this research, since delamination occurs inside of the material and is difficult to see with the naked eye, two approaches were used to study delamination. The first method used was the Ultrasonic C-scan method. After scanning was completed, the damaged specimens were cut into halves to reveal the damaged cross- sectional area.

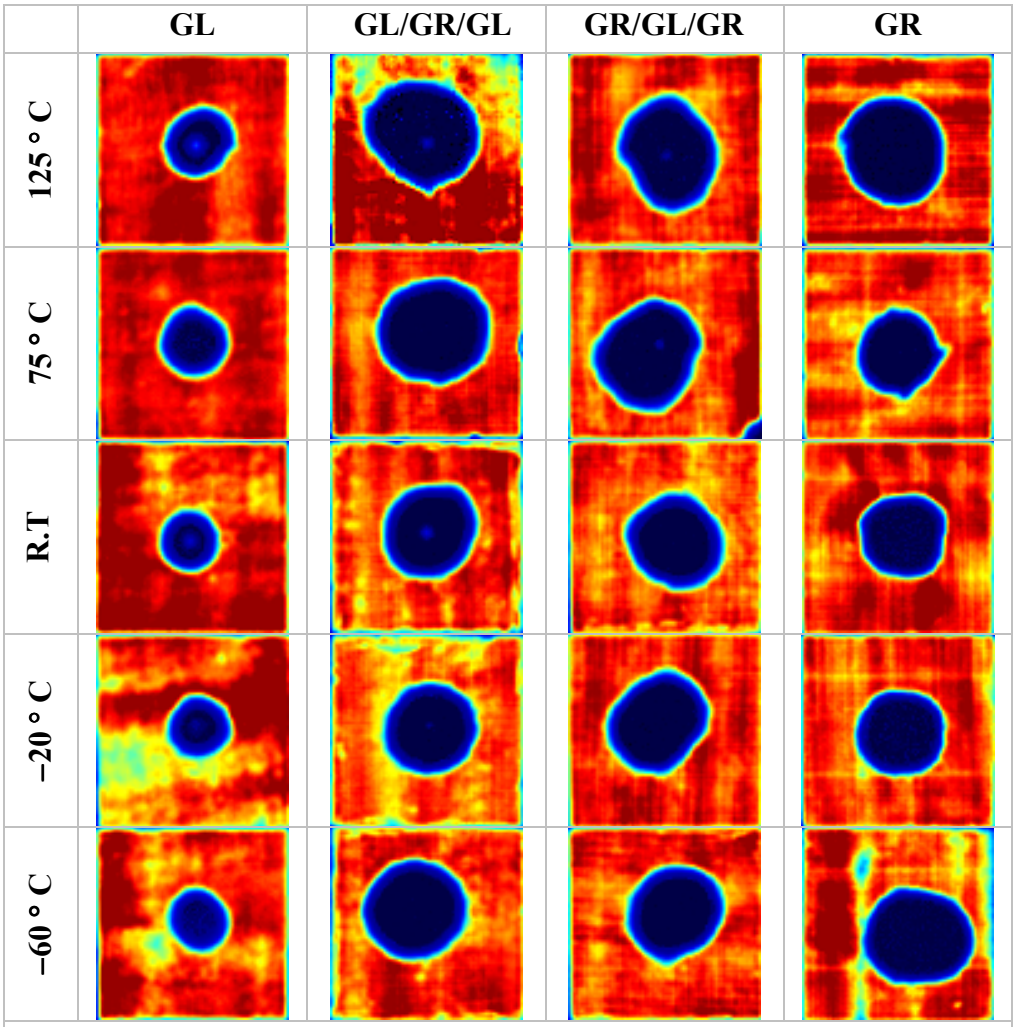

Figure 6.22 C-scan images of all impacted specimens

In Figure 6.22 the C-scan images of the delaminated areas of the impacted specimens at all test temperatures are shown. Using these images the delamination area was measured in order to quantify the effect of temperature on it. It can be seen that for the non hybrid composites, the delamination area is smaller and symmetric while that of the non hybrids is more asymmetric and larger. This is due to the bonding of different materials, in which the adhesion strength between the dissimilar materials is weaker and the propagation of delamination and failure is not uniform in all directions, thus giving rise to an

unsymmetrical delamination pattern. The delamination area of glass tends to decrease with a decrease in temperature; this contradicts our intuition that the delamination area is expected to increase with a decrease in test temperature. With the exception of −60 ° C, it can also be seen the GL/GR/GL follows a similar pattern, where the delamination area decreases with a decrease in temperature. With the exception of 125 ° C, it can be seen that GR tend to follow the general intuition that the delamination area increases with a decrease in test temperature. This can be explained by the fact that as temperature decreases, cracks and delamination tend to propagate easier due to a reduction in the fracture toughness of the material. Graphite is also brittle; hence, its behavior is more unstable under impact. GR/GL/GR delamination area seems to be quite unpredictable; this can be due to the combination of a few factors such as, brittle behavior of graphite, poor bonding between GR and GL and material imperfections in the hybrid composite.

Figure 6.23 shows the cross-sectional view of GL specimens at all the test temperatures after impact. At high temperature a darker center core can be seen throughout the thickness of the cross-section, and is due to compression of the material. As the temperature decreases, due to brittleness of the material, the compression effect is significantly smaller so from the figure it can be seen that this core fades away. It can also be seen that at the point of impact, the delamination area is very small but the delamination area tend to get larger further away from the point of impact.

(a)

(b)

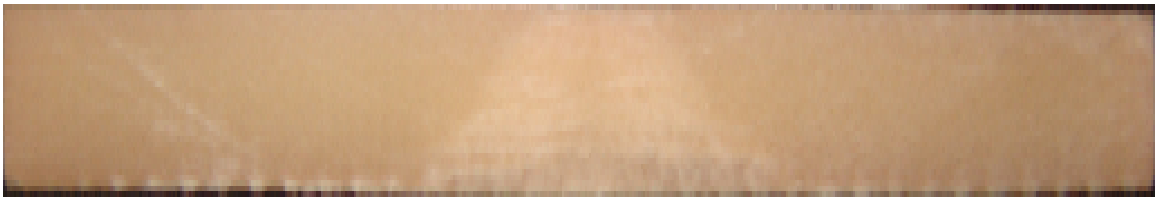

(c)

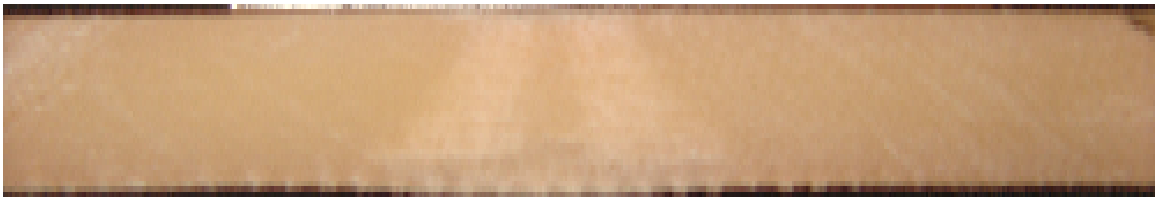

(d)

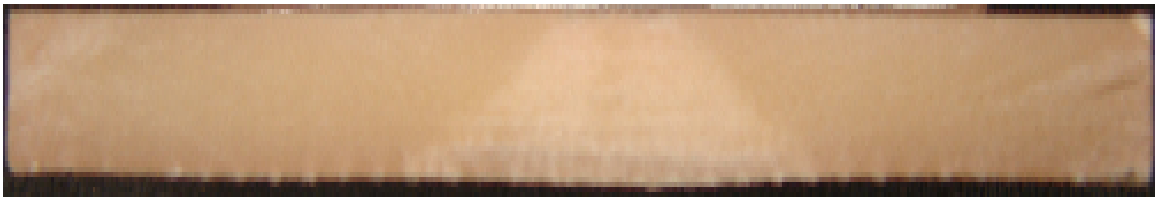

(e)

Figure 6.23. Optical fractographs of sectioned composites after drop impact conducted at 30 J on GL: (a) 125°C, (b) 75°C, (c) R.T (d) –20°C, (e) –60°C.

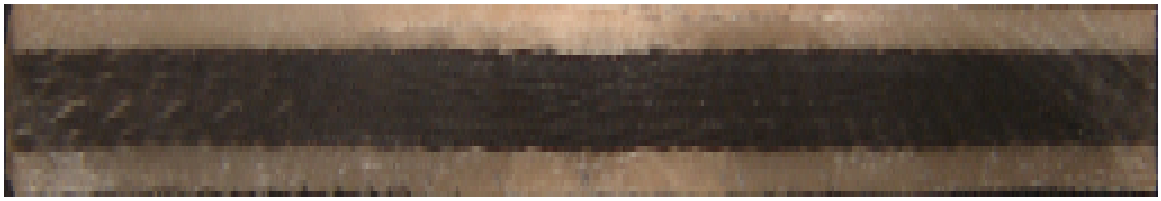

(a)

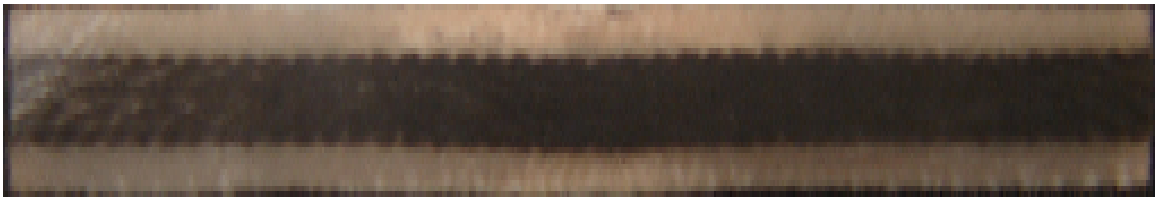

(b)

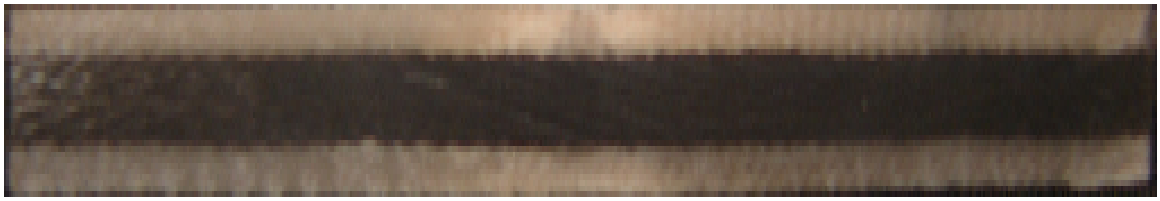

(c)

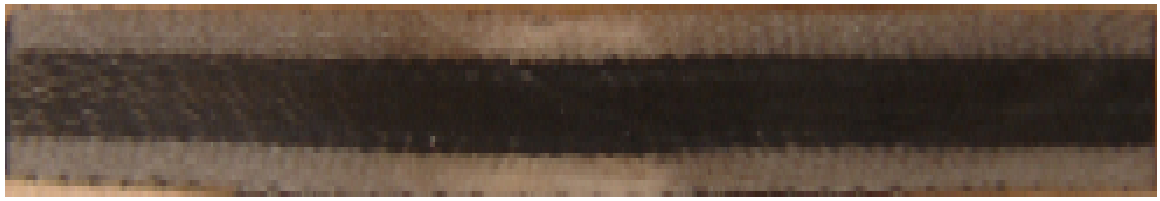

(d)

(e)

Figure 6.24. Optical fractographs of sectioned composites after drop impact conducted at 30 J on GL/GR/GL: (a) 125°C, (b) 75°C, (c) R.T (d) –20°C, (e) –60°C.

(a)

(b)

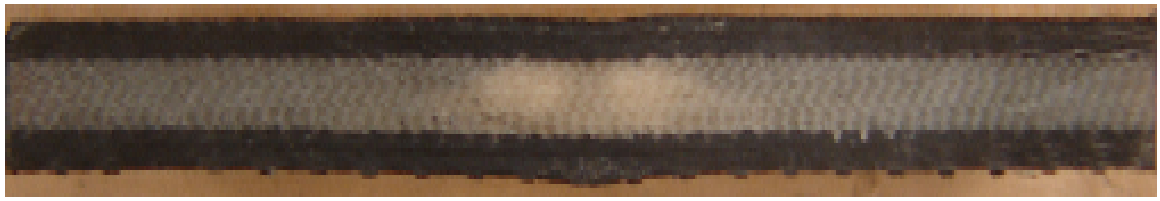

(c)

(d)

(e)

Figure 6.25. Optical fractographs of sectioned composites after drop impact conducted at 30 J on GR/GL/GR: (a) 125°C, (b) 75°C, (c) R.T (d) –20°C, (e) –60°C.

(a)

(b)

(c)

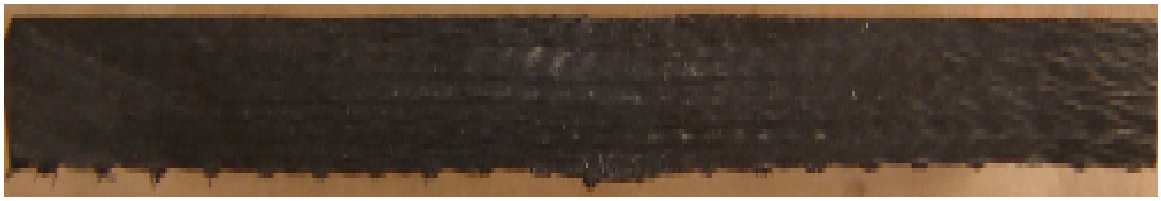

(d)

(e)

Figure 6.26. Optical fractographs of sectioned composites after drop impact conducted at 30 J on GL/GR/GL: (a) 125°C, (b) 75°C, (c) R.T (d) –20°C, (e) –60°C.

It is interesting to note that in Figure 6.23 the rate of increase of delamination from the top surface to the bottom surface is a lot greater for the low temperature tests and this rate decreases with an increase in temperature. This can be easily seen by the white area of the cross-section. In looking very carefully in Figure 6.22 at the C-scan results for the GL specimens and in Figure 6.23 at the cross-section revealing the damage area, our question as to why GL appears to have a decrease in delamination area as temperature decreases is answered. At high temperature the dark core at the center is the effect of compression and is not the actual delamination of the specimen. This can be verified by looking at the C-scan images where at high temperature a white core is seen surrounded by the delamination area which is darker. Therefore at high temperature although the delamination area is small, it appears to be large because it surrounds a large compressive core. This compression area along with the delamination surrounding it has also been reported in literature. At lower temperature, this compression effect is minimal and the entire area is delamination. This can be verified by the absence of the white core in the C-scan images and also the dark core in the cross-sectional images. Therefore the actual delamination area increases as temperature decreases but only appears at first to be the reverse. This compression effect is not seen in the GR specimens; hence the actual delamination area from the C-scan follows intuition and increases with a decrease in temperature. One reason why this compression is not seen in the GR specimen is due to the fact that the graphite is quite brittle and at this impact energy, there is delamination and fiber fracture before compression can occur. In Figure 6.24, none of the specimens experienced back splitting; one reason for this could be that there is GL on the outside which is more ductile so there is more room for deformation. Figure 6.25 shows the

cross-sectional view of the hybrid GR/GL/GR specimens. It can be seen that at R.T, –20°C and –60°C there is back splitting of the material. Usually, when a material is impacted, energy transferred by the impactor is dissipated by the damage mechanisms in the composite material. The first major form of energy dissipation is usually delamination. When delamination can not occur fast enough to dissipate the energy, then the material seeks other methods to dissipate the energy. The two other major energy dissipation mechanisms in composites are fiber shear out and fiber fracture. In Figure 6.25, fiber shear out is seen, this is when material near the impactor cannot remain perpendicular to the impactor anymore so it start to shear out. The back splitting is due to fibers failing in tension since the back end of the specimens elongates to its fracture point due to the deflection of the specimen. It can also be seen clearly from the GL layer in Figure 6.25, that on the surface closer to the impactor the delamination is smaller and further away from the impactor the delamination area increases. Figure 6.26 shows the GR specimens which all have some damage on the surface and back splitting. This is due to the brittle nature of graphite. When examined closely, it is also seen that even though back splitting and surface damage occurred, there was no case where the impactor totally perforated the specimen.

6.2 Conclusions

a) As the test temperature decreases, the peak force of the composite tends to increase slightly.

b) For GL and hybrid GL/GR/GL, the delamination area tends to decrease with a decrease in test temperature, while that of GR increases. The delamination pattern of GR/GL/GR was not clear.

c) As the test temperature decreases, the strain rate of the material due to impact also tends to decrease.

d) The first major form of energy dissipation in the composite material was delamination which was directly linked to the material peak force. Other dissipation methods seen were fiber shear out and fiber breakage.

e) Among the four layups, it can be seen that GL specimen is more impact resistant and hence the strongest while GR was the weakest.

f) Hybridization tends to increase the impact resistance of GR

Chapter 7

BALLISTIC IMPACT TESTS ON WOVEN HYBRID COMPOSITES

Impacts are usually classified into three categories: low velocity impact, high velocity (ballistic) impact and hyper velocity impact. The characteristics of these categories are quite different in terms of energy transfer between the projectile and target, energy dissipation and damage propagation mechanisms [101]. In this part of the research, ballistic impact tests were conducted using an in-house high pressure gas gun together with an environmental chamber. High pressure helium provides the force needed to accelerate a 22-caliber copper bullet through the gun barrel to the desired velocity. Near the muzzle of the gun barrel, two sets of laser-amplified photo diode pairs form two continuous optical paths. The distance between the two diodes is 101.6 mm. As the projectile travels through the gun barrel, it interferes with this continuous optical path, which in turn creates a voltage change which is recorded by an oscilloscope. Knowing the distance between the two diodes and the time difference in the interference between the two optical paths the projectile velocity can be estimated.

The high and low temperatures testing conditions were controlled by an attached environmental chamber. The same environmental chamber used for temperature control during tensile testing was used here; therefore the mechanisms used to attain the testing temperatures are the same. Inside the environmental chamber, a fixture was used to clamp the specimen on each side. After clamping, the temperature was raised to the desired test temperature, and then the specimen was soaked for approximately 30 minutes before testing. Soaking is done to remove any temperature gradient which may exist in the specimen. The existence of temperature gradient usually causes the surface to expand or contract more than the center of the composite, thus giving rise to unwanted skin-core stresses.

Ballistic impact tests were conducted on the four different layups of composites, i.e. GL, GL/GR/GL, GR/GL/GR and GR. Each panel had dimensions of 152.4mm×101.6 mm ×6.35 mm. They were clamped over a length of 25.4 mm on both sides (Fig. 7.1). Two strain gages were mounted approximately 25.4 mm away from the impact location on the impact side of the specimens. SG-1 (strain gage #1) measured the radial strain during and after impact while SG-2 (strain gage #2) measured the hoop strain.

Once an experiment was completed, the composite panels were ultrasonically C-scanned and optical pictures were taken. Finally the specimens were cut longitudinally along the center to reveal the internal damage and delamination.

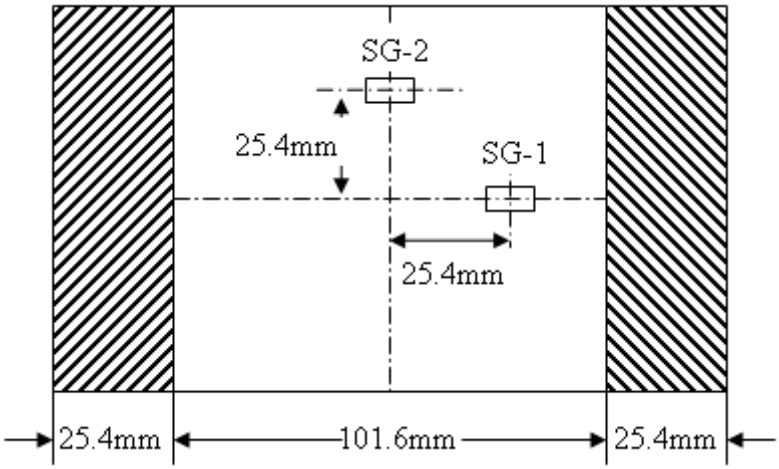

Figure 7.1 A typical composite panel specimen mounted with two strain-gages on the ballistic impact side

7.1 Ballistic impact tests on woven hybrid composite panels

During the ballistic impact tests at various test temperatures, the main objective was to obtain an estimate of the ballistic limit of the four layups of composite. There are many definitions of ballistic limit, however, in this research the definition of ballistic limit was taken from [101] where ballistic limit is looked at in terms of not only velocity but also energy. During ballistic impacts, one of three outcomes is possible [101]:

1) The projectile impacts the front surface of the composite with a certain velocity, perforates it and exits with a certain residual velocity. In this case the projectile's initial energy is larger than the energy than the composite can absorb.

2) The projectile partially penetrates the composite i.e. the projectile gets stuck in the composite or rebounds. In this case the projectile's initial energy is less than what the composite can absorb.

3) The projectile perforates the target completely with a zero exit/residual velocity. In this case the initial velocity of the projectile is called the **ballistic limit** or V_{50}. Here, the entire energy of the projectile is absorbed by the target.

In the experiments conducted, the procedure used to obtain the ballistic limit was by finding an impact velocity which causes perforation in the target by the projectile and one that causes only partial penetration of the projectile in the target. More tests were conducted within this range of these two extremes velocities in order to find the maximum impact velocity which causes a zero exit/residual velocity. Due to the limited number of specimens available for testing, the exact ballistic limit could not be obtained experimentally. Hence, minimal tests were conducted as needed to obtain a reasonable range in velocities i.e. minimum velocity that causes perforation and maximum velocity that causes partial penetration.

In Tables 7.1-7.4, the impact velocities which cause full and partial penetration in the composite specimens are given. It can be seen that in quite a few cases, the projectile was partially imbedded in the GL specimen, while this never occurred in the case of the GR specimens. One explanation of this fact is that GL is more ductile than GR.

The interval of V_{50} velocity for all panels was roughly estimated using experimental data.

(a) Experimental results

Table 7.1 Parameters of ballistic impact tests on woven GL composite panels

Materials	Temperature	Impact velocity	Penetration type	Impact energy
GLASS	125 °C	282 m/s	Partial (stuck)	119 J
	125 °C	299 m/s	Partial (stuck)	134 J
	125 °C	325 m/s	Full	158 J
	75 °C	322 m/s	Partial	156 J
	75 °C	346 m/s	Partial	180 J
	75 °C	365 m/s	Full	200 J
	R.T	360 m/s	Partial	194 J
	R.T	387 m/s	Partial (stuck)	225 J
	R.T	400 m/s	Partial*	240 J
	R.T	403 m/s	Full	244 J
	−20 °C	382 m/s	Partial (stuck)	219 J
	−20 °C	404 m/s	Full	245 J
	−60 °C	397 m/s	Partial*	236 J
	−60 °C	404 m/s	Full	245 J

*** Severe splitting on the back surface of specimen**

In Table 7.1, it can be seen that as the temperature decreases the ballistic limit increases. At high temperature the ballistic resistance decreases severely when compared to room temperature. At low temperature however, the impact resistance of the composite increases only slightly when compared to room temperature.

In Table 7.2, it can be seen that the impact resistance and ballistic limit tend to increase slightly with an increase of temperature.

Table 7.2 Parameters of ballistic impact tests on woven GR composite panels

Materials	Temperature	Impact velocity	Penetration type	Impact energy
GRAPHITE	125 °C	203 m/s	Partial	62 J
	125 °C	275 m/s	Partial	113 J
	125 °C	299 m/s	Full	134 J
	75 °C	258 m/s	Partial*	100 J
	75 °C	275 m/s	Full	113 J
	R.T	254 m/s	Partial	97 J
	R.T	272 m/s	Full	111 J
	−20 °C	252 m/s	Partial	95 J
	−20 °C	261 m/s	Full	102 J
	−60 °C	233 m/s	Partial*	81 J
	−60 °C	256 m/s	Full	98 J
	−60 °C	299 m/s	Full	134 J
	−60 °C	318 m/s	Full	152 J

*** Severe splitting on the back surface of specimen**

Table 7.3 Parameters of ballistic impact tests on woven GL/GR/GL composite panels

Materials	Temperature	Impact velocity	Penetration type	Impact energy
GL/GR/GL	125 °C	308 m/s	Partial (stuck)	142 J
	125 °C	325 m/s	Full	158 J
	125 °C	338 m/s	Full	171 J
	75 °C	306 m/s	Partial*	140 J
	75 °C	317 m/s	Full	151 J
	R.T	306 m/s	Partial	140 J
	R.T	313 m/s	Partial*	147 J
	R.T	319 m/s	Full	153 J
	−20 °C	301 m/s	Partial	136 J
	−20 °C	320 m/s	Full	154 J
	−60 °C	295 m/s	Partial	131 J
	−60 °C	322 m/s	Partial	156 J
	−60 °C	345 m/s	Full	179 J
	−60 °C	368 m/s	Full	203 J

*** Severe splitting on the back surface of specimen**

Table 7.4 Parameters of ballistic impact tests on woven GR/GL/GR composite panels

Materials	Temperature	Impact velocity	Penetration type	Impact energy
GR/GL/GR	125 °C	299 m/s	Partial	134 J
	125 °C	342 m/s	Partial	175 J
	125 °C	368 m/s	Full	203 J
	75 °C	312 m/s	Partial	146 J
	75 °C	339 m/s	Full	172 J
	R.T	327 m/s	Partial	160 J
	R.T	343 m/s	Partial	176 J
	R.T	362 m/s	Full	197 J
	−20 °C	299 m/s	Partial	134 J
	−20 °C	324 m/s	Partial*	158 J
	−20 °C	338 m/s	Full	171 J
	−60 °C	275 m/s	Partial	113 J
	−60 °C	297 m/s	Partial	132 J
	−60 °C	312 m/s	Full	146 J
	−60 °C	358 m/s	Full	192 J
	−60 °C	390 m/s	Full	228 J

*** Severe splitting on the back surface of specimen**

Tables 7.3 and 7.4 shows the results for the hybrid composites tested at all the test temperature. The impact resistance and ballistic limit as a function of temperature can be seen, but to have a clearer understanding of the behavior, the impact velocity has been plotted against temperature in Figure 7.2.

The ballistic limit in Figure 7.2 is obtained by taking the average of the minimum velocity that causes perforation and the maximum velocity that causes partial penetration at that particular test temperature. The error bar is added to each curve to represent the difference in these two velocities. It can be seen from Figure 7.2 that as temperature decreases, the ballistic limit for GR decreases while those of GL increases. At temperatures above room temperature, the ballistic limit for GL has a sharp drop. The ballistic limit for the hybrid GR/GL/GR follows a similar trend as GR but the effect of

temperature has a more distinct effect in this case. The ballistic limit for the hybrid GL/GR/GL also follows a similar trend as GR but at –60ºC, the ballistic limit seems to deviate from this trend.

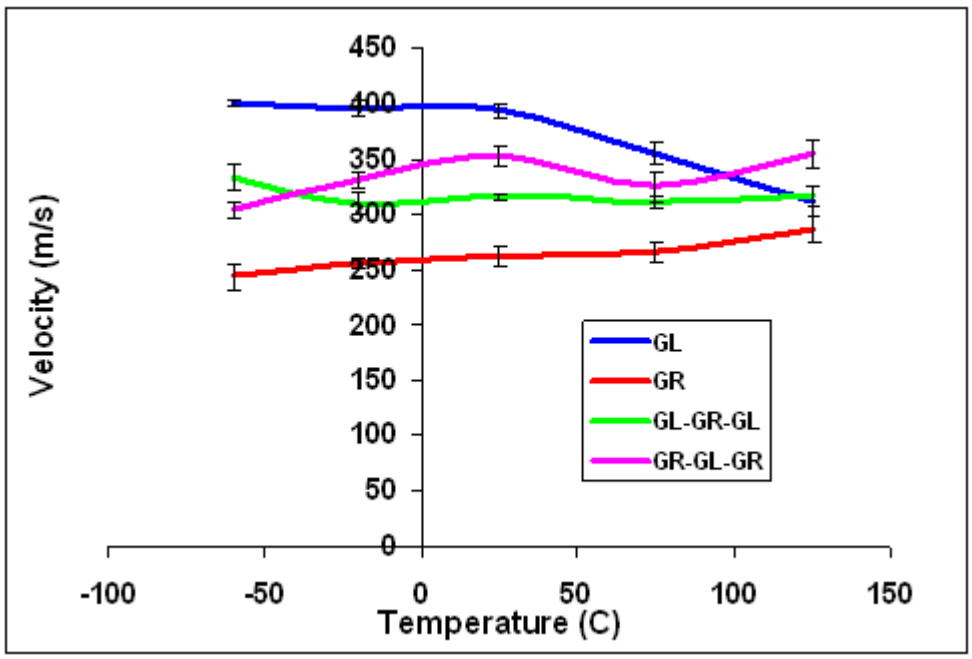

Figure 7.2 Temperature vs. ballistic limit for all the layups

In order to explain these trends of ballistic limit as a function temperature for the four different layups of composite, attention must be given to the contribution of thermal stresses developed during the soaking period. First, before the composites are soaked, they are clamped at both ends. During soaking, some thermal stress will develop in the material. To study the effect of clamping and of the resulting stresses on the trend shown in Fig 7.2, clamped-clamped boundary conditions are removed from the two ends and are replaced with simply supported boundary conditions. Then tests were conducted on the non- hybrid composites at extremes of the testing temperatures and the results are given in Table 7.5.

Table 7.5 Parameters of ballistic impact tests on non-hybrid simply supported composite panels

Material	Temperature	Velocity	Penetration type
GRAPHITE	–60 °C	264 m/s	Full
	125 °C	279 m/s	Partial*
GLASS	–60 °C	394 m/s	Partial*
	125 °C	332 m/s	Full

From Table 7.5, it can be seen that the boundary conditions and the resulting thermal stress do not affect the trend of ballistic limit as a function of temperature, i.e. as temperature decreases, the impact resistance of GR decreases while those of GL increases. In quantitatively comparing the results in Table 7.5 with those of Table 7.1 and 7.2, it can also be concluded that the acquired residual stress buildup during soaking has negligible effect on the ballistic limit.

Intra-laminar thermal stresses, or stresses within each layer of the composite which are caused by a difference in the thermal expansion coefficients between matrix and fibers are believed to have only a small effect on the trend of the ballistic limit. Research [102] has showed that biaxial preloading a woven glass composite plate by 31% of its unidirectional tensile strength then impacting it at high velocity, increases the ballistic limit only by 11%. During the soaking period of the composites for ballistic tests at high temperature, the glass and graphite fibers are in tension due to the larger thermal expansion coefficient of the matrix material. However, as the test temperature increases and approaches its curing temperature (177 °C), the intra laminar stresses in the composites become smaller. At low test temperatures (– 20 °C and – 60 °C), the intra laminar stresses are however larger. In this research, we are studying the impact behavior of composite materials initially at room temperature as temperature changes, so the

assumption is made that no thermal stress is in the composite panel after manufacturing. This means that at room temperature, the thermal residual stress in the composite is zero.

Calculations (see chapter eight) show that intra laminar stresses developed during soaking are small and hence their effect is negligible on the ballistic limit trend.

It has been shown by many researchers [101, 103, 104] that some of the major damage mechanisms involved in ballistic impact of composites includes, cone formation on back surface of the target, deformation of secondary yarns, deformation/failure of primary yarns, delamination, matrix cracking, shear plugging and friction between projectile and target.

Morye et al. [103], Naik et al. [101] showed that the major form of energy absorption in composites is usually due to cone formation. Since GL is more ductile and has a higher modulus of toughness than GR, it is able to absorb more energy from the projectile in the form cone formation. This is one possible reason why GL is more impact resistant than GR as seen in Figure 7.2.

Taking a close look at Figure 7.3, it can be seen that the dominant damage mechanism in GR at low temperature is shear plugging. It is interesting to note that at high temperature, this dominant mechanism for GR becomes similar to that of GL. It is also interesting to note that both GL and GR at high temperatures have a higher ballistic impact resistance than GR at low temperature. It can be said that very brittle materials will most likely have shear dominant failure mechanism under ballistic impact. Shear dominant failure mechanism and brittle materials are therefore unfavorable choices for impact resistant materials [101]. Lee and Sun [105] and Ellis [106] reported shear plugging to be one of

the major damage modes on impact of angle ply graphite/bismaleimide by blunt/flat projectiles.

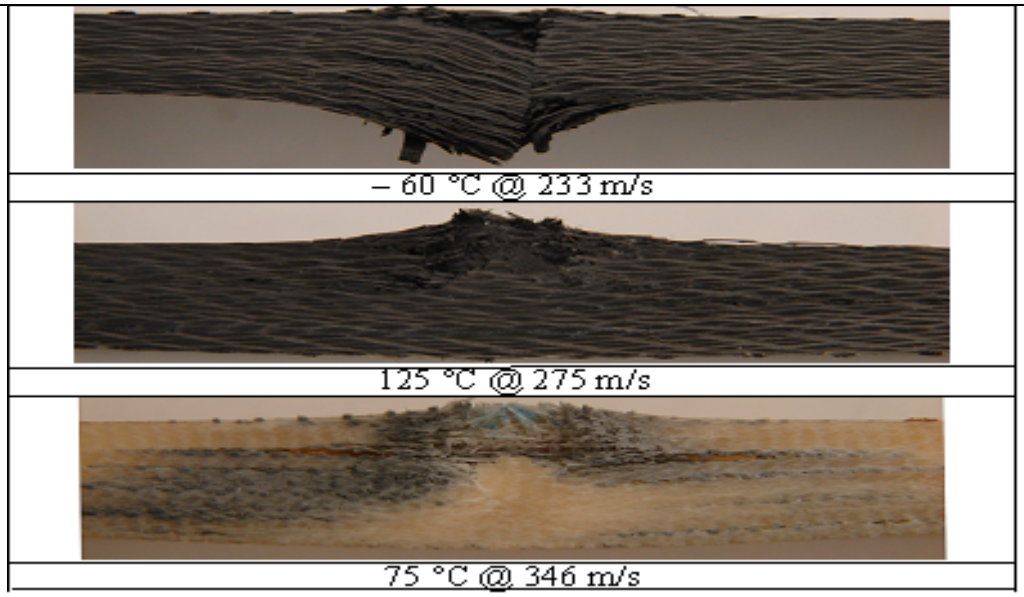

Figure 7.3 Cross-sectional view of GR and GL at high and low temperatures

(b) Dynamic strains

The ballistic impact event takes place in an extremely short time. Accordingly the frequency of the recording device should be high enough to capture the strain gauge readings in such a short time. The oscilloscope used in this study to capture the strain output from the strain gages has a maximum frequency of 500 KHz. In other words, it was only able to record a strain data every 2μs.

Assuming that the ballistic impact event takes 100μs, the dynamic strain curve from experiment would have captured only 50 data points, resulting in significant under sampling. Thus, the strain curve constructed using these data points will not represent the actual response of the composite during the impact. The strain measurements obtained are mainly for vibration of impacted composite panel and not necessarily the transient

response of composite during ballistic impact. Experiments were conducted at five temperatures but only the strain results at extreme temperatures are presented here, i.e.125 °C and – 60 °C.

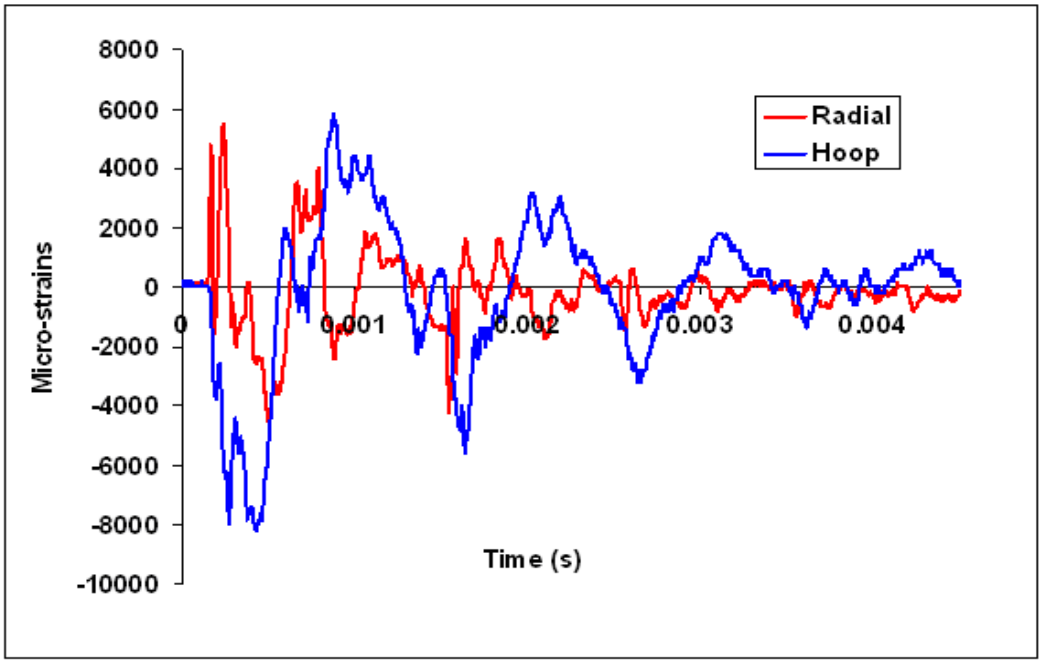

(a)

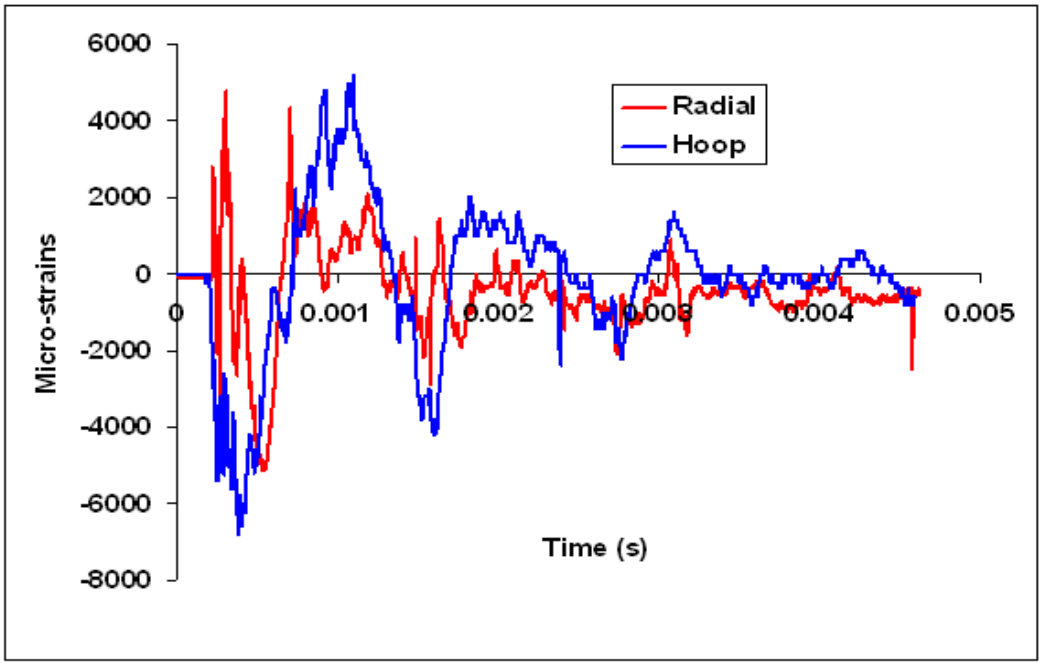

(b)

Fig 7.4 Hoop and radial experimental strain histories for GL at (a) 125 °C (b) – 60 °C

Figure 7.4 shows the dynamic strain histories for GL at 125 °C and – 60 °C. It can be seen that at both temperatures, the frequency is higher in the radial direction than the hoop. This can be an effect of the boundary (Fig 7.1). Comparing the magnitudes of the signals, it is observed that the strain values at 125 °C are higher than those at – 60 °C. This can be explained by the increase ductility of the material at high temperatures. It can also be observed that the absolute magnitude of the hoop strain is approximately 1.5 to 2 times that of the radial strain.

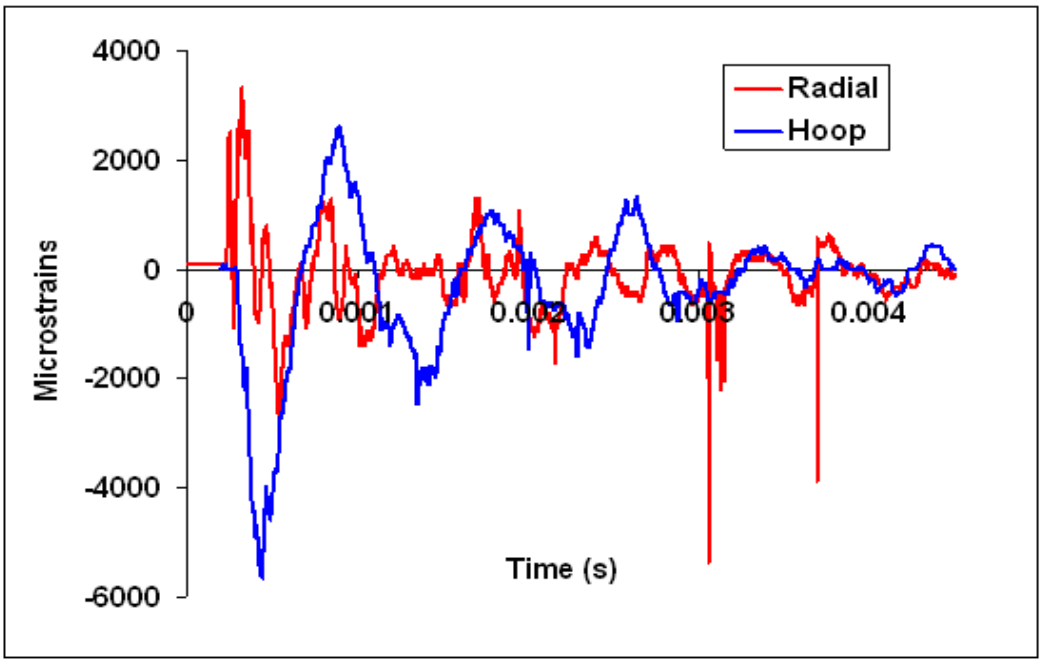

(a)

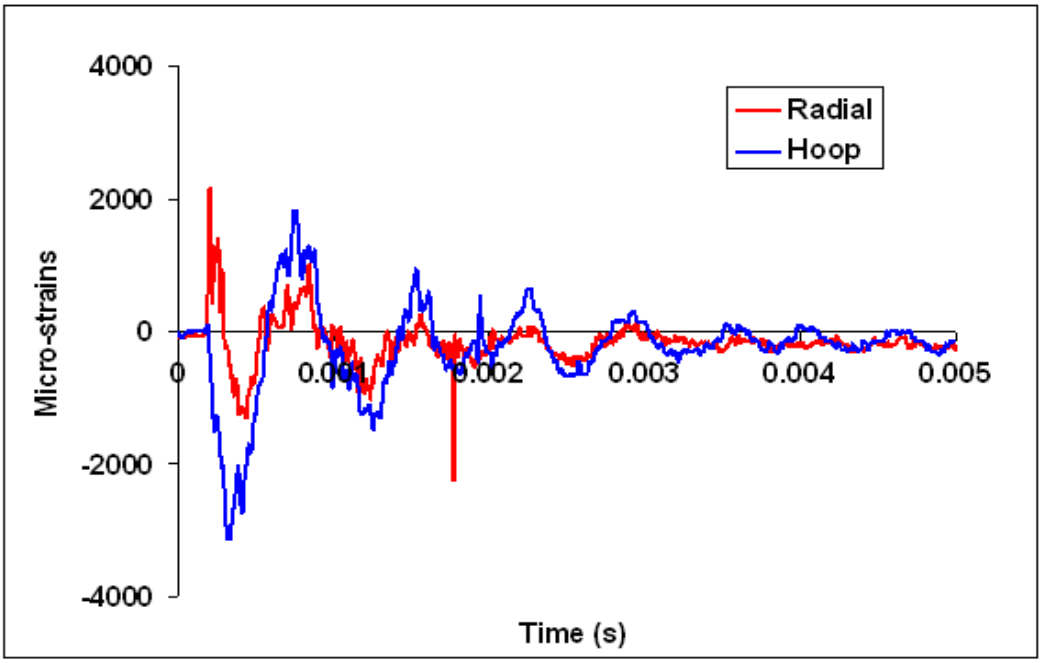

(b)

Fig 7.5 Hoop and radial experimental strain histories for GR at (a) 125 °C (b) – 60 °C

Figure 7.5 shows the dynamic strain histories of composites for GR at 125 °C and – 60 °C. It follows a similar trend to the GL composite. However, at both temperatures, the strains for GR are less that those of GL composite.

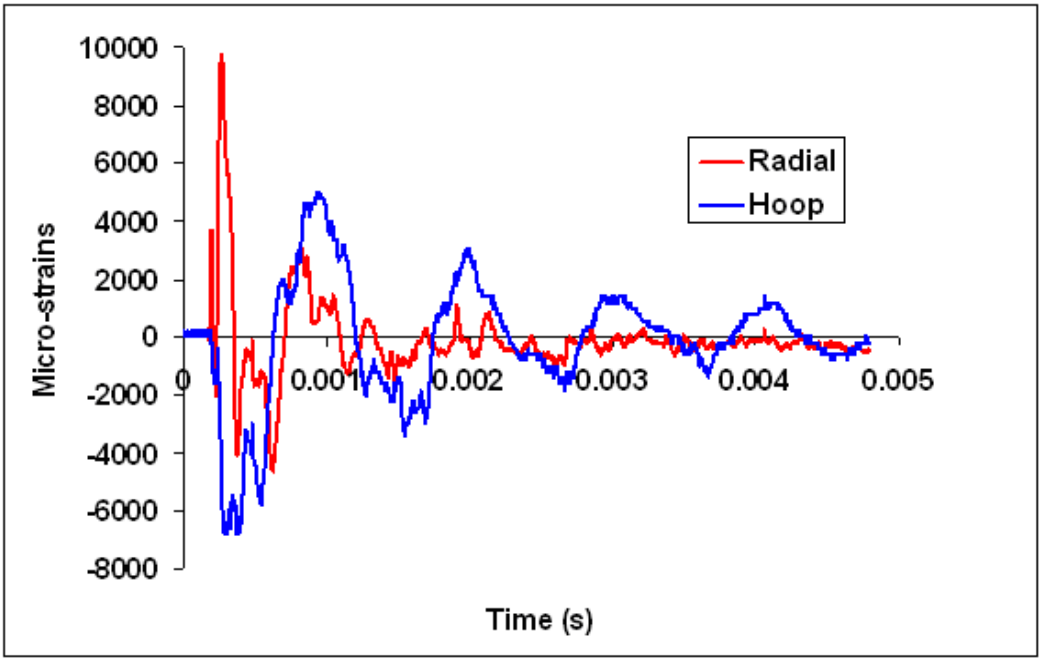

(a)

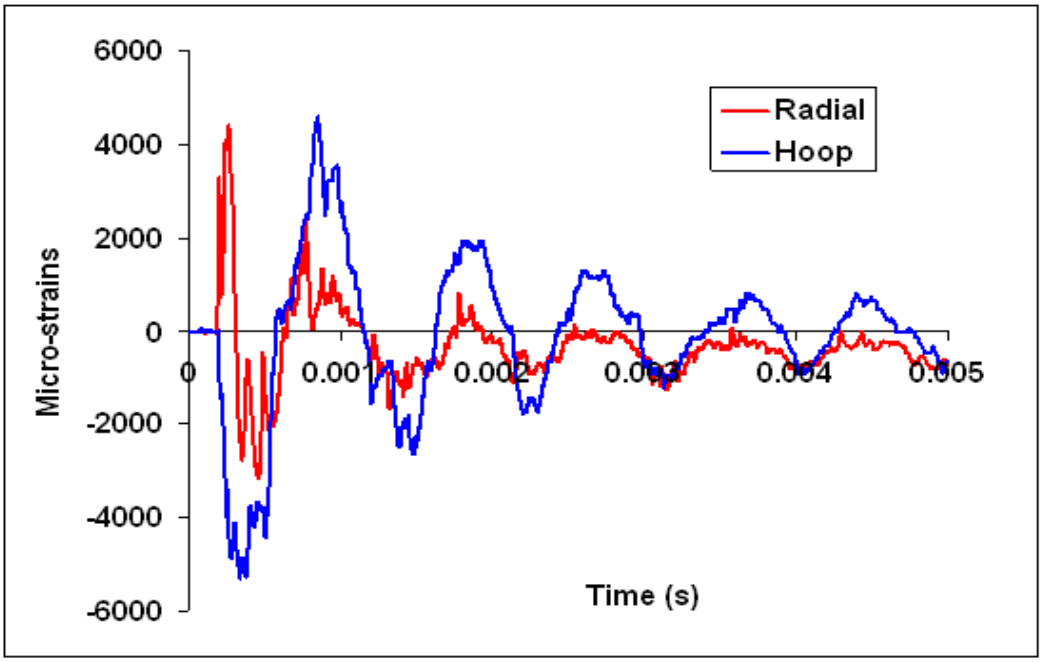

(b)

Fig 7.6 Hoop and radial experimental strain histories for GL/GR/GL at (a) 125 °C (b) – 60 °C

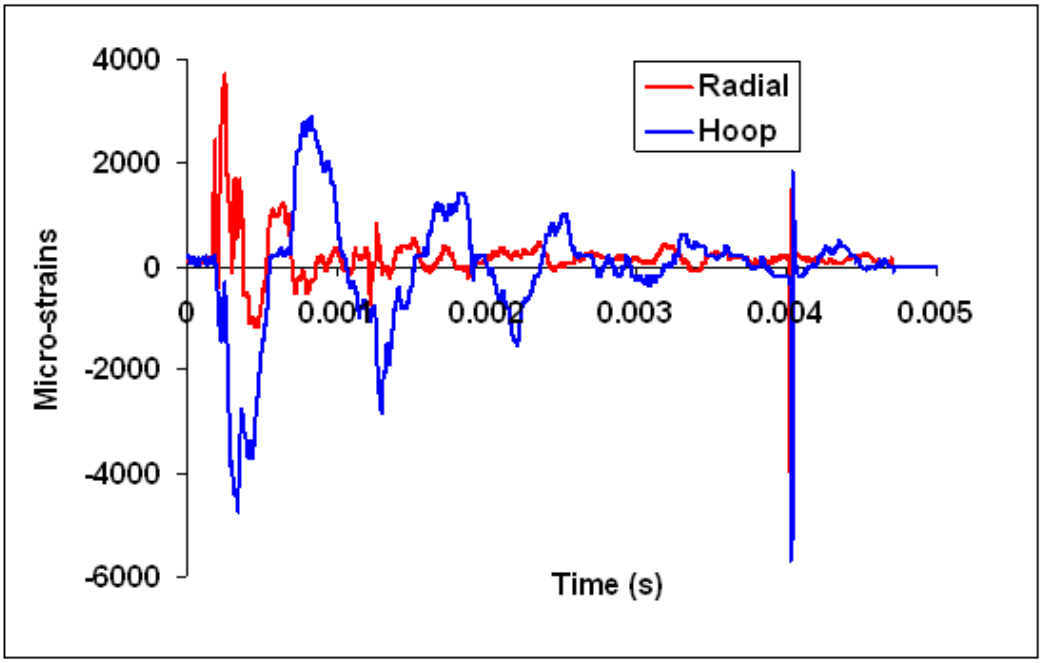

(a)

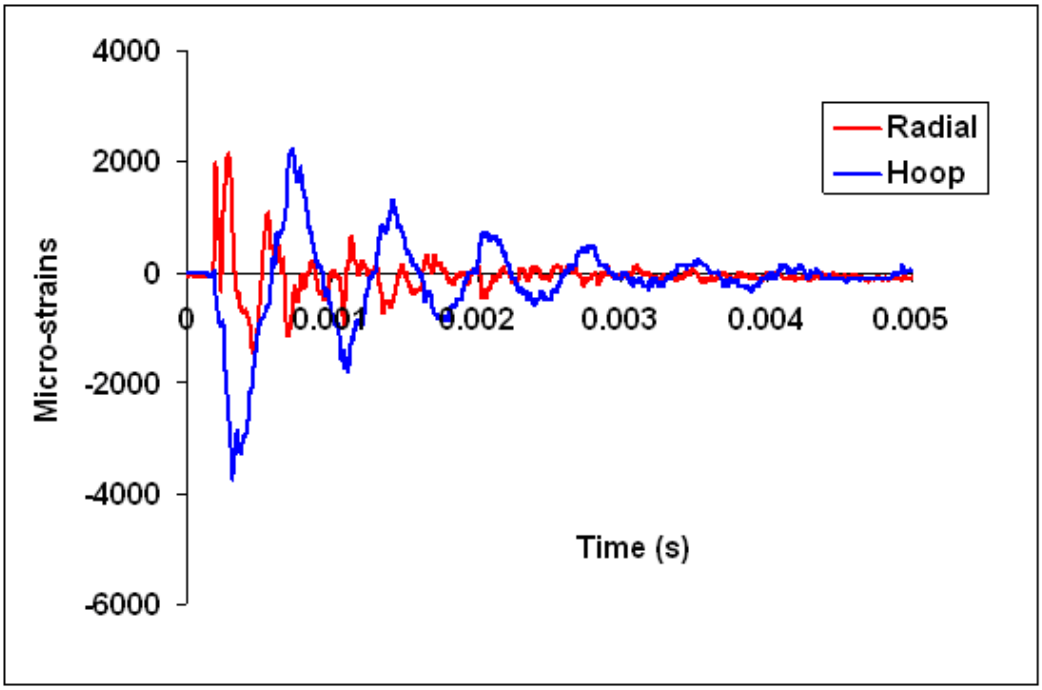

(b)

Fig 7.7 Hoop and radial experimental strain histories for GR/GL/GR at (a) 125 °C (b) – 60 °C

Figures 7.6 and 7.7 show the dynamic strain histories for GL/GR/GL and GR/GL/GR composites at 125 °C and – 60 °C, respectively. It is observed that for the hybrid

GL/GR/GL, the magnitude of the strains is larger than that of GR/GL/GR. One explanation for this is probably because GR is more brittle than GL, hence instead of large deformations, GR will fail. One important piece of information to keep in mind while comparing these strains is that they are measured on the surface of the impacted specimen.

(c) Post Mortem analysis of specimens

In order to better investigate the damage mechanisms and damage patterns of the composites and how they change with temperature, optical pictures of the specimens were taken and then they were C-scanned and finally cut in two halves to analyze the cross-sectional view.

Figure 7.8(a, b, c and d) shows optical pictures of impacted composites. The length of the vertical and horizontal front surface cracks (micro buckling) increased with increasing velocity for partial penetration cases. However, increasing velocity resulted in smaller horizontal and vertical cracks in case of perforation. In some specimens the bullet can be seen stuck in the specimen. This is due to the ductile nature of the GL specimens.

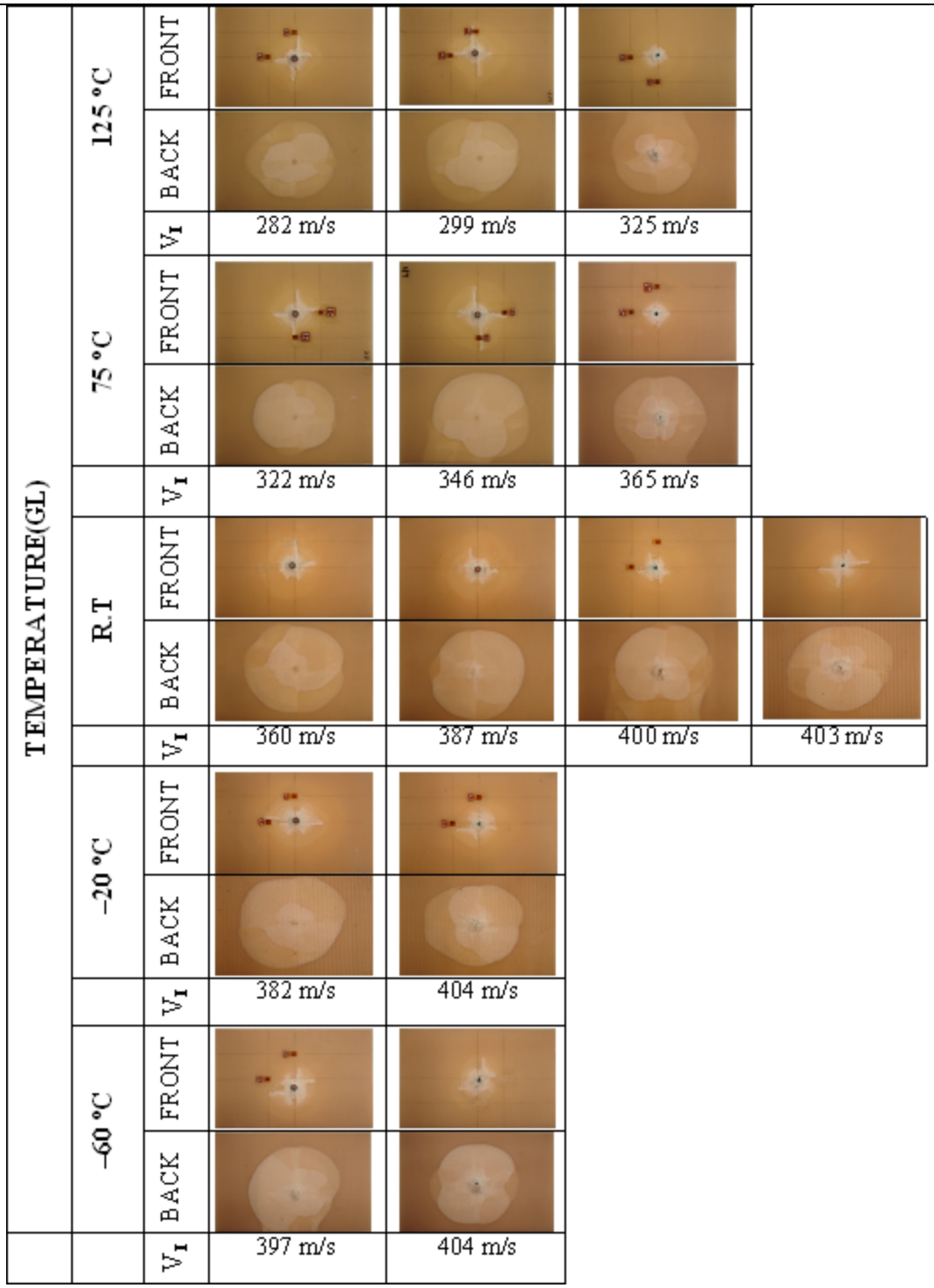

Figure 7.8 (a) Optical pictures of GL composite specimens after impact

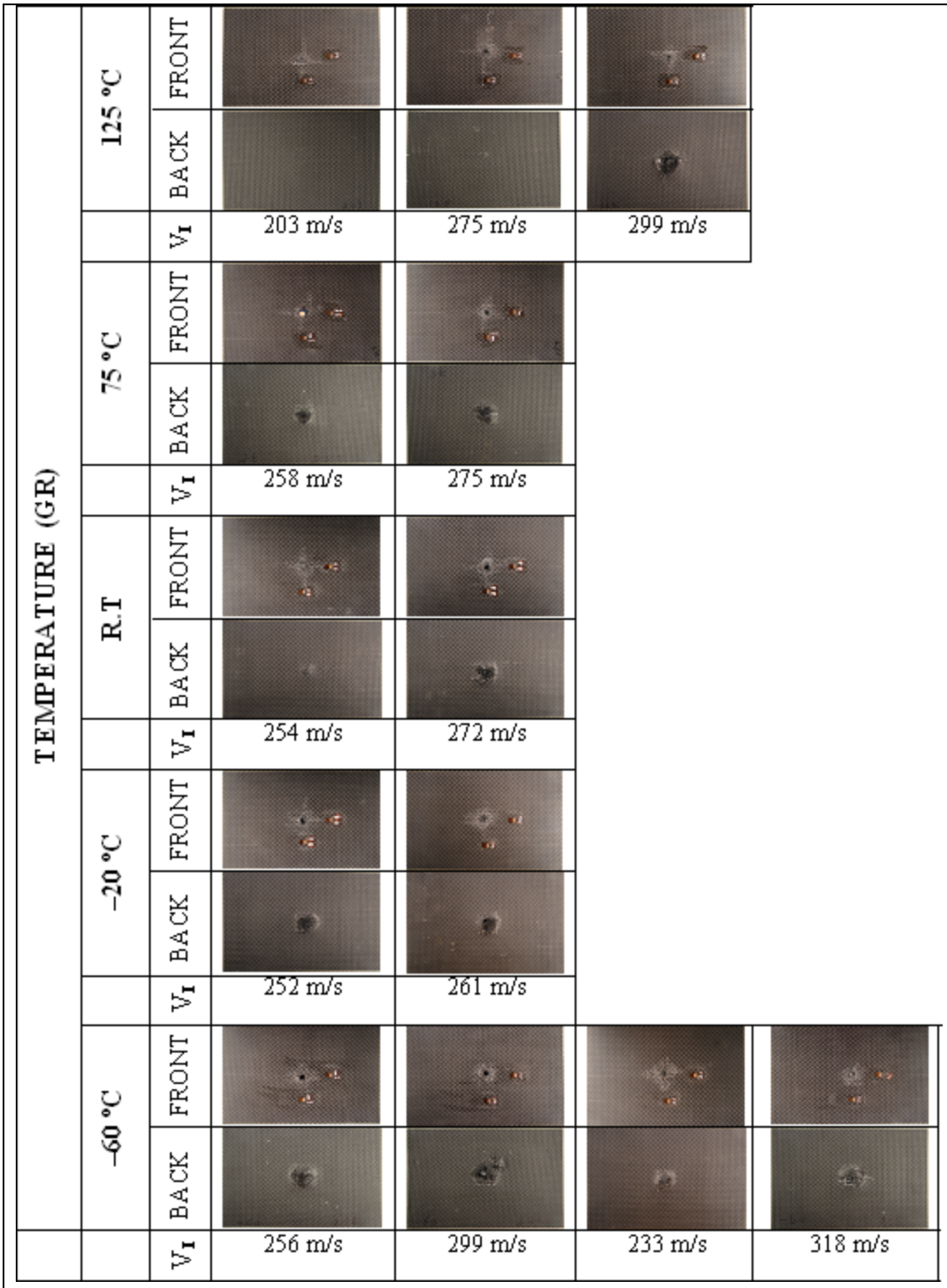

Figure 7.8 (b) Optical pictures of GR composite specimens after impact

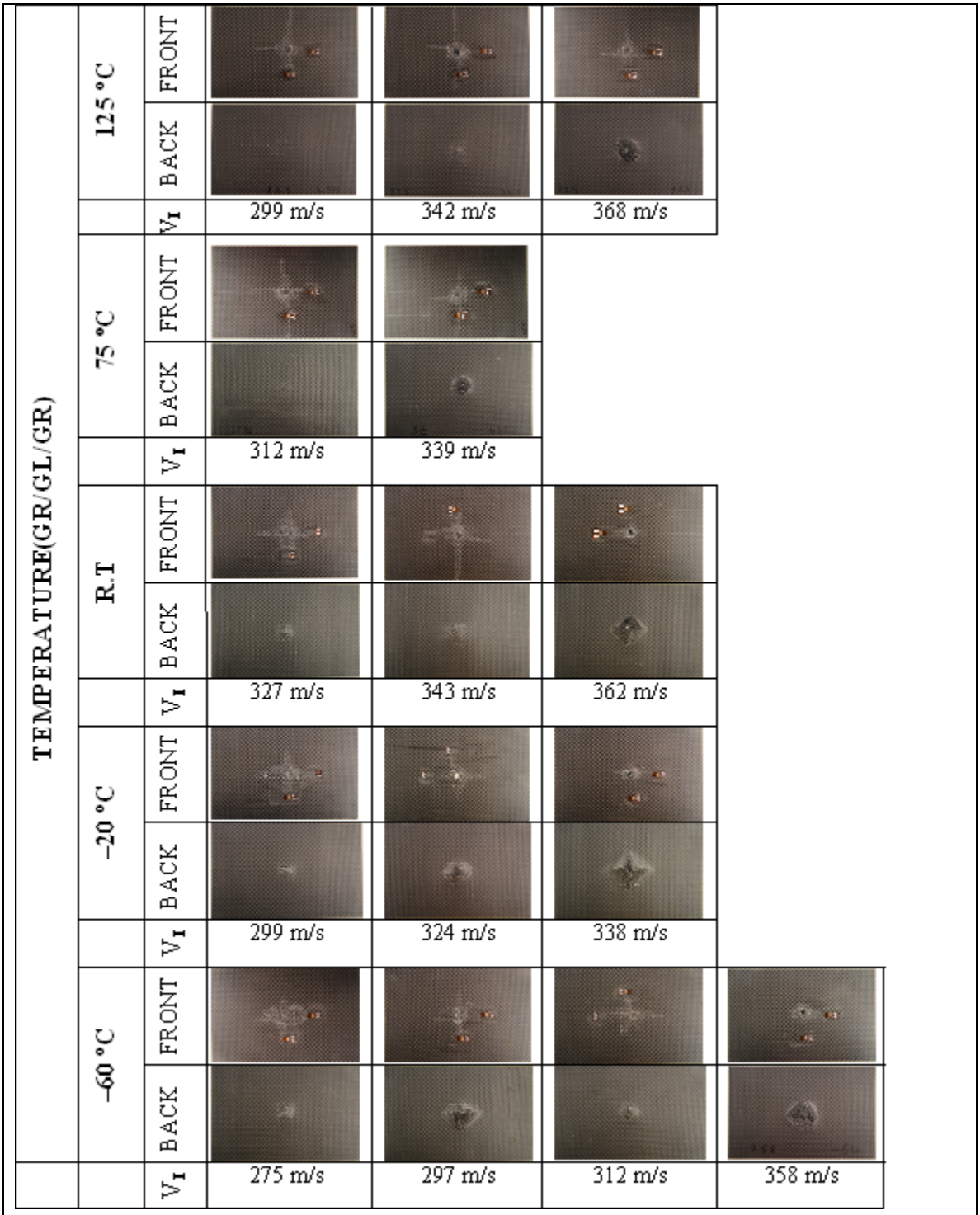

Figure 7.8 (c) Optical pictures of GR/GL/GR composite specimens after impact

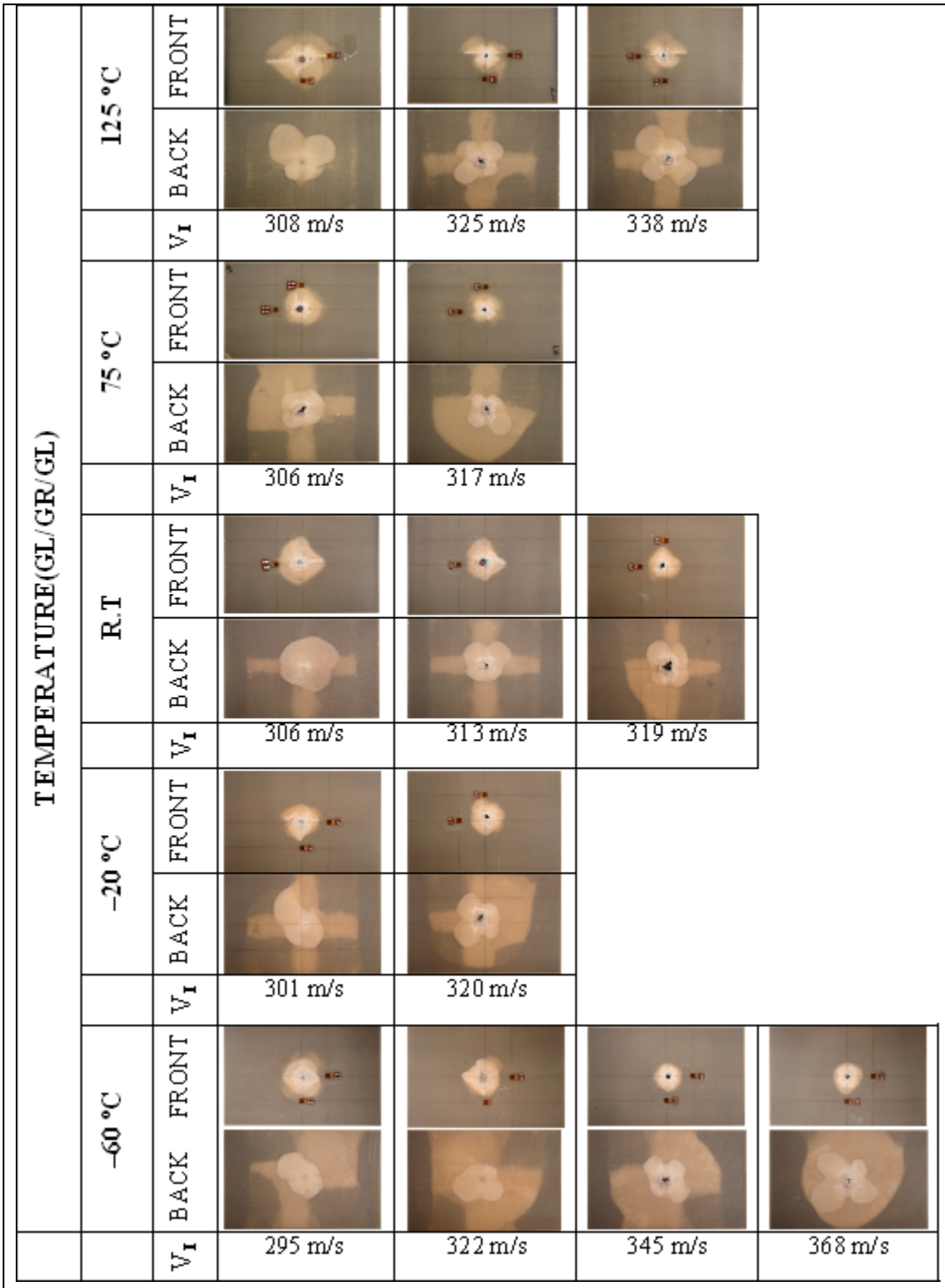

Figure 7.8 (d) Optical pictures of GL/GR/GL composite specimens after impact

In Figure 7.8(b) the optical pictures of GR are shown. It can be seen that even though there is partial penetration, almost all of the specimens had back splitting. This is due to

the brittle nature of the GR. Figure 7.8(c) shows the optical pictures of GR/GL/GR specimens. It can be seen that the behavior is similar to that of the GR specimens in terms of back splitting. In Figure 7.8(d) the internal delamination of the hybrid GL/GR/GL specimens can be easily seen. It can also be seen that there is less back splitting as compared to the GL and GL/GR/GL specimens. This is because the outer layer of this hybrid composite is GL which is ductile and can undergo larger deformations before fracture. In most of the pictures of the impact surface, micro buckling is seen; this is a form of energy absorption in the composite, however, it is usually considered as a secondary damage mechanism since the fibers require only small amount of energy to buckle.

(d) Delamination

Figures 7.9 a-d show the fractographs of layups of sectioned composites after ballistic impact conducted at various temperatures and velocities. For each temperature, two cross-sectional views are shown. The lower velocity is the maximum partial penetrating velocity and the higher velocity is the minimum perforating velocity obtained during the experiments. In Figure 7.9 (a) however, the bullet was stuck in the specimen for the partial penetration cases. Attempt to remove the bullet was not a trivial task and leads to increase delamination. Hence, for these cases where the bullet cannot be removed, only fractographs for the perforation velocities are shown.

The delamination of GL composites is shown in Figure 7.9 (a), where it is seen that the delamination area is smaller and much localized on the impact side and widens once it moves to the tension side of the composite. In the image that shows partial penetration at 75 ° C, it can be seen that there is a compressive zone right below the impact point.

The dark color of around the impact region is due to the diamond blade cutter. During the impact event, delamination propagation is usually of mode II type. In studies on delamination initiation and propagation on woven fabric composites, it has been observed that the delamination propagation is more along the fill and warp directions and less along the other directions. This is usually attributed to the difference in material properties in different directions. As a result, the delaminated area is quasi- lemniscate shape rather than circular. This shape is usually seen in C-scan images.

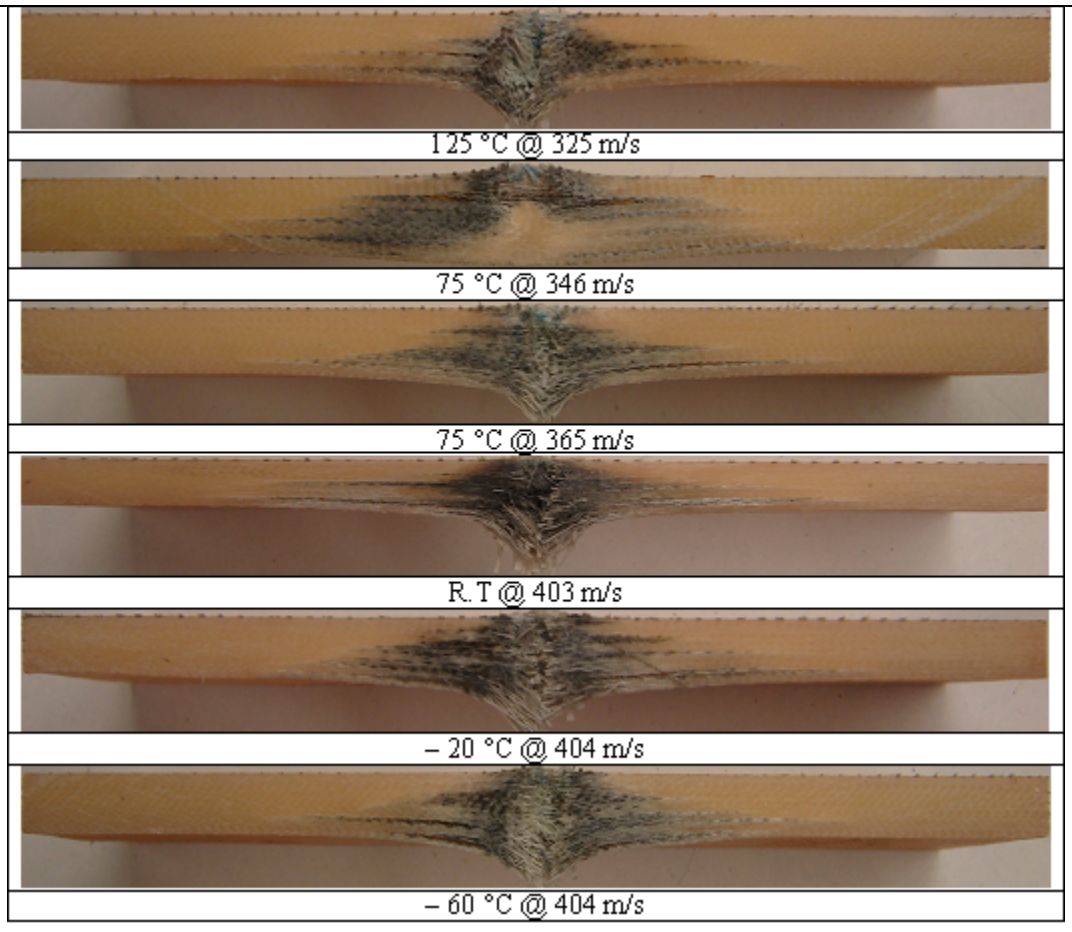

Figure 7.9 (a) Fractographs of sectioned GL composites after ballistic impact conducted at various test temperatures and also at perforating and partial penetrating velocities

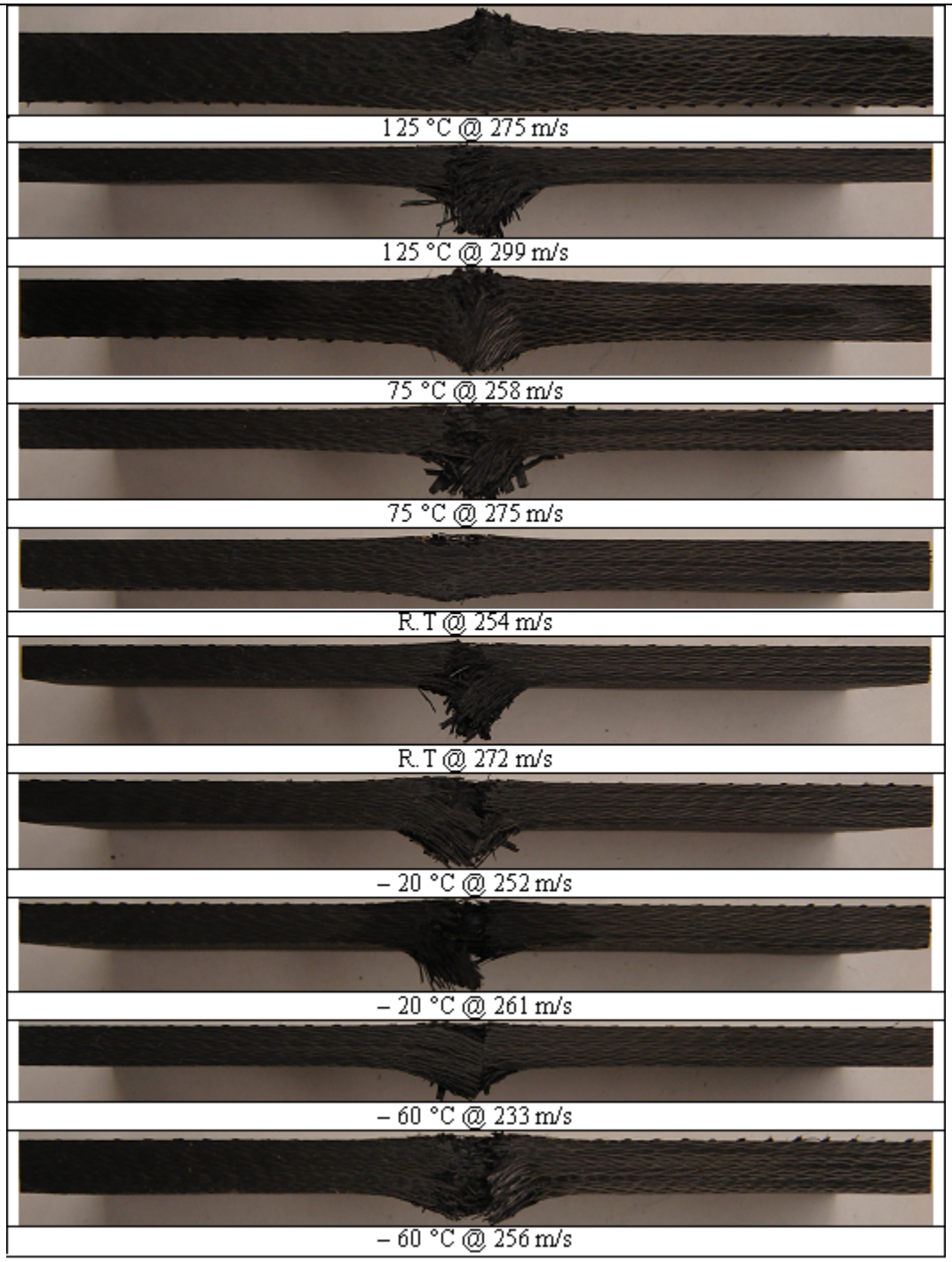

Figure 7.9 (b) Fractographs of sectioned GR composites after ballistic impact conducted at various test temperatures and also at perforating and partial penetrating velocities

Figure 7.9 (c) Fractographs of sectioned GL/GR/GL composites after ballistic impact conducted at various test temperatures and also at perforating and partial penetrating velocities

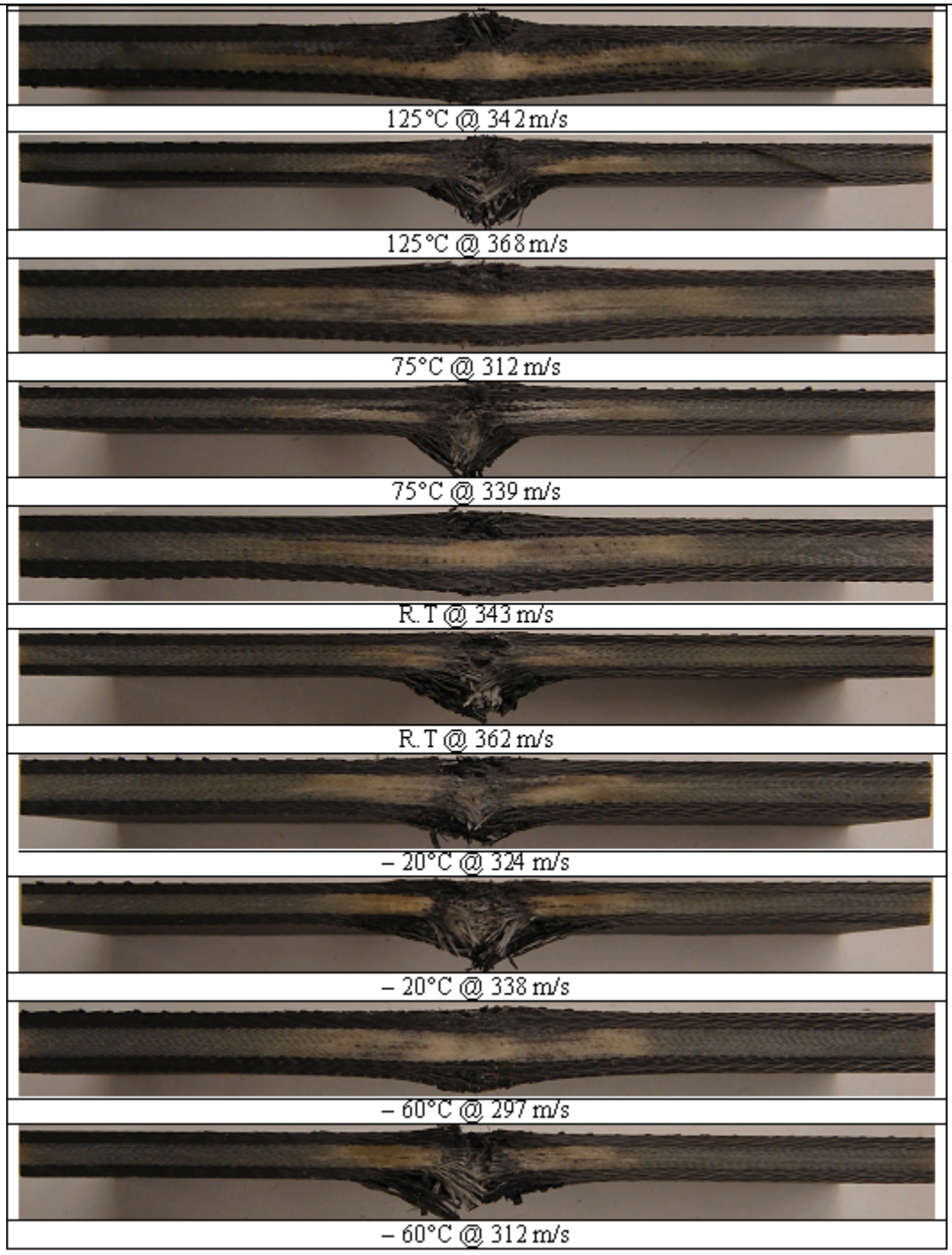

Figure 7.9(d) Fractographs of sectioned GR/GL/GR composites after ballistic impact conducted at various test temperatures and also at perforating and partial penetrating velocities

Delamination in GR specimens was much more localized and did not exhibit much spreading on the tension side (Fig.7.9 (b)). One quite interesting observation is that at low temperature, shear seems to be the dominant damage mechanism, while as the test temperature increases, this shear dominant damage mechanism seems to fade away and the GR composite specimens seem to fail similar to those of GL. One reason that may explain this behavior is, GL has high failure strain at high strain rate [101] while GR doesn't. Also at low temperature, GR is quite brittle and stiff while GL is more ductile.

Ballistic impact tests created quite extended delamination in hybrid composites especially at the interface of GL and GR layers (Fig.7.9.c-d). This may be due to greater incompatibility between dissimilar layers. Both hybrid composites delaminated more than non-hybrid composites. However splitting that occurred between hybrid layers was more severe in GL/GR/GL composite (Fig.7.9 (c)) compared to that in GR/GL/GR composites (Fig.7.9 (d)).

Figures 7.10 a-d show ultrasonic C-scans of the impacted composites. The C-Scans show that hybrid composites delaminated more than non-hybrid composites. Delamination in hybrid composites where GL was used as an outer skin was more pronounced compared to that in the other hybrid composites. All C-Scan images exhibited increased delamination up to the ballistic limit and gradual decrease was observed after this critical velocity.

In the non hybrid composites, it is interesting to observe that GR has a smaller delamination area than that of GL. Again this can be attributed to the fact that GR is quite brittle, hence its damage is more highly localized that the GL composites. This assumption is also supported by the observation that the delamination area of GR composite at low temperature is smaller than that observed at high temperature.

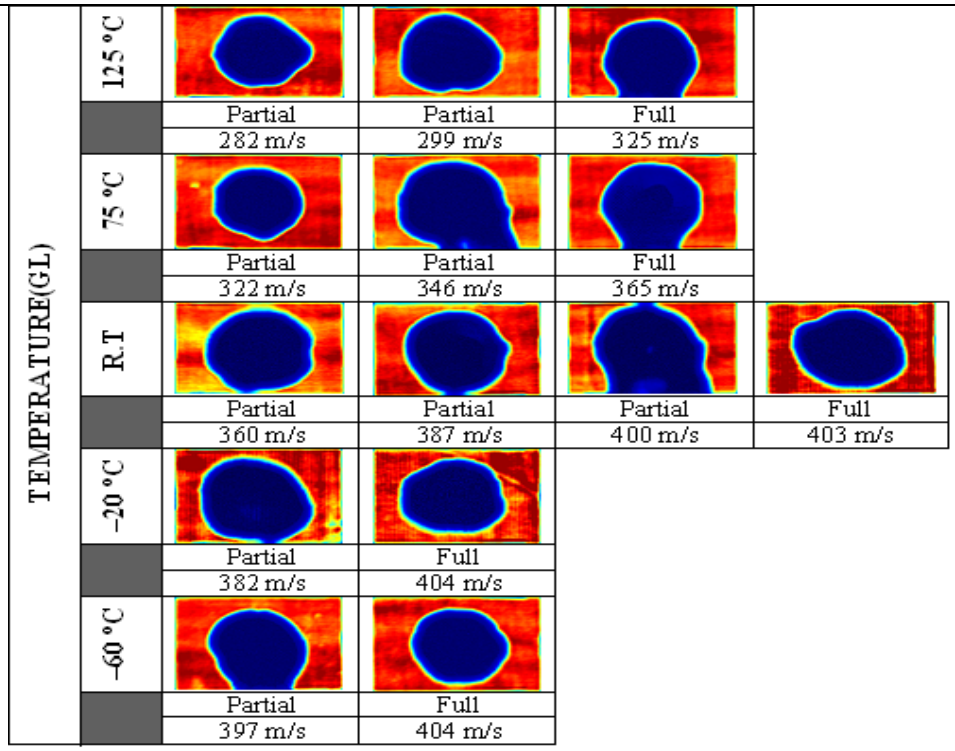

Figure 7.10 (a) Ultrasonic C-scan images of impacted GL composites at various test temperature and velocities

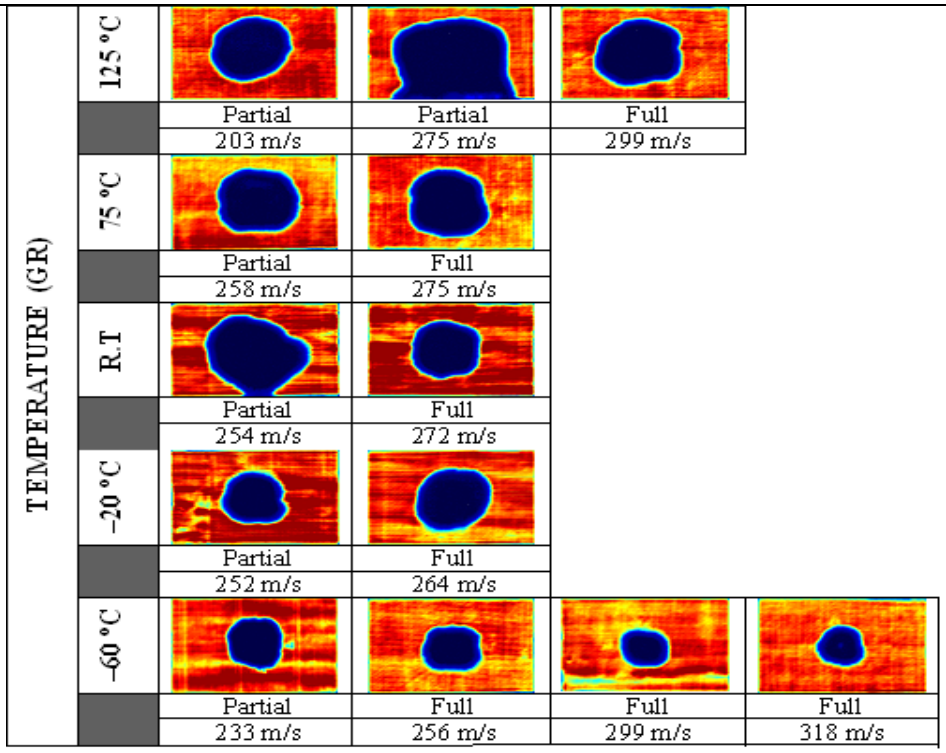

Figure 7.10 (b) Ultrasonic C-scan images of impacted GR composites at various test temperature and velocities

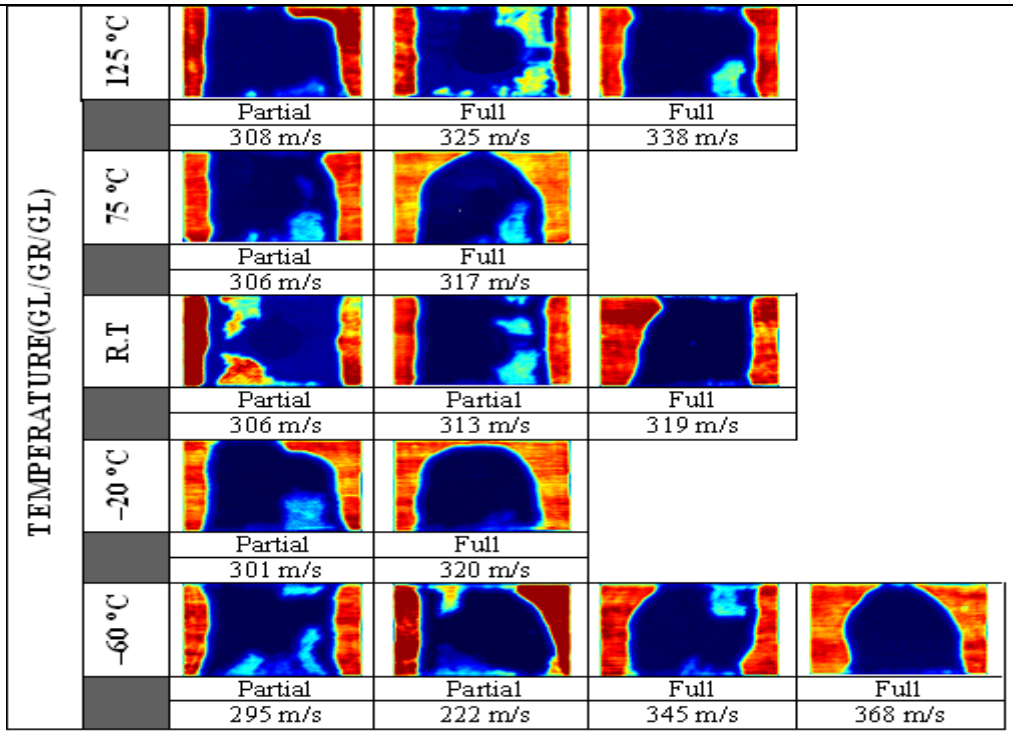

Figure 7.10 (c) Ultrasonic C-scan images of impacted GL/GR/GL composites at various test temperature and velocities

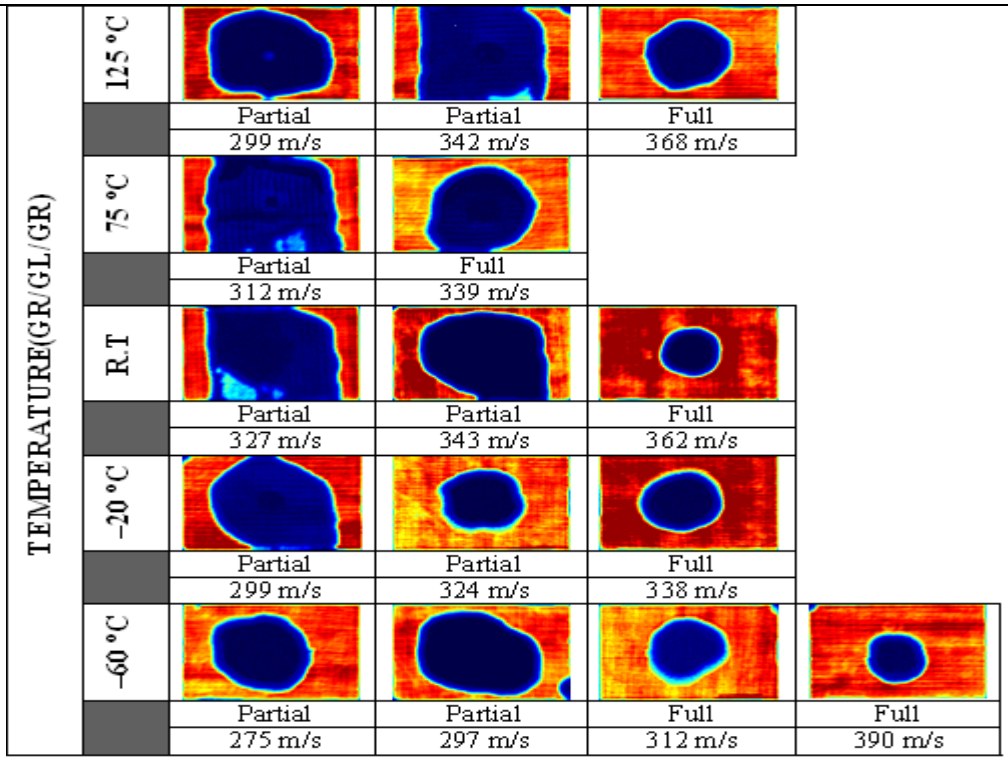

Figure 7.10 (d) Ultrasonic C-scan images of impacted GR/GL/GR composites at various test temperature and velocities

Looking back at the C-scan for low velocity impact, it can be seen that the delamination areas of GR composite were larger than those of GL specimens, whereas at high velocity impact this pattern is reversed. From this we can conclude that the damage mechanisms are not the same or do not follow the same order in high velocity and low velocity impact cases. Another conclusion that one can make is that the delamination area increases with an increased velocity to the ballistic limit, and then gradually decreases with an increase in impact velocity. The C-scan images can give estimation or a range of velocities for the ballistic limit (V_{50}) of the composite will be.

7.2 CONCLUSIONS FOR BALLISTIC IMPACT STUDIES

a) Temperature has an effect on the ballistic limit of both hybrid and non hybrid composites.

- As the temperature increases, the ballistic limit of GL composites decreases. The ballistic limit decreases severely as the test temperature increases from room to high temperature. At cryogenic temperatures, the change in temperature has only a very slight effect on the ballistic limit.
- As the test temperature increases, the ballistic limit of GR specimens increases.
- For hybrid GL/GR/GL composites, from – 20 °C to 125 °C, temperature has negligible effect on the ballistic limit. However at – 60 °C, the ballistic limit increases.
- For hybrid GR/GL/GR, the ballistic limit increases with an increase in test temperature with a drop in ballistic limit only at 75 °C.

b) After ballistic impact tests, specimens and projectile were examined and fiber shear out, shear plugging, delamination, matrix failure, fiber breakage and projectile deformation were observed.

c) From C-scan images and cross-sectional fractographs, larger delamination was seen in the hybrid composites. Also, among the non hybrids, the GR specimens had a smaller delamination area.

d) Delamination increased with increasing velocity for partial penetration cases. It then decreased with an increasing velocity for the full penetration cases.

e) The interval of the ballistic limit velocity can be estimated using ballistic tests and Ultrasonic C-Scans.

Chapter 8

Theoretical determination of thermal stresses in hybrid composites

In this study, specimens were tested at various temperatures. The specimens were soaked at this temperature for approximately thirty minutes before testing. This was done to reach a steady state test temperature so that the effect of any thermal gradient would not affect the results. In soaking the specimens, thermal stresses inevitably develop in the composite material. To accurately predict the behavior of the composite material using finite element analysis, these stresses need to be quantified and if large enough, should be incorporated in the analysis and all other calculations. Thermal stresses that develop in composite material due to temperature change can be classified in three categories. The first type of thermal stress is known as intralaminar stress which develops due to the difference in thermal expansion coefficients between the matrix and fiber materials. An approximate method was used to calculate these stresses. They were found to be negligible and hence neglected. The second type of stress is known as interlaminar stress and is due to the difference in expansion coefficients between the different layers of the composite material (hybrid GL/GR/GL and GR/GL/GR in this case). In this chapter, classical lamination theory was used to determine the interlaminar thermal stresses and if necessary, they will be included in the analysis. The third and final type of thermal stress is known as global (skin-core) stress. This is due to the thermal gradient that may exist in the material during testing. In this case, since the composite is soaked for thirty minutes until this gradient vanishes, the global stress has no effect on the material response and will be neglected.

8.1 Formulation and solution technique for intra laminar stresses

During soaking of the composite at elevated and low temperatures for testing, one type of thermal stress that is developed is known as intra laminar stress. This is the stress that develops in a single lamina and is due to the difference in thermal expansion between fibers and matrix materials. An attempt is made here to estimate this intra laminar stress by making a few simplifying assumptions. If this stress is small it will be neglected from all further analysis.

Procedure used for the estimation of intra laminar thermal stress

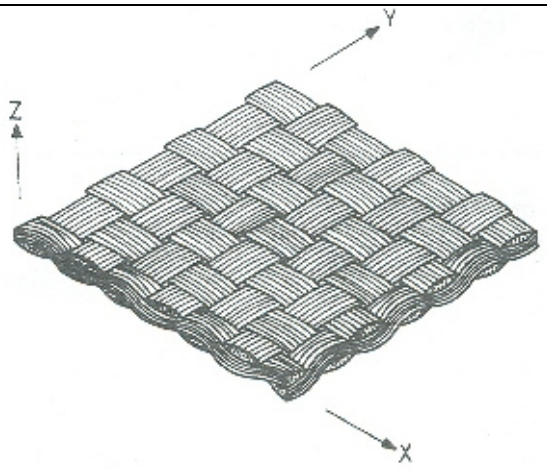

Figure 8.1 Plain weave fabric structure

In Figure 8.1, a plain weave fabric structure is shown. The basic idea here is to take a unit cell of this fabric as shown in Figure 8.2, where‘t’ represents the thickness of the lamina (fiber and matrix) and ‘t_f’ represents the thickness of the fabric alone.

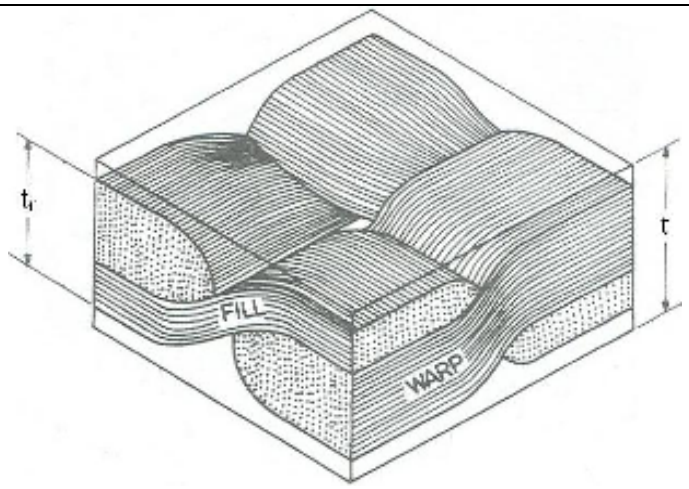

Figure 8.2 A unit cell plain weave fabric lamina

The first simplifying assumption is similar to that of the mosaic model for analyzing woven composites, i.e. neglecting fiber undulation or waviness.

If we were to neglect this undulation then we would have four little squares of cross ply of fibers, lying beside each other forming a square, covered by a sheet of matrix material at the top and bottom as shown in figure 8.3.

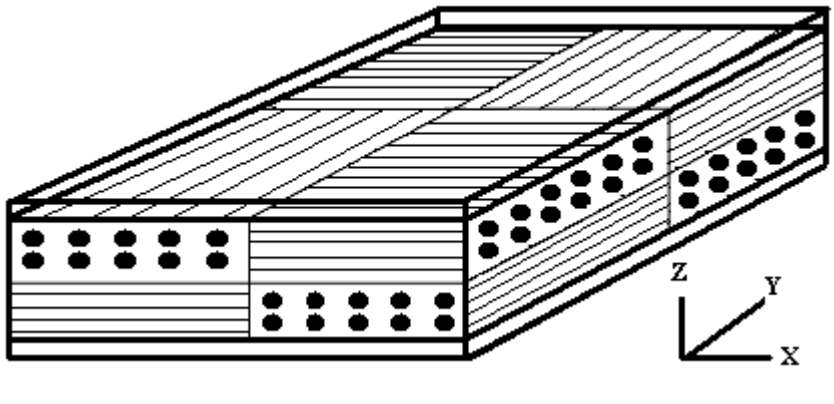

Figure 8.3 Fiber idealization sandwiched by matrix

In order to calculate the thermal stress in the composite layer, it is assumed that the two layers have the same material properties in the 'X' and 'Y' directions, and the two layers can be combined into a single layer.

Since the fiber volume fraction in the composite used in this research is 60%, it can be said that each layer of the composite is made up of 60% fibers and 40% matrix material. Figure 8.4 shows the proportion of fiber and matrix contribution in the thickness (t) of a lamina

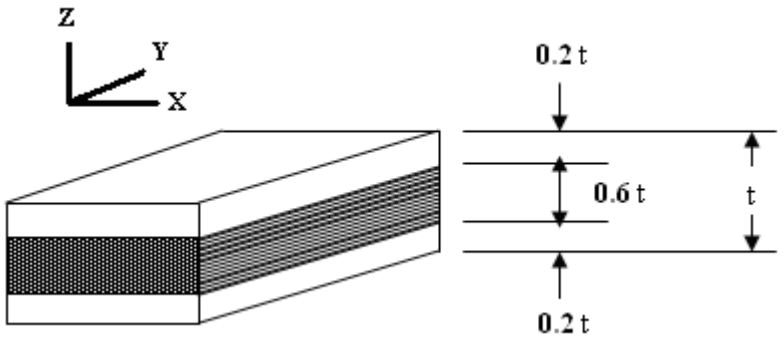

Figure 8.4 Idealized unit cell from a lamina

If the temperature changes by ΔT in the lamina shown in figure 8.4, we can derive the relationship of the stresses in the fiber and matrix layers.

From equilibrium equation:

$$\sigma_M \times \frac{t}{5} + \sigma_F \times \frac{3t}{5} + \sigma_M \times \frac{t}{5} = 0$$

$$\frac{2\sigma_M}{5} + \frac{3\sigma_F}{5} = 0$$

Therefore, $\sigma_M = -\frac{3}{2}\sigma_F$ (1)

where σ_M is the stress in the matrix and σ_F is the stress in the fibers

The total strain in each layer is as follows:

$$(\varepsilon_1)_M = \frac{1}{E_M}\left[\sigma_M - (\nu)_M \sigma_M\right] + \alpha_M \Delta T \quad (2)$$

$$(\varepsilon_1)_F = \frac{1}{E_F}\left[\sigma_F - (\nu)_F \sigma_F\right] + \alpha_F \Delta T \quad (3)$$

Assuming that the fiber and the matrix deform together (i.e. $(\varepsilon_1)_M = (\varepsilon_1)_F$**) and using eq. (1),**

$$\frac{1}{E_M}\left[\sigma_M - (\nu)_M \sigma_M\right] + \alpha_M \Delta T = \frac{1}{E_F}\left[\sigma_F - (\nu)_F \sigma_F\right] + \alpha_F \Delta T$$

$$(\alpha_M - \alpha_F)\Delta T = \sigma_F\left[\frac{1-(\nu)_F}{E_F} + \frac{3\left(1-(\nu)_M\right)}{2E_M}\right]$$

$$\sigma_F = \frac{(\alpha_M - \alpha_F)\Delta T}{\left[\frac{1-(\nu)_F}{E_F} + \frac{3\left(1-(\nu)_M\right)}{2E_M}\right]} \quad (4)$$

Equation (4) can be used to approximate the thermal intra laminar stress developed in the fabric of the composite layers during soaking of the specimen. Since the fabric carries most of the load we are more interested in the stress developed in it, and therefore will calculate the approximate stress in the fabric. Table 8.1 shows the material properties that are used in the calculations. Since the stresses in the fabric are of greater interest, they are calculated at the various test temperatures and shown in Table 8.2. These stresses are then compared to the composites' ultimate tensile strength (UTS). It can be seen that the intra laminar stresses are negligible compared to the UTS, hence they will be neglected in future analysis.

Table 8.1 Material property for matrix and fibers

Properties	SC-79 Epoxy	S-2 Glass	IM-Graphite
Elastic Modulus (GPa)	3	86.9	276 (12-transverse)
Poisson's Ratio	0.42	0.22	0.25
CTE ($\times 10^{-6}$ °C^{-1})	45	1.6	-0.396 (21.6-transverse)

Table 8.2 Intra laminar stresses induced in fibers at different test temperatures

Material	Temperature (ºC)	Theoretical (MPa)	Experimental (MPa)	% of UTS
Glass	– 60	– 12.33	469.1	2.6
	– 20	– 6.53	443.0	1.4
	R.T	0	426.8	0
	75	7.25	342.2	2.1
	125	14.51	325.9	4.4
Graphite	– 60	– 13.18	633.4	2.0
	– 20	– 6.98	627.7	1.1
	R.T	0	614.3	0
	75	7.75	586.4	1.3
	125	15.5	544.1	2.8

8.2 Formulation and solution technique for inter laminar stresses

Here the thermal stresses developed in the hybrid composite (GL/GR/GL) were calculated using the classical lamination theory.

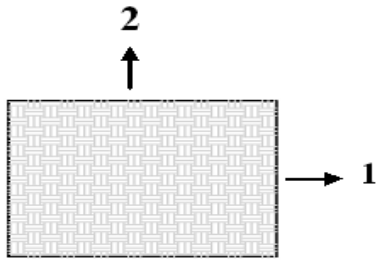

Fig 8.5 Top view of hybrid composite with defined coordinate axes

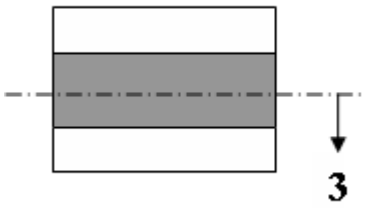

Fig 8.6 Transverse section of the woven hybrid composite

In Figures 8.5 and 8.6 above, the specimen coordinates are shown. For woven composites, the 1 direction here is referred to as the fill direction, the 2 direction is referred to as the warp direction, and the 3 direction is the thickness direction. The thermal expansion coefficients for the non hybrid composites were determined experimentally as follows:

For Non-Hybrid Glass
$\alpha_1 = \alpha_2 = 7.1 \times 10^{-6}$ 1/°C

For Non-Hybrid Graphite
$\alpha_1 = \alpha_2 = 3.38 \times 10^{-6}$ 1/°C

Table 8.3 gives a summary of the material properties obtained experimentally and which will be used in determining the thermal stresses:

Table 8.3 Material properties used in determining the interlaminar stresses

Composite	Test Temperature	$E_1=E_2$ (GPa)	σ_{max} (MPa)	G_{12} (GPa)	ν_{12}	$\nu_{13}=\nu_{23}$
Non- Hybrid GL	–60 °C (–76 °F)	19.395	469.12	2.980	0.152	0.370
	–20 °C (–4 °F)	18.927	443.02	2.785	0.145	0.361
	R T (R T)	17.047	426.80	2.742	0.13	0.41
	75 °C (167 °F)	16.139	342.32	1.893	0.128	0.436
	125°C (257 °F)	15.038	286.00	1.444	0.121	0.453
Non- Hybrid GR	–60 °C (–76 °F)	43.820	633.39	3.975	0.140	0.382
	–20 °C (–4 °F)	43.715	627.74	3.935	0.129	0.462
	R T (R T)	42.559	614.26	3.080	0.121	0.427
	75 °C (167 °F)	41.497	585.40	1.998	0.116	0.627
	125°C (257 °F)	40.392	544.11	1.670	0.099	0.649

In performing the calculations, the following assumptions were made:

1) The laminae are orthotropic with $E_1=E_2$, therefore $\nu_{12}=\nu_{21}$
2) The composite is stress-free at room temperature
3) The laminate is symmetric
4) There is no external mechanical load applied to the composite during thermal loading

For the laminae considered here, the transformed reduced stiffnesses $\overline{Q}_{ij}$ are the same as the reduced stiffness matrix Q_{ij} and were calculated using the following formulas:

$$Q_{11}=\frac{E_1}{1-\nu_{12}\nu_{21}}, Q_{12}=Q_{21}=\frac{\nu_{12}E_2}{1-\nu_{12}\nu_{21}}=\frac{\nu_{21}E_1}{1-\nu_{12}\nu_{21}}, Q_{22}=\frac{E_2}{1-\nu_{12}\nu_{21}} \text{ and } Q_{66}=G_{12}$$
$$Q_{16}=Q_{61}=Q_{62}=Q_{26}=0$$

where G_{12} is the shear modulus of the non hybrid material,

The extensional stiffnesses, A_{ij} were then computed using the formula,

$$A_{ij} = \sum_{k=1}^{N} (\overline{Q}_{ij})_k (z_k - z_{k-1}),$$

where 'z' is the coordinate in the thickness direction.

From known values for the thermal expansion coefficients α, temperature change ΔT, and reduced stiffnesses $\overline{Q}_{ij}$, the thermal forces in the composite laminate can easily be calculated using the formula,

$$\begin{Bmatrix} N_x^T \\ N_y^T \\ N_{xy}^T \end{Bmatrix} = \int \begin{bmatrix} \overline{Q}_{11} & \overline{Q}_{12} & \overline{Q}_{16} \\ \overline{Q}_{21} & \overline{Q}_{22} & \overline{Q}_{26} \\ \overline{Q}_{61} & \overline{Q}_{62} & \overline{Q}_{66} \end{bmatrix}_k \begin{Bmatrix} \alpha_x \\ \alpha_y \\ \alpha_{xy} \end{Bmatrix} \Delta T \, dz .$$

The mid surface strains were then calculated for the hybrid laminate using,

$$\begin{Bmatrix} \varepsilon_x^0 \\ \varepsilon_y^0 \\ \gamma_{xy}^0 \end{Bmatrix} = \begin{bmatrix} A_{11} & A_{12} & A_{16} \\ A_{21} & A_{22} & A_{26} \\ A_{61} & A_{62} & A_{66} \end{bmatrix}^{-1} \begin{Bmatrix} N_x^T \\ N_y^T \\ N_{xy}^T \end{Bmatrix}$$

Then, the stresses in the k^{th} layer of the laminate can be computed as:

$$\begin{Bmatrix} \sigma_1 \\ \sigma_2 \\ \tau_{12} \end{Bmatrix}_k = \begin{bmatrix} Q_{11} & Q_{12} & Q_{16} \\ Q_{21} & Q_{22} & Q_{26} \\ Q_{61} & Q_{62} & Q_{66} \end{bmatrix}_k \begin{Bmatrix} \varepsilon_1 - \alpha_1 \Delta T \\ \varepsilon_2 - \alpha_2 \Delta T \\ \gamma_{12} \end{Bmatrix}_k$$

Following this procedure the thermal stress buildup in the hybrid composite, i.e. GL/GR/GL was calculated for the different test temperatures and the results are shown in Table 8.4.

Table 8.4 Interlaminar thermal stresses in plain weave 0°/90° hybrid composite

Temperature	Stress (MPa) 0°/90°		Stress (MPa) ±45°	
–60 °C (–76 °F)	GL layer	–5.36	GL layer	–5.36
	GR layer	5.36	GR layer	5.36
–20 °C (–4 °F)	GL layer	–2.68	GL layer	–2.68
	GR layer	2.68	GR layer	2.68
R T (R T)	GL layer	0	GL layer	0
	GR layer	0	GR layer	0
75 °C (167 °F)	GL layer	2.25	GL layer	2.25
	GR layer	–2.25	GR layer	–2.25
125°C (257 °F)	GL layer	4.44	GL layer	4.44
	GR layer	–4.44	GR layer	–4.44

8.3 Conclusion

It can be concluded that the intra laminar and interlaminar thermal stresses developed in the non-hybrid and hybrid composites respectively, during soaking are negligible when compared to the ultimate tensile strength of the material (less that 5%). For this reason, the intra laminar and interlaminar thermal stresses will be neglected in the finite element modeling and all other calculations. Due to steady state temperature during testing, the skin-core thermal stresses are also assumed to be zero, and thus will not be taken into consideration in any modeling and analysis.

Chapter 9

Finite Element Analysis

Finite element analysis (FEA) is a very useful tool in solving complex problems and also predicts the behavior of structures when actual testing may not be cost effective or practical. In this study, low velocity and ballistic impact problems at various temperatures are modeled and analyzed using the finite element software, LS-DYNA. To validate the reliability of the model, the finite element results will be compared to those obtained experimentally. These results include strain-time histories, damage patterns, and in the event of low velocity impact, stiffness, contact force and energy. If the model is valid, it will be assumed that it can be used to predict the behavior of composites under different loading conditions.

9.1 Finite element modeling of experiment

Since the geometries of the composite plate, bullet and impactor are all symmetric, it is customary that only a quarter of these parts be modeled to save computational time. Therefore, in these simulations only a quarter of the geometry will be modeled. All the parts will be modeled using 8-node solid elements.

9.1.1 Material Models

(a) MAT_ELASTIC (MAT_001): In the modeling of the impactor, the elastic material model was used. The choice of elastic model was due to the fact that the impactor stiffness was much greater than that of the specimen. In this case, no deformation is expected of the impactor but in the event of deformation, it will be elastic. So the choice of an elastic impactor seems appropriate. The choice of the more conventional rigid

material model was not chosen for the impactor because in a rigid impactor, there is assumption of no deformation. This means that no energy is used up in elastically deforming the impactor and also the resulting displacement of the impactor will be less accurate that of an elastic impactor. In using MAT_ELASTIC, the required input material properties for impactor are Young's' modulus, Poisson's ratio and material density.

(b) MAT_COMPOSITE_DAMAGE (MAT_022): In modeling the composite plate, MAT_022 also called the Chang-Chang composite damage model was used. This model is an orthotropic material model with optional brittle failure for composites. From tensile testing of GL, GL/GR/GL, GR/GL/GR and GR, it can be seen that especially at high temperatures, the material behavior is non-linear. In order to use MAT_22 (best suited to describe a linear elastic behavior), we use the idea of strain energy. Here we calculate the strain energy from the non linear stress strain behavior. Knowing the strain energy and the initial Young's modulus, a new linear stress-strain curve is redrawn where the strain energy and Young's modulus is maintained but the failure strain and ultimate stress are changed. Figure 9.1 shows an example of the approximation of the true stress-strain curve for a given material. The approximate curve was inputted in LS-DYNA instead of the true curve. It can be seen that in the approximate curve the ultimate strength of the material is higher and its failure strain is lower. This serves us well, since as the strain rate increases, the material behavior becomes more brittle and the ultimate strength increases. Since drop weight is at a higher strain rate relative to tensile testing, the approximate curve is assumed to be somewhat a better representation of the stress-strain behavior than the tensile testing curve, since tensile testing was done at low strain rate.

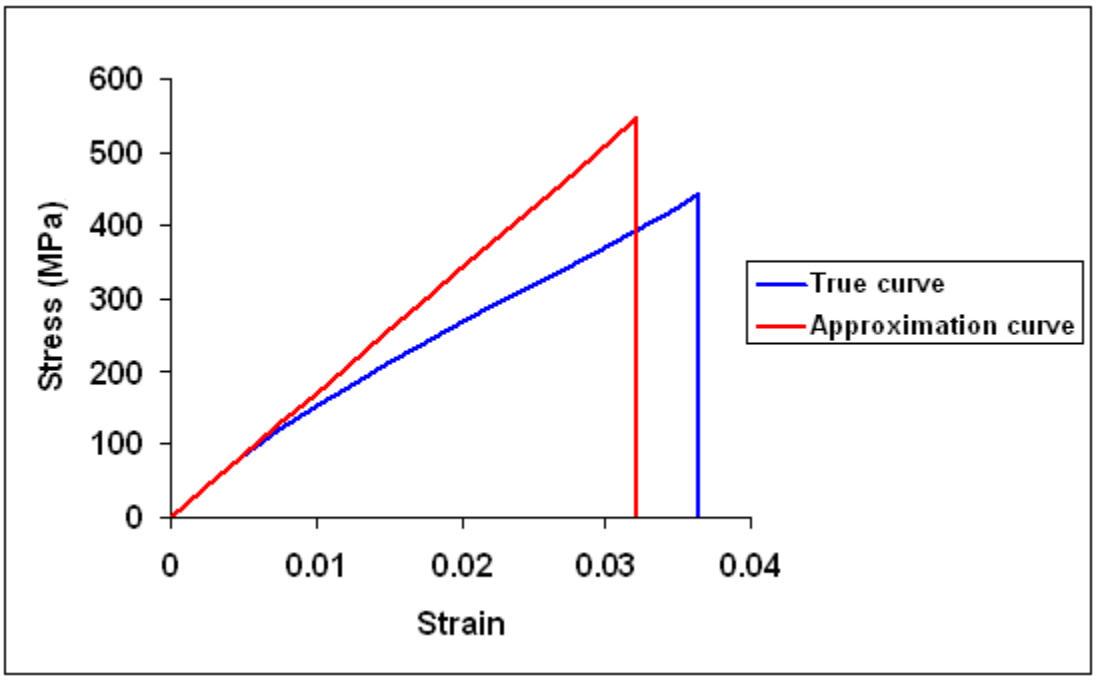

Figure 9.1 Linearization of non linear stress-strain curve obtained from tensile testing while maintaining the same strain energy

In the Chang-Chang model five material parameters are used (in three possible failure criteria):

S_1 = Longitudinal tensile strength

S_2 = Transverse tensile strength

S_{12} = Shear strength

C_2 = Transverse compressive strength

α = Non linear shear stress parameter

Here, S_1, S_2, S_{12}, and C_2 are obtained from material strength measurements and α is defined by a material shear stress-strain measurement.

The three failure criteria used are matrix cracking, fiber breakage and compressive failure.

(1) Matrix cracking:

$$F_{matrix} = \left(\frac{\sigma_2}{S_2}\right)^2 + \bar{\tau} \qquad \text{where } \bar{\tau} = \frac{\frac{\tau_{12}^2}{2G_{12}} + \frac{3}{4}\alpha\tau_{12}^4}{\frac{S_{12}^2}{2G_{12}} + \frac{3}{4}\alpha S_{12}^4}$$

here σ_2 is the tensile stress in the transverse direction whereas τ_{12} is the in-plane shear stress between fibers and matrix. Failure is assumed whenever $F_{matrix} > 1$. Once this type of failure occurs, the material constants E_2 (Young's modulus in the transverse direction), G_{12} (in-plane shear modulus in the 1-2 plane), ν_{12} and ν_{21} (generalized Poisson's ratios in the 1-2 plane) are set to zero.

(2) Compressive failure:

$$F_{comp} = \left(\frac{\sigma_{12}}{2S_{12}}\right)^2 + \left[\left(\frac{C_2}{2S_{12}}\right)^2 - 1\right]\frac{\sigma_2}{S_2} + \bar{\tau} \qquad (6.3)$$

Failure is assumed when $F_{comp} > 1$. When this type of failure occurs, the material constants E_2, ν_{12} and ν_{21} are all set to zero.

(3) Fiber breakage:

$$F_{fiber} = \left(\frac{\sigma_1}{S_1}\right)^2 + \bar{\tau}$$

where σ_1 is the tensile stress in the longitudinal direction. Failure occurs when F_{fiber} >1. After fiber breakage, E_1 (Young's modulus in the longitudinal direction), E_2, G_{12}, ν_{12} and ν_{21} are all set to zero.

(c) MAT_PLASTIC_KINEMATIC (MAT_003): This model is used for isotropic and kinematic hardening plasticity with the option of including rate effects. E_t is the slope of the second arm of the bilinear stress strain curve (Fig.9.2) and l_o and l are undeformed and deformed lengths of uniaxial tension specimen respectively. This material was used for the 22 caliber copper bullet.

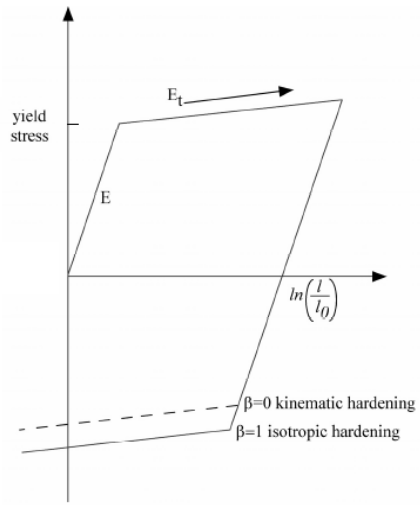

Figure 9.2 Elastic-plastic behavior with kinematic and isotropic hardening. (Picture is taken from LS-DYNA theoretical manual).

MAT_ADD_EROSION (MAT_00). This failure criterion was added to all the materials used in our modeling although it is used mostly for material models which do not have a failure or erosion criterion. It is basically an additional criterion which when satisfied, the element is deleted from the calculation. It is a good tool to use when comparison is needed between animation and real specimen.

9.1.2 Contact and delamination Model

The contact between the composite layers was defined using the option, CONTACT_AUTOMATIC_SURFACE_TO_SURFACE_TIEBREAK. By using this contact definition, delamination between the composite layers is governed by the criterion: $\left[\frac{\max(0,\sigma_n)}{NFLS}\right]^2+\left(\frac{\sigma_s}{SFLS}\right)^2\geq 1$

where σ_n and σ_s are normal and shear stresses acting on the layer interface, respectively, while *NFLS* and *SFLS* are normal and shear failure strengths of interface, respectively. It is assumed that delamination occurs mainly by shear failure; hence, *NFLS* is set to a very large number so delamination in the model is controlled by *SFLS*. Since SFLS was not obtained experimentally, it was varied in order to fit experimental results. It was found that 70MPa between GR and GL layers and a range of 90-120MPa between GL-GL and GR-GR layers give good results.

Additionally, ERODING_SURFACE_TO_SURFACE contact model was used between the impactor and the composite. This model allows elements to be eroded when certain failure criteria are met. In this study a strain-based failure criterion was used for element erosion elements; that is, when $\varepsilon \geq \varepsilon_{\text{erosion}}$, the element was eroded and removed from

calculation. The contact and delamination models as well as the erosion option were used for all the composites.

9.2 Boundary Conditions

To model the impact event properly, correct boundary conditions should be chosen. Preliminary simulations were carried out, and it was determined that a fixed-fixed boundary condition was best suited to model the low velocity impact.

9.3 Finite element simulations for low-velocity impact tests

9.3.1 Effect of Temperature on the low velocity impact response of woven composites

Figure 9.3 shows the mesh of a quarter model of the plate used in simulating the drop-weight impact test. Fine mesh was used around the center which is the critical location while coarse mesh was used away from center. One advantage of this is to reduce computation time.

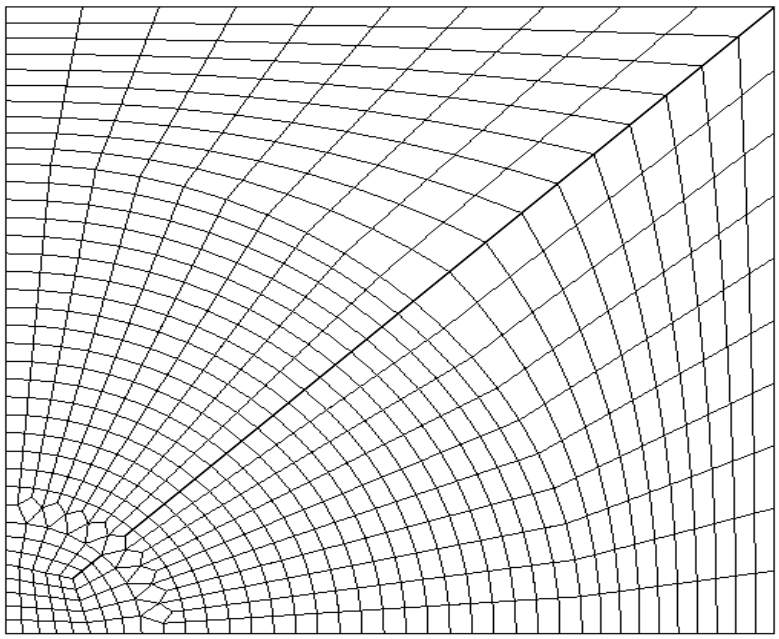

Figure 9.3 Quarter model of meshed plate used in drop impact simulation

Figure 9.4 shows the entire drop weight model of both the composite panel and the impactor for a non hybrid specimen for low velocity impact.

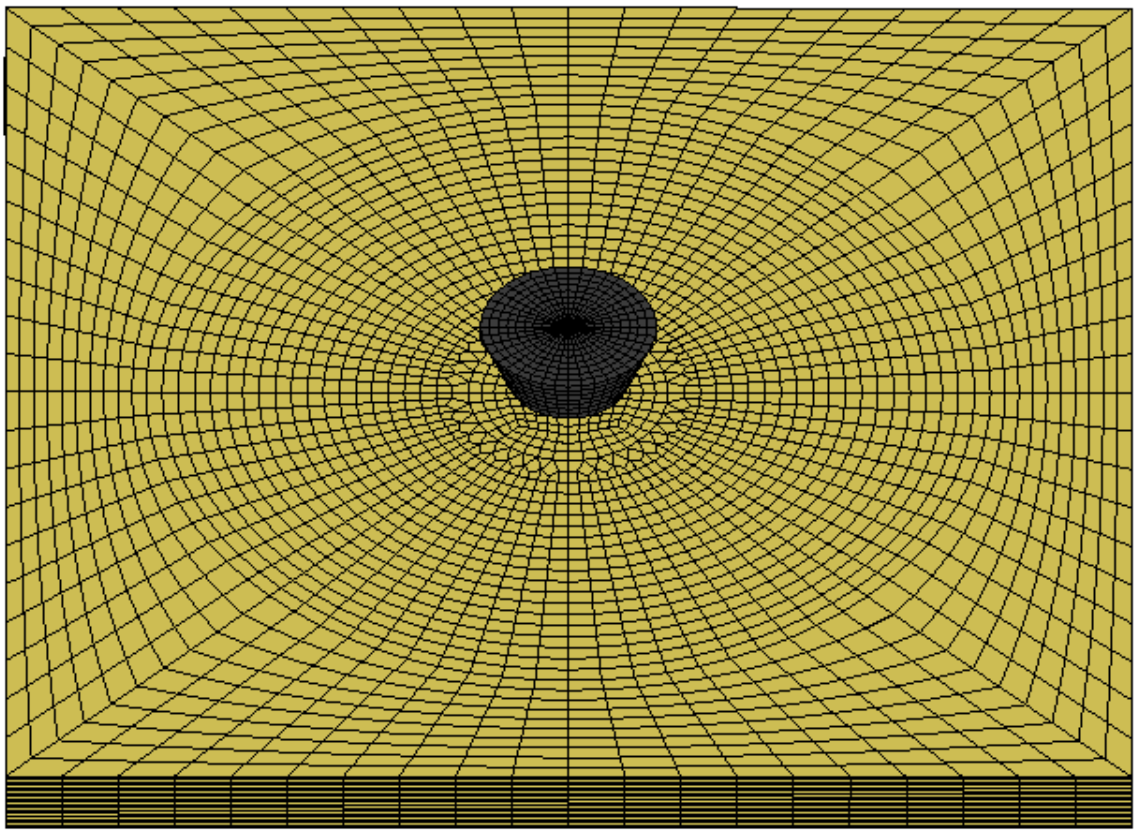

Figure 9.4 Mesh of the entire composite plate and impactor for low velocity impact

Figure 9.5 shows the LS-DYNA finite element meshes used simulating drop-weight impact onto (a) a woven non hybrid composite (b) a woven hybrid composite. In the models, 18 layers were used for GL, 14 layers for GR and 16 layers for the hybrid composite.

(a) Comparison of Force-Time histories

In obtaining experimental data from the Dynatup 930-I data acquisition system, only the contact force i.e. resistive force of the specimen vs. time and initial impact velocity (just

prior to impact) is directly measured. Therefore, it can be said that the most accurate and valuable date obtained from the Dynatup 930-I data acquisition system would be the force-time histories. Simulations were done for all four layups of composites at all test temperatures. Since the number of simulations turns out to be twenty, and the correlation of results with experiments is good, only simulation and experimental results for the highest and lowest test temperatures will be presented i.e. for 125 °C and –60°C, respectively.

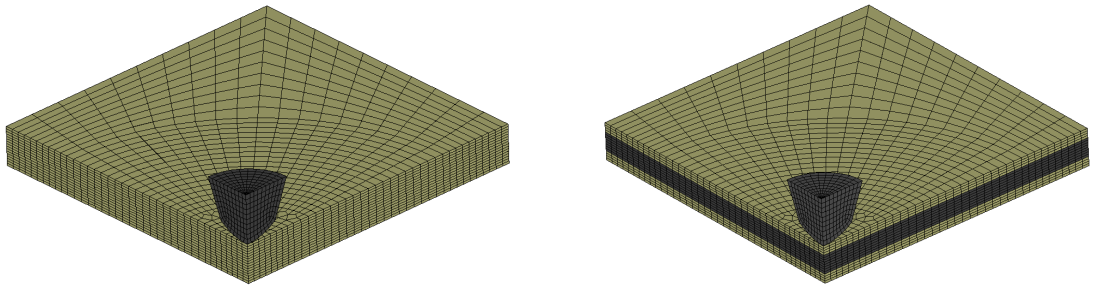

(a) (b)

Figure 9.5 Finite element simulation models. (a) Drop-weight impact model for the non hybrid specimen (b) Drop-weight impact model for the hybrid specimen

In Figure 9.6, the force-time histories of the impact tests conducted on all four layups of composite specimens at 125 °C were compared with FE simulations. The FEM and experimental force-time histories show good agreement. It can be observed that for the force-time histories of GL composite the contact duration matched very well however there was more oscillation in the curve after initiation of delamination for the simulation results compared to the experiment. The contact duration matches also quite well for the hybrid composites, however, the initiation of delamination seems to be delayed in the FEM simulation when compared to experimental results. Also the FEM simulation

produced a little higher value for the contact force. Predicted force-time histories of GR composites showed a contact duration that is smaller than that obtained experimentally. Also, the predicted contact force was a little larger than that obtained from experiments. The initial peak of force predicted from the FEM model is higher that the experimental value for the GL and the hybrid composites, but matches very well for the GR specimens.

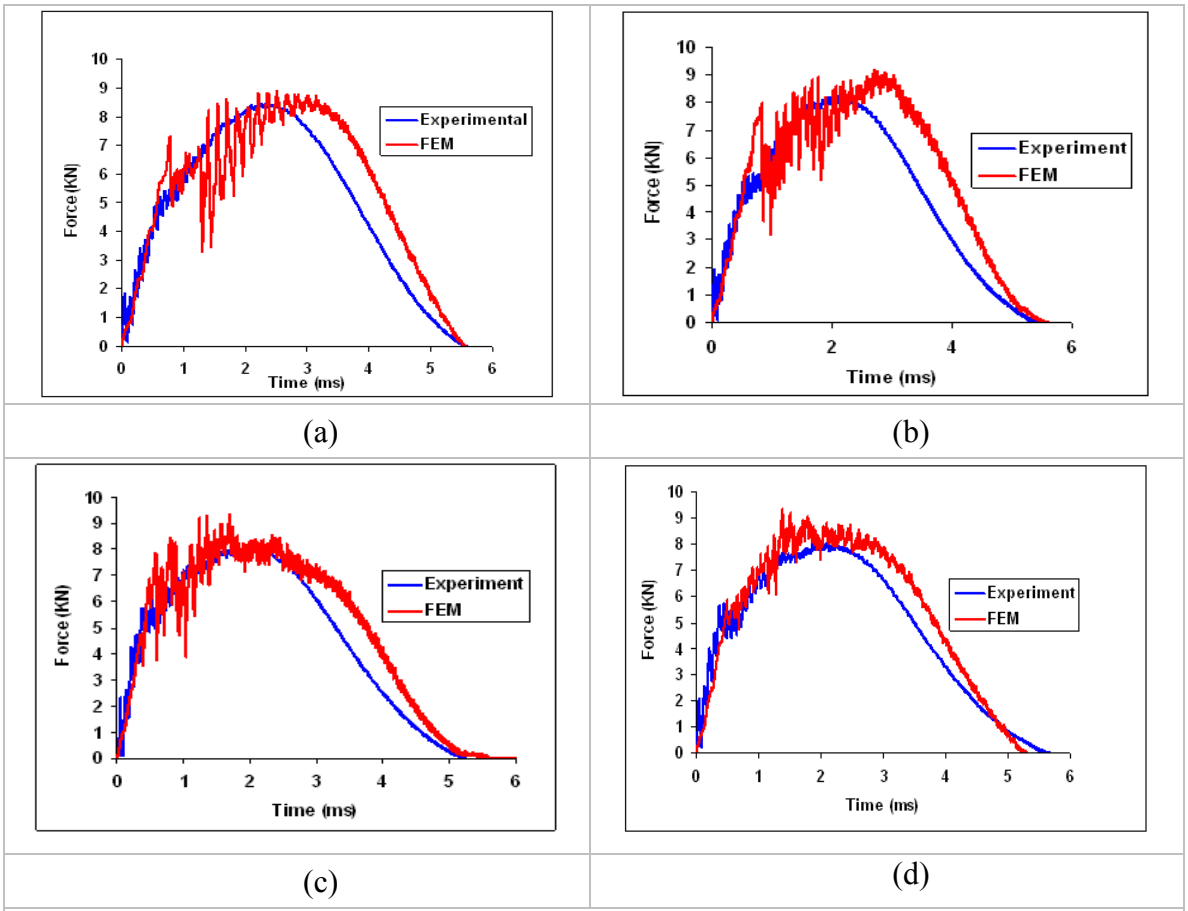

Figure 9.6 Comparison of FEM and experimental force-time histories for (a) GL, (b) GL/GR/GL, (c) GR/GL/GR, (d) GR composite plates impacted at 125 °C.

Figure 9.7 shows the comparison of FEM and experimental force-time histories for tests conducted at −60°C. It can be seen that the initial peak of the force for the FEM model matches the experimental results quite well.

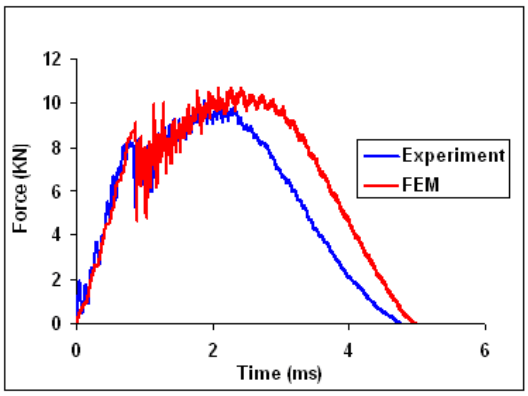

(a)

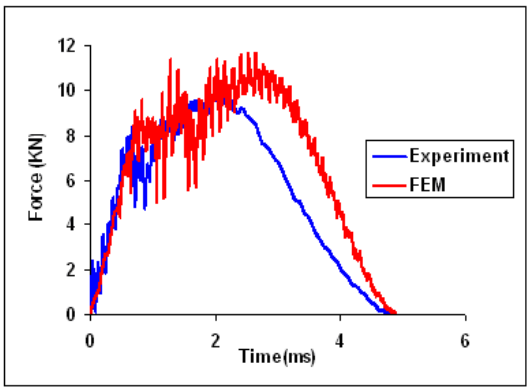

(b)

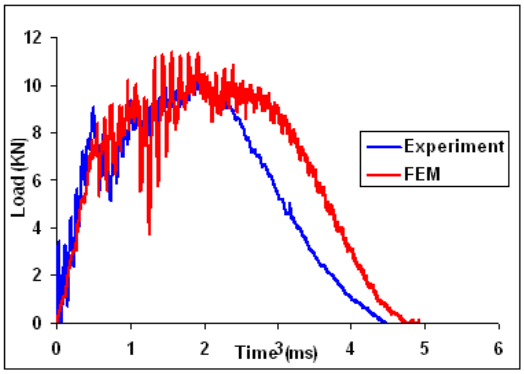

(c)

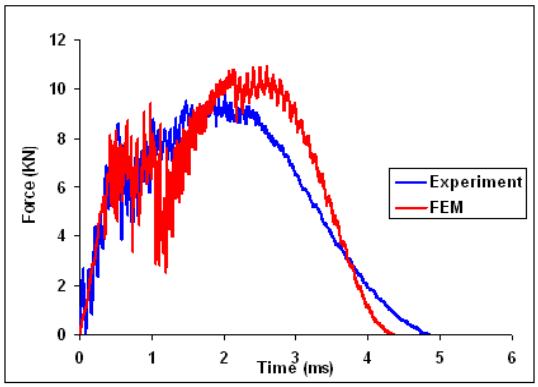

(d)

Figure 9.7 Comparison of FEM and experimental force-time histories for (a) GL, (b) GL/GR/GL, (c) GR/GL/GR, (d) GR composite plates impacted at –60 °C.

(b) Comparison of Energy-Time histories

Dynatup 930-I data acquisition system calculates the total energy of impactor/specimen system at time t using the equation

$$E(t) = K(t) + V(t) + E_a(t) = K(0)$$

where *E(t)* is the total energy of the impactor /specimen system at time t, *K(t)*, kinetic energy of the impactor at time t, *V(t),* potential energy of the impactor at time t, and $E_a(t)$, the energy absorbed by the specimen at time t. $K(0) = \frac{1}{2}mv_i^2$ is the kinetic energy

of the impactor at time t=0. The potential energy can be neglected, since the displacement is small. Therefore the energy absorbed by the specimen can be computed as follows:

$$E_a(t) = K(0) - K(t) = \tfrac{1}{2} m\{v_i^2 - [v(t)]^2\}$$

where v_i is the impact velocity measured by photodiodes and *v(t)* is the velocity of the impactor at time t.

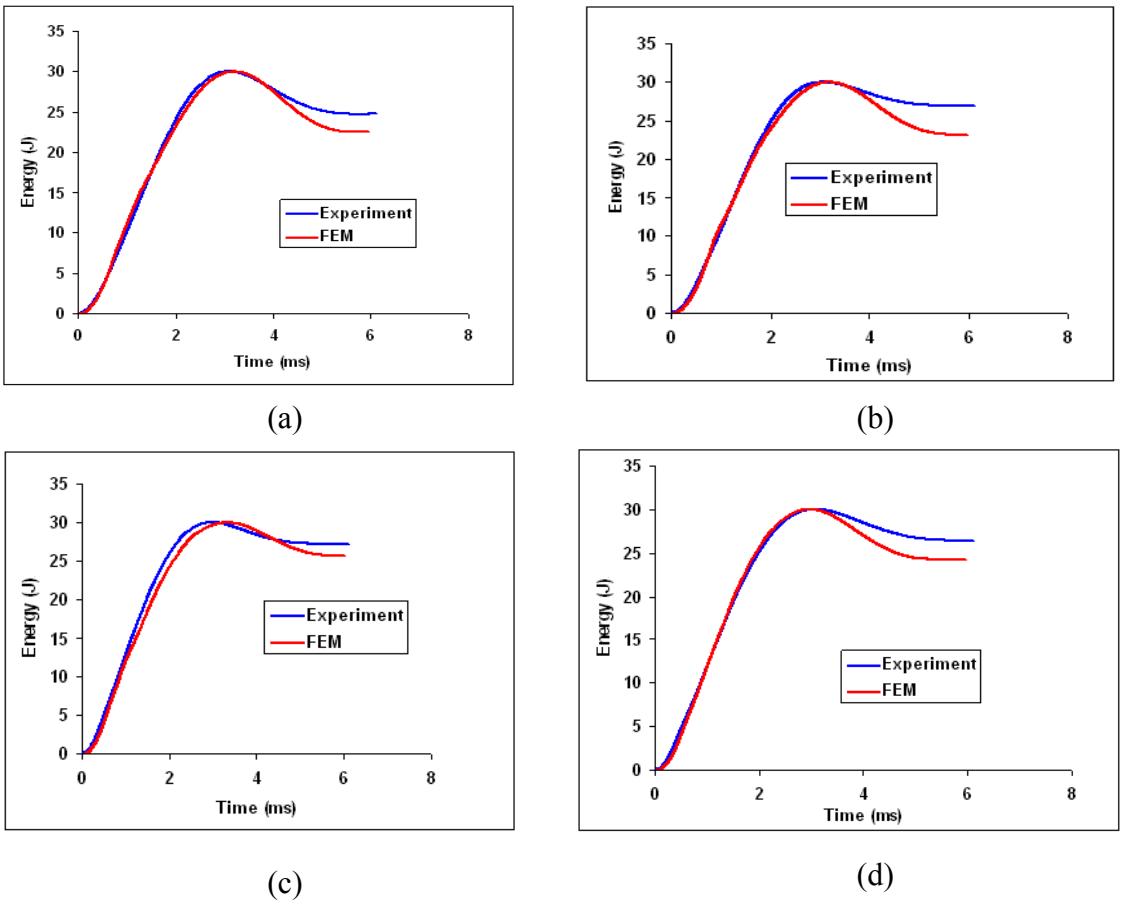

Figure 9.8 Comparison of FEM and experimental energy histories for (a) GL, (b) GL/GR/GL, (c) GR/GL/GR, (d) GR composite plates impacted at 125 °C.

A simple trapezoidal numerical approximation is used to evaluate the integrals in the formulae for v (t) which are used to generate absorbed energy values at a given time (t). Since FEM and experiments generate energy curves based on approximation, neither will generate the exact value for the absorbed energy.

Figure 9.8 shows the energy time histories for tests conducted at 125 °C. It can be seen that both experiments and FEM gives comparable results to the point of maximum impact energy. After this point the impactor starts to rebound and it can be seen that the FEM model under-predicts the absorbed energy.

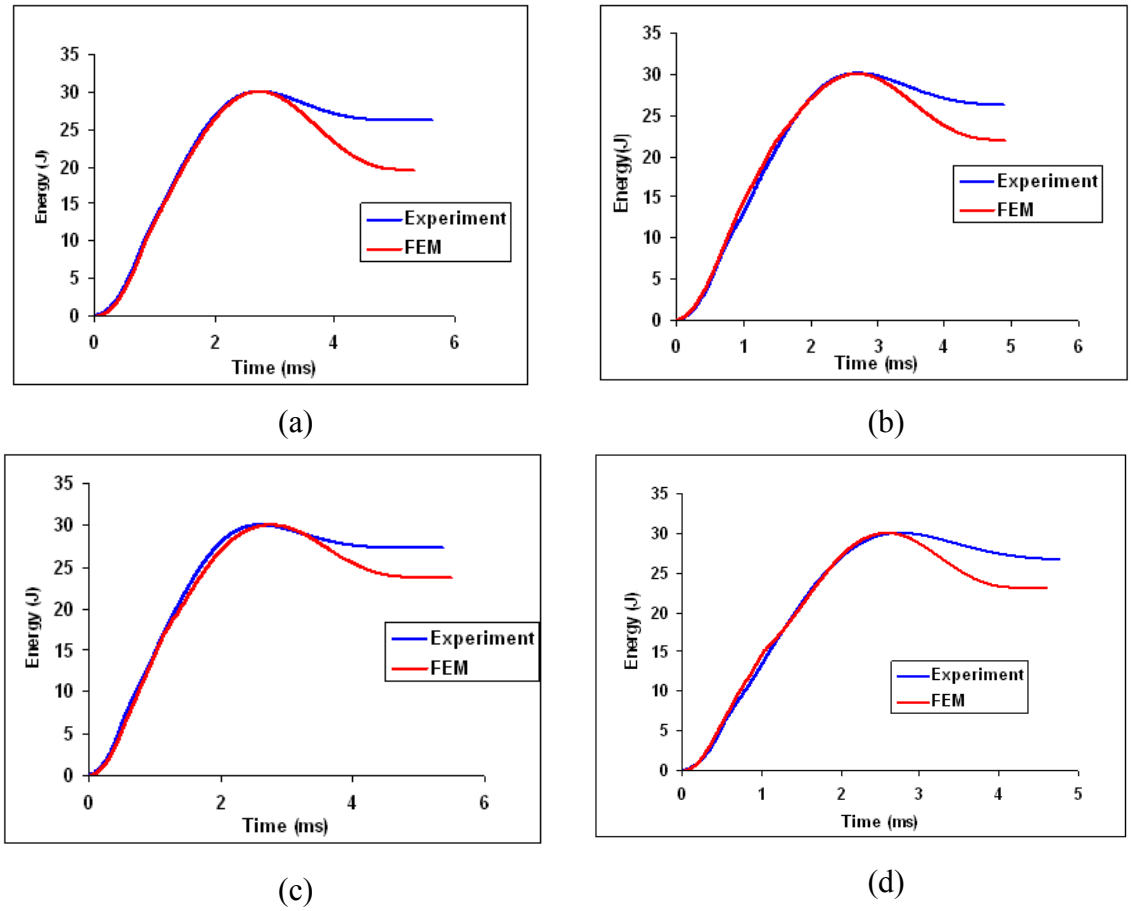

Figure 9.9 Comparison of FEM and experimental energy histories for (a) GL, (b) GL/GR/GL, (c) GR/GL/GR, (d) GR composite plates impacted at –60 °C.

In Figure 9.9, again there is a mismatch in the absorbed and rebound energy when comparing the experimental and FEM results. A higher rebound energy means that the impactor has a higher kinetic energy and hence a higher velocity. This high rebound velocity is the result of the impactor striking a stiffer material. With this in mind, the

mismatch in experimental and FEM results can be expected since in our model, we assume the material to be linear elastic. Our material model used the initial elastic modulus as a constant for the entire behavior, whereas the real material behavior is non linear with decreasing elastic modulus. Another contributing factor for this mismatch in the energy is that in FEM the boundary conditions are assumed as prefect fixed-fixed conditions whereas in the experiments the boundary conditions are somewhere between fixed-fixed and roller-fixed. At low temperatures, this roller condition is more dominant due to ice formation on the surface of the specimen, leading to a more accentuated difference in the results between FEM and experiments. This can be seen in the comparison between the high temperature and low temperature results for a given composite layup in Figures 9.8 and 9.9.

(c) Comparison of contact stiffness

Figure 9.10 shows the comparison of the contact stiffness between experiments and FEM. The predicted curve matches quite well with the experimental curve especially in the initial portion. After damage initiates, there is a little variation in results between the two curves, especially in the unloading portion. Again this can be explained by the approximation of the material stiffness in the material model and also the idealization of the boundary conditions.

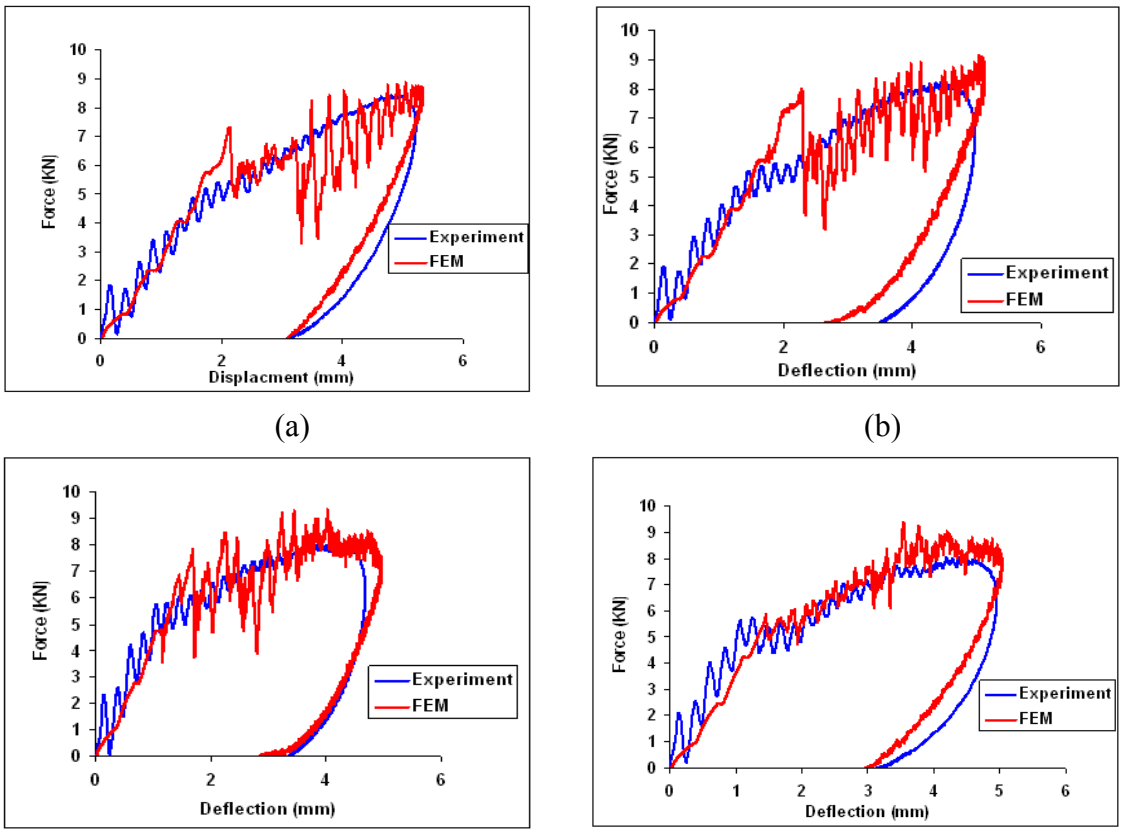

Figure 9.10 Comparison of FEM and experimental contact stiffness for (a) GL, (b) GL/GR/GL, (c) GR/GL/GR, (d) GR composite plates impacted at 125 °C.

In Figure 9.11 the contact stiffness is compared between experiment and FEM for test temperature of –60 °C. The stiffness shows good comparison during the loading portion but some differences are observed after damage initiates and during unloading. This difference is larger when compared to that for 125 °C. This again can be explained by the idealization of our material model, boundary conditions and also the effect of ice on the surface which leads to sliding in the gripping area.

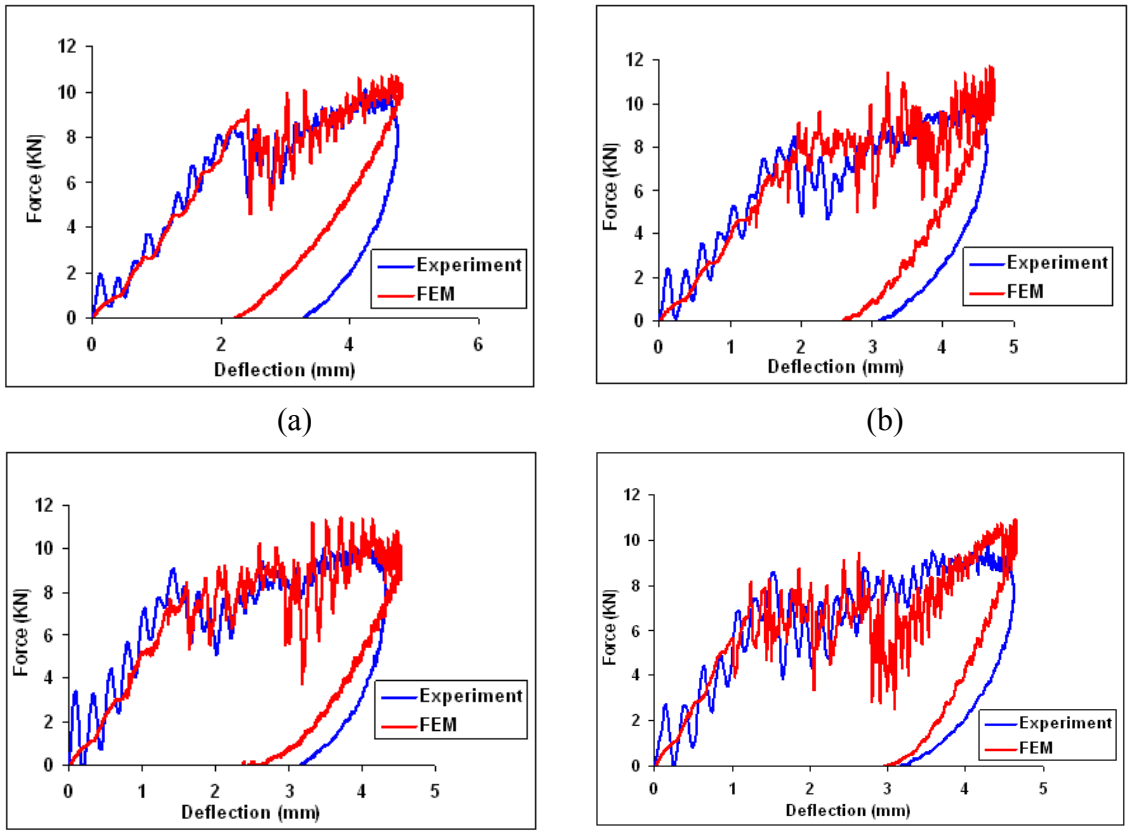

Figure 9.11 Comparison of FEM and experimental contact stiffness for (a) GL, (b) GL/GR/GL, (c) GR/GL/GR, (d) GR composite plates impacted at –60 °C.

(d) Comparison of Strain-Time histories

In Figure 9.12 the experimental and FEM dynamic surface strain histories are shown. The experimental curves are a lot smoother then the predicted curves generated by FEM. This can be explained by the fact that experimental strain measurements were obtained through a strain gage amplifier, whereas actual readings might have been filtered. One reason why the FEM results were not very smooth is due to the fact that the contact between layers was held by the nodes of the contacting layers. As the material is being stressed, the stress buildup continues at the contacting nodes until delamination failure.

When delamination occurs, the stress at the nodes suddenly drops and the crack progresses further to near-by nodes in contact where the stress builds up again until delamination occurs. Then the process gets repeated. This rise and fall in stress causes the strain output to have a lot of oscillations. In order to increase the smoothness of the strain curve, the specimen should be modeled with finer meshes where the nodes will be closer to each other and delamination will have a smoother transition.

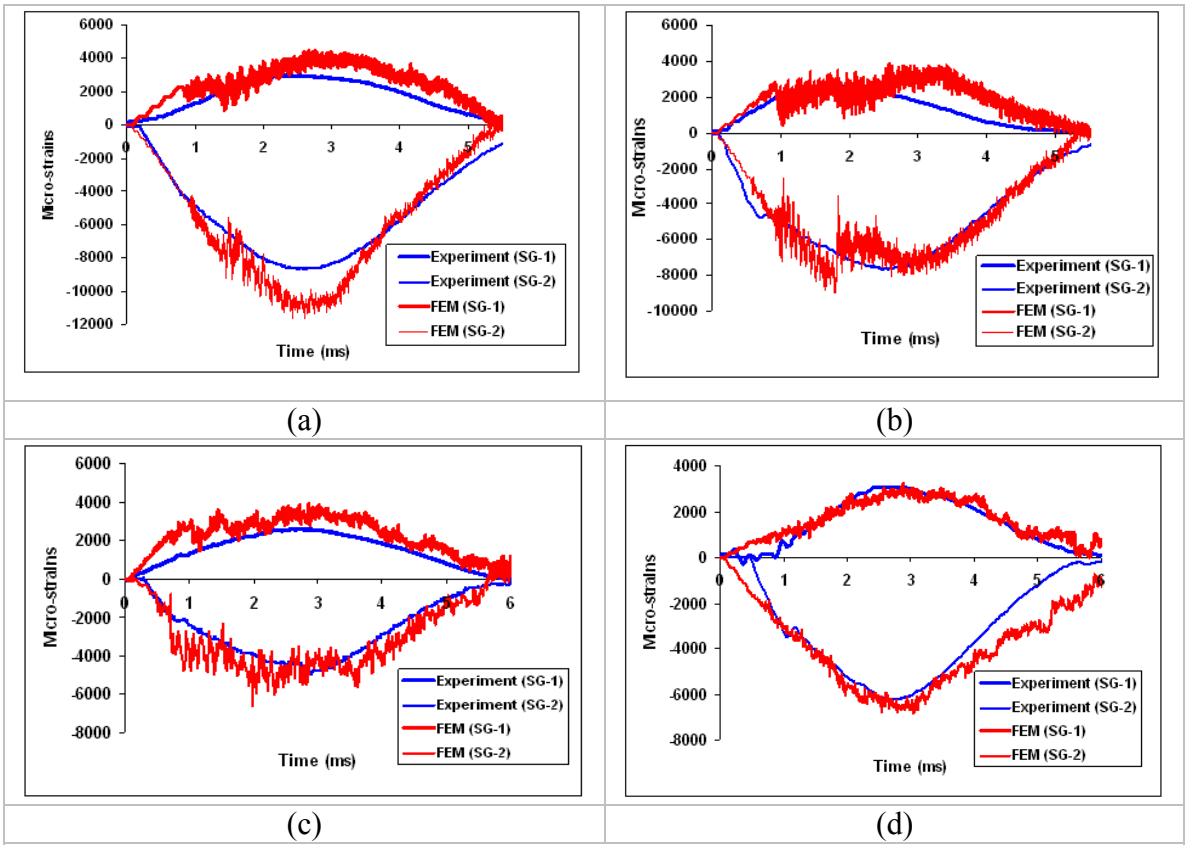

Figure 9.12 Comparison of dynamic strain histories of (a) GL (b) GL/GR/GR/GL (c) GR/GL/GL/GR and (d) GR composite plates impacted at 125°C.

The strain outputs in Fig 9.12 above are in good agreement with each other, but the model could not predict the initial portion of the strain curve quite well.

(e) Comparison of post-impact damage patterns

Figures 9.13 and 9.14 show the post impact damage patterns for all four layups at 125 °C and −60 °C, respectively. Impacted specimens were cut into half at impact location to reveal the internal damage and possible visible delamination. Even though just one quarter of the composite was modeled in FEM calculations, half of the composite is shown for comparison. It can be seen in both figures that the FEM model has more deformation than the actual specimens after impact. One reason for this is due to the fact that our model was stiffer than the actual specimen; hence the deformation which leads to shear failure or shear out of the lamina increases. In the FEM modeling also, erosion factor should be taken into account while comparing the cross sections in Figures 9.13 and 9.14. Erosion is an artificial value which is entered into the program to prevent numerical instability. When this value is reached, the element disappears (is removed) from the animation, which is not the case in the real specimen. In the model, when the failure criterion is reached for a particular element, it material properties are set to zero (see Chapter 3). However, in the actual specimens, even though the material may fracture, it still interacts with material around it and may be also with the impactor depending on its location. This interaction could lead to a contribution in friction, compressive resistance, etc.

	EXPERIMENT	FEM
(1)		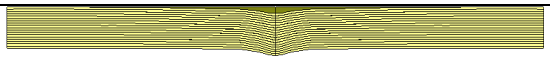
(2)		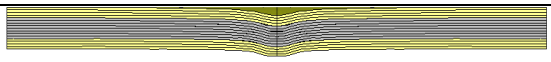
(3)		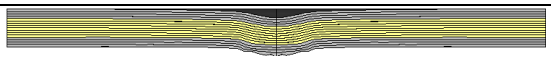
(4)		

Figure 9.13 Comparison of post impact damage patterns of FEM and experimental results for drop-weight tests at 125 °C for (1) GL, (2) GL/GR/GL (3) GR/GL/GR and (4) GR using 16mm hemispherical impactor.

	EXPERIMENT	FEM
(1)		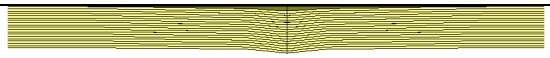
(2)		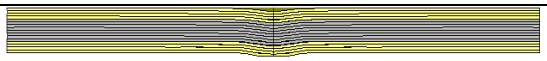
(3)		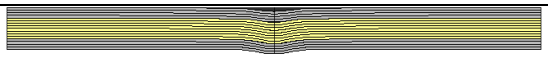
(4)		

Figure 9.14 Comparison of post impact damage patterns of FEM and experimental results for drop-weight tests at −60 °C for (1) GL, (2) GL/GR/GL (3) GR/GL/GR and (4) GR using 16mm hemispherical impactor.

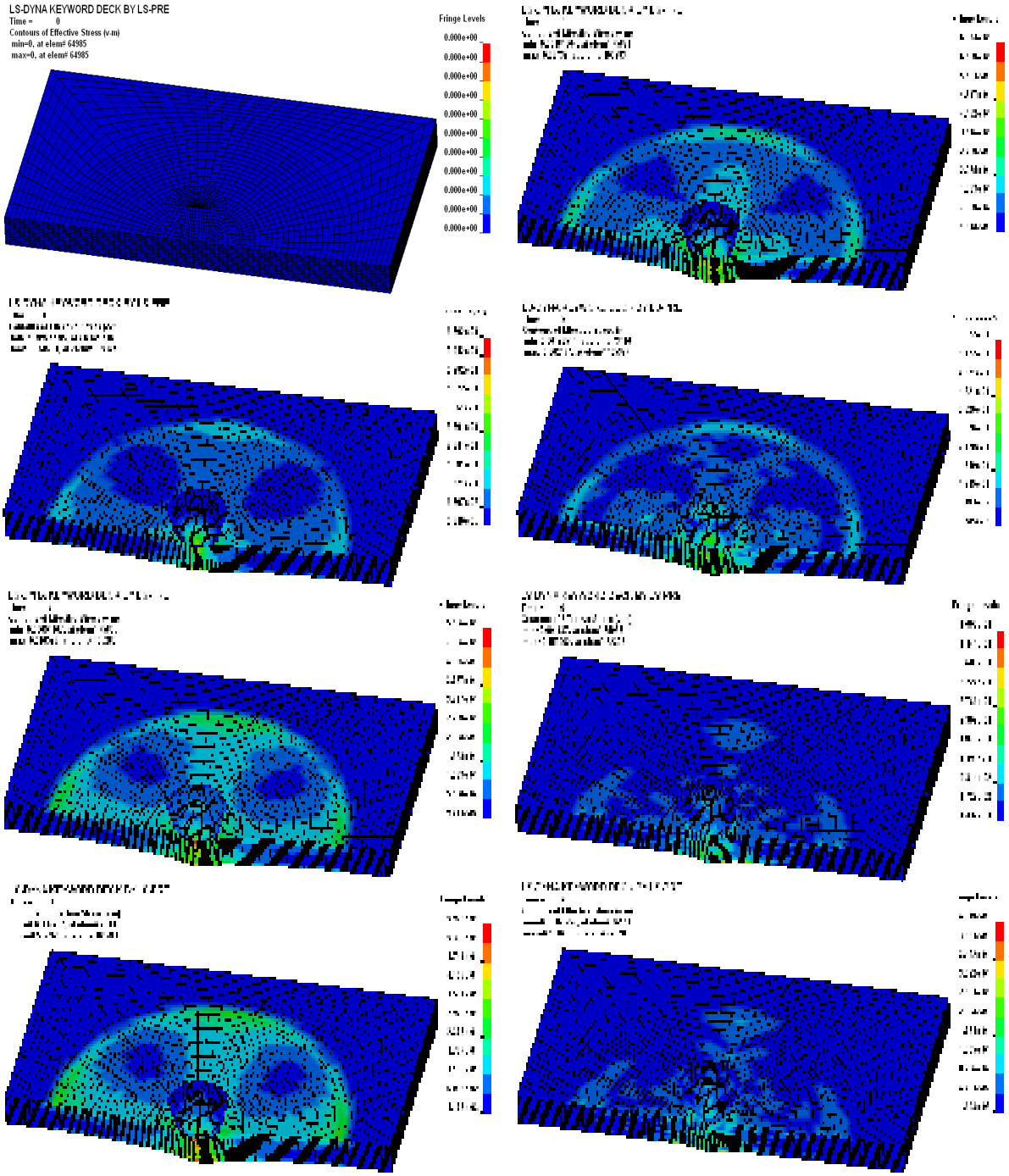

Figure 9.15 Damage progression and stress counters of FEM simulation for non-hybrid woven GL composite plate impacted at test temperature of 125 °C. (Time interval between each plot is 1ms)

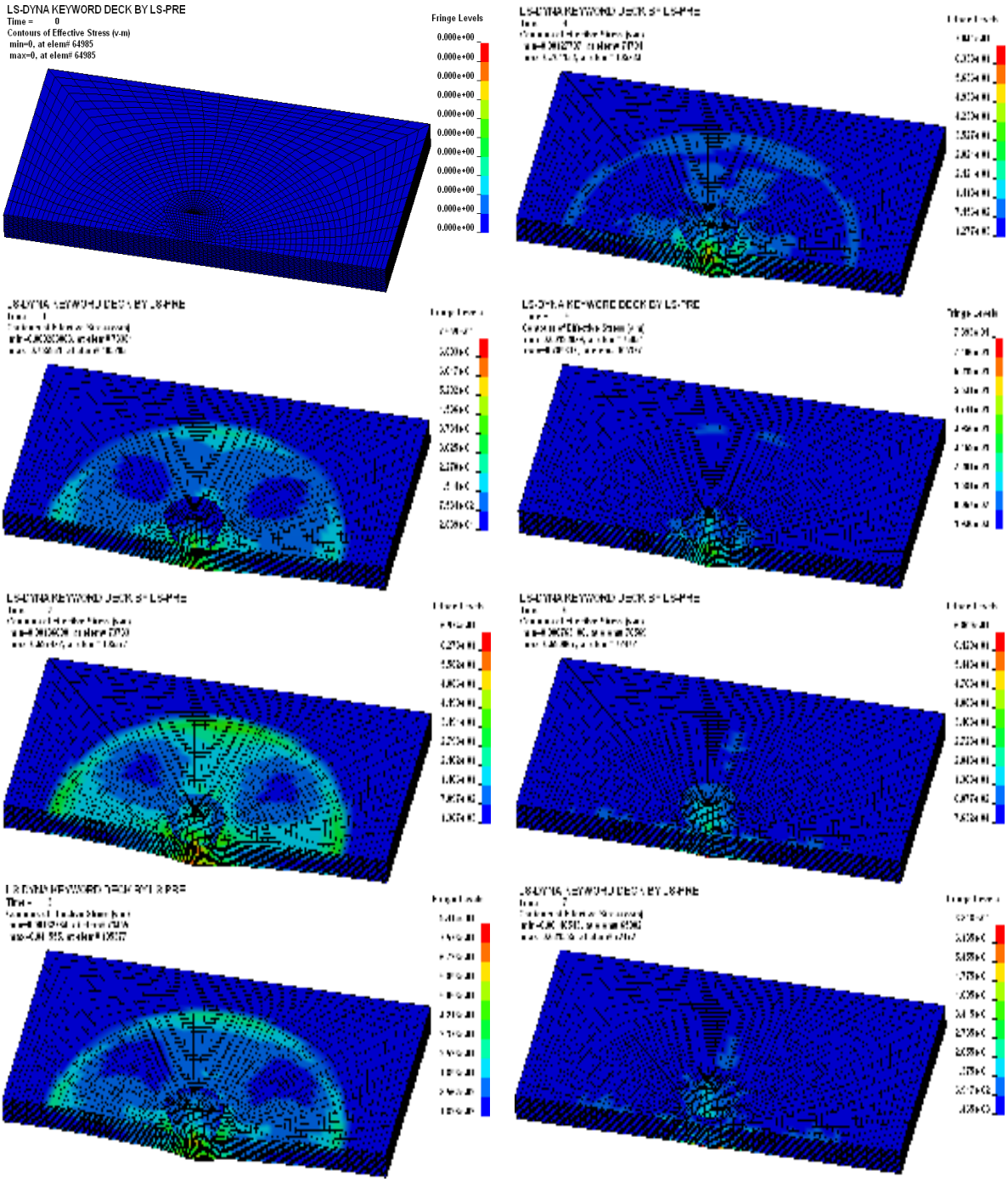

Figure 9.16 Damage progression and stress counters of FEM simulation for non-hybrid woven GL composite plate impacted at test temperature of –60 °C. (Time interval between each plot is 1ms)

Figure 9.15 and 9.16 show damage progression and stress counters of FEM simulation for woven GL composite plate impacted at test temperatures of 125 °C and –60 °C,

respectively. It is interesting to note that in Figures 9.15 and 9.16 that for the low temperature, the stress distribution is more concentrated in the region of impact than it is for high temperature. This is more evident during the period when the impactor is rebounding.

9.4 Finite element simulations for ballistic impact tests

9.4.1 Effect of Temperature on the ballistic impact response of woven composites

Figure 9.17 shows the mesh of a quarter model of the plate used in simulating the ballistic impact test. Fine mesh was used around the center which is the critical location while course mesh is used away from center. One advantage of this is to reduce computation time.

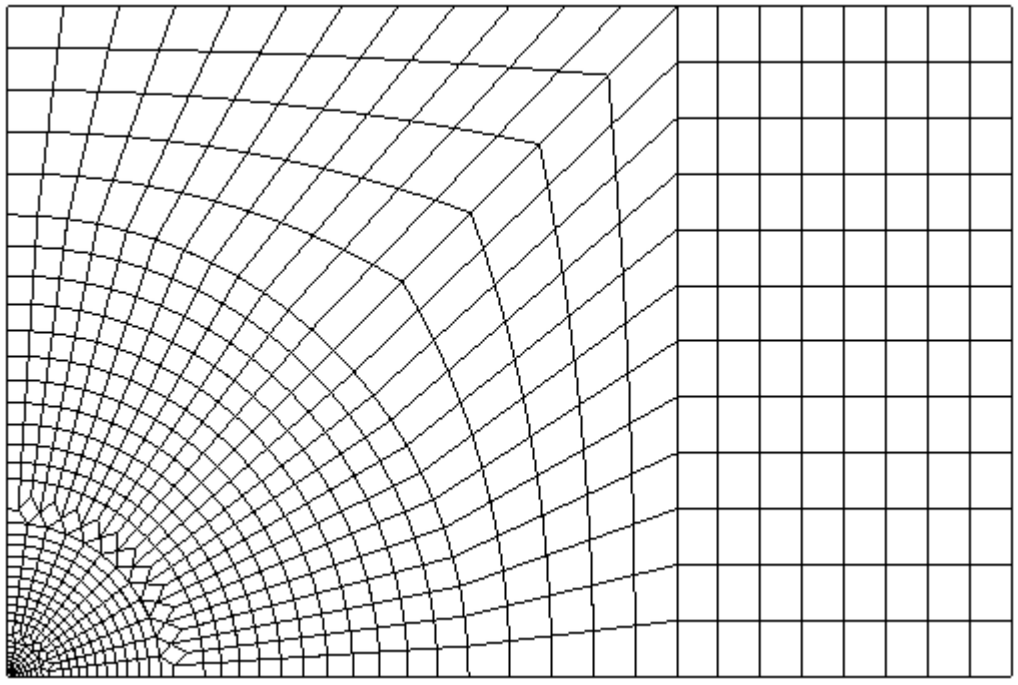

Figure 9.17 Quarter model of meshed plate used in ballistic impact simulation

Figure 9.18 shows the entire ballistic model of both the composite panel and also the bullet for a non hybrid specimen for the ballistic impact simulation.

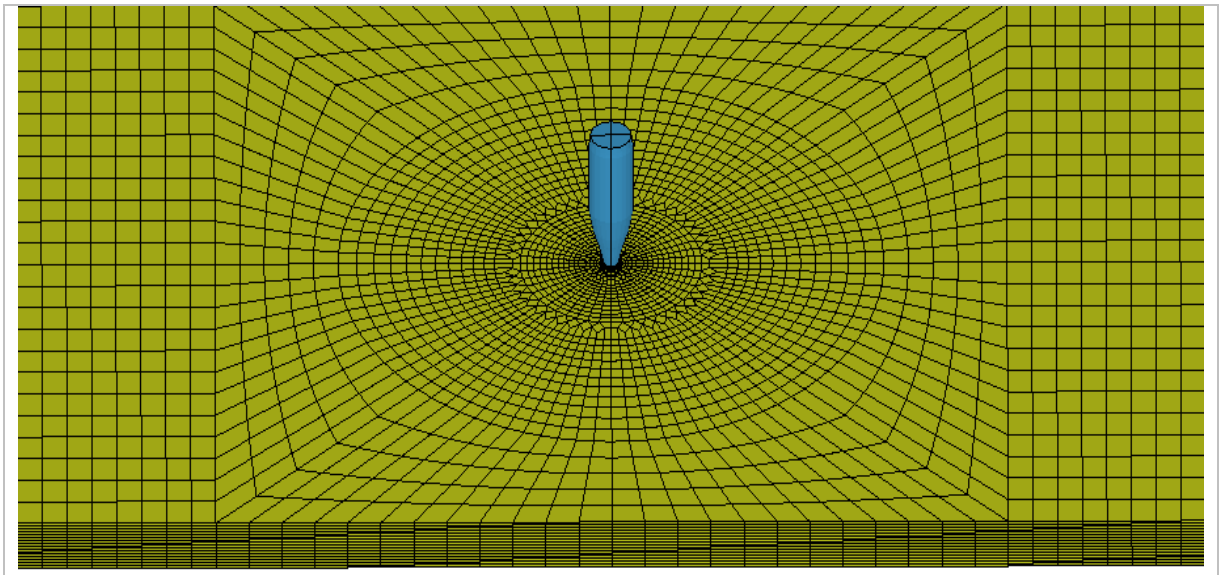

Figure 9.18 Mesh of entire composite plate and bullet for the ballistic impact model

Figure 9.19 shows the LS-DYNA finite element meshes used for simulating ballistic impact onto (a) a woven non hybrid composite (b) a woven hybrid composite. In the models, 18 layers were used for GL, 14 layers for GR and 16 layers for the hybrid composite.

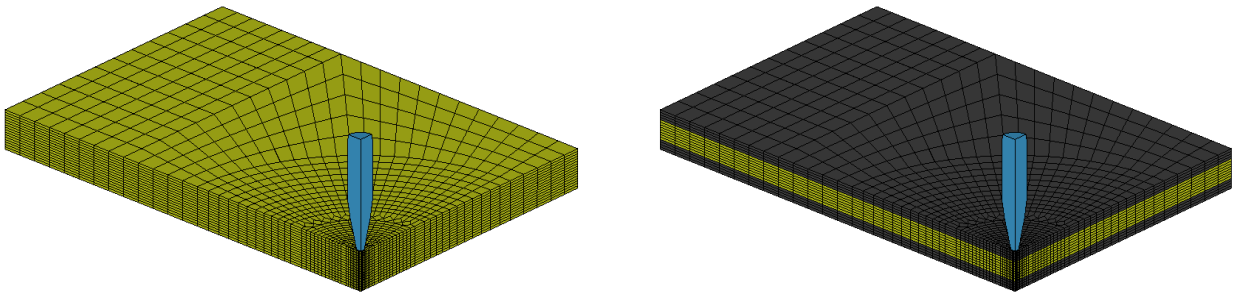

(a) (b)

Figure 9.19 Finite element simulation models. (a) Ballistic impact model for the non hybrid specimen (b) Ballistic impact model for the hybrid specimen

(a) Determination of damping constant

In analyzing the dynamic strain histories recorded during the ballistic impact tests, it can be seen that the response of the composite was damped. Slipping between layers of laminated structures such as composites introduces high internal damping to the system; therefore damping was required to be incorporated into the FE model. However, the damping constant is not easy to determine. In order to successfully incorporate a reasonable damping constant into the model, two options were used. The first option is to incorporate damping between layers in the form of a viscous damping coefficient in terms of percentage of critical damping. This helps to eliminate undesirable oscillation in contact. Between layers of similar materials, 10% damping was used and between layers of dissimilar materials, 20% damping was used. The second option where damping was introduced was through DAMPING_PART_STIFFNESS. In this option a Raleigh damping coefficient is specified which is uniformly applied to each element of the part. LS-DYNA suggests a value of 0.01 to 0.25 or in other words, 1% to 25% of the critical damping coefficient. Different values were used in the model and the strain outputs from the model were compared to those obtained experimentally. Best results were obtained when 10% damping was used.

(b) Comparison of Strain-Time histories

In this study FE predictions were compared with experimental results mainly for dynamic strain histories and post-impact damage patterns, since it was not possible to obtain force and energy-time histories experimentally. As shown in Figures 9.20-23 the dynamic

strains obtained from experiments and the FE results are in good agreement. The strains obtained using the Chang-Chang model exhibited some magnitude and frequency mismatch in comparison with experimental data. This may be because the nonlinear material behavior could not be represented perfectly by the linear Chang-Chang model. It should be noted that the strain comparisons made here are mainly for vibration of impacted composite beams. It would be better to compare the transient response of composite during ballistic impact. However ballistic impact takes place in an extremely short time. In order to capture strains in such a short time, the frequency of the strain amplifier should be very high.

Since dynamic strains obtained from the numerical models were in good agreement with the experimental results, only comparisons for the extreme temperatures (i.e. 125 °C and – 60 °C) are presented in Figures 9.20-23 (a) and (b) respectively. In Figure 9.20, the dynamic strain comparison is shown for the non hybrid GL composite. It can be seen that the magnitude of the strain output from LS-DYNA was slightly lower than that obtained experimentally. However, the magnitude of strain for the low temperature was in better agreement than that for high temperature. This difference in magnitude of strains between the model and experiment can be due to the fact that the LS-DYNA model is stiffer than the actual composite that is being tested. It can also be observed from the strain results that only for the first half cycle, the frequency of vibration of the model and specimen match each other. After this point it is seen that the model was slightly out of phase with the experimental results. Again, this can be attributed to the model being stiffer than the actual composite.

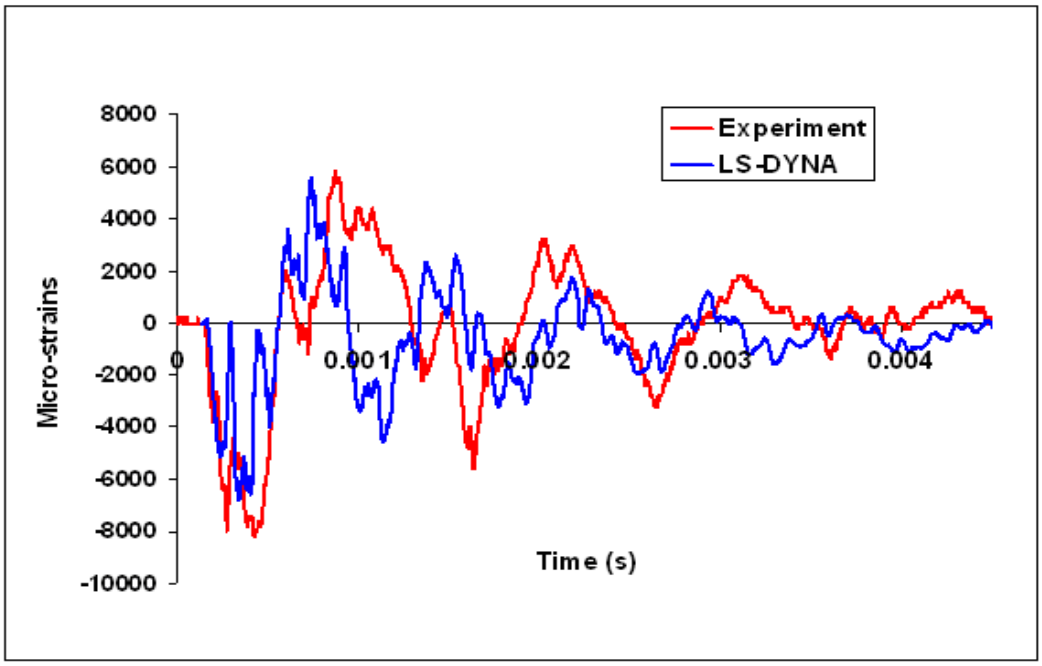

(a)

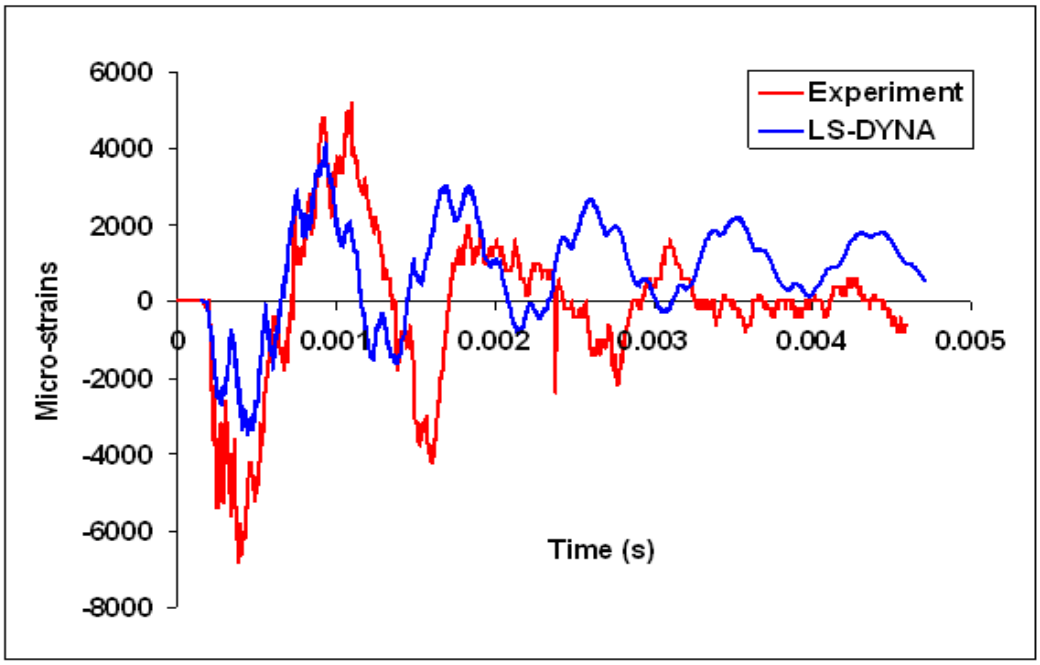

(b)

Fig 9.20 Comparison of LS-DYNA and experimental strain histories for GL at 125 °C (b) – 60 °C (a)

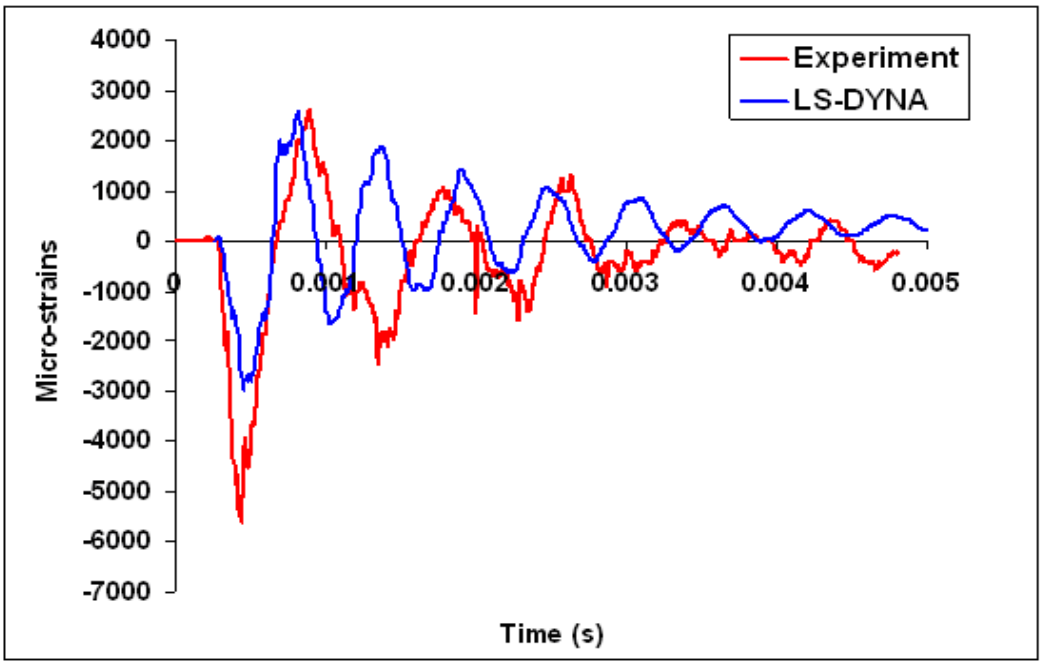

(a)

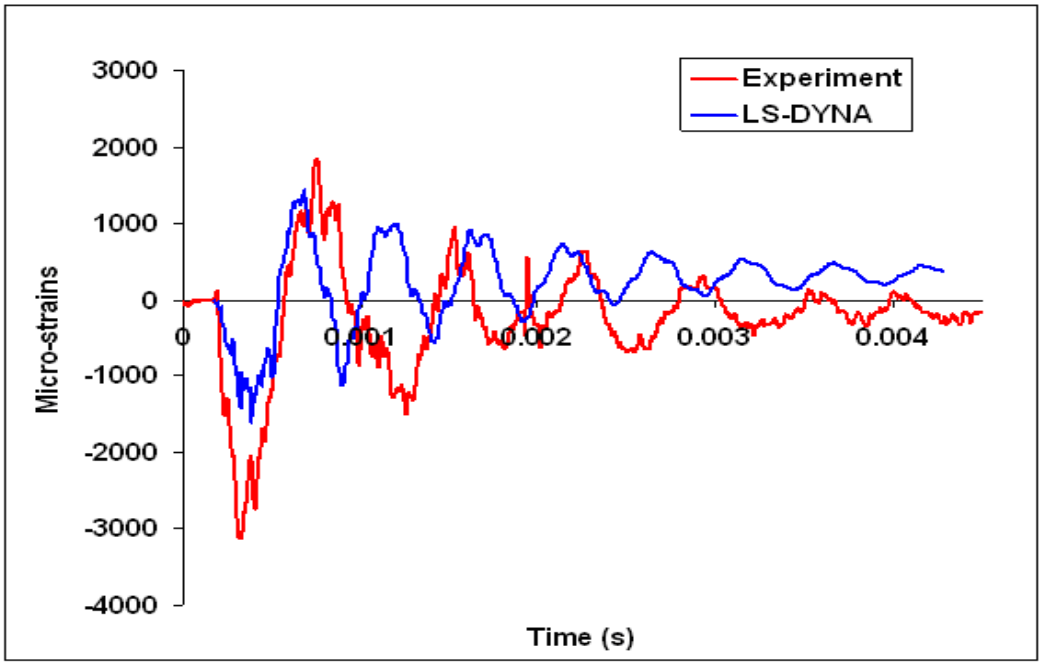

(b)

Fig 9.21 Comparison of LS-DYNA and experimental strain histories for GR at 125 °C (b) – 60 °C (a)

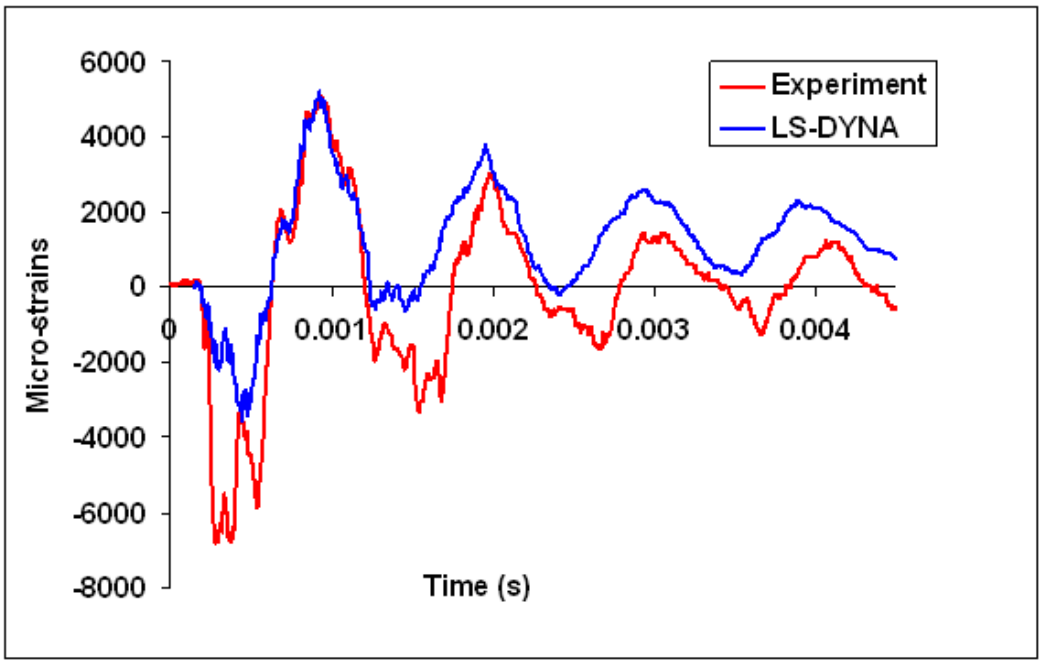

(a)

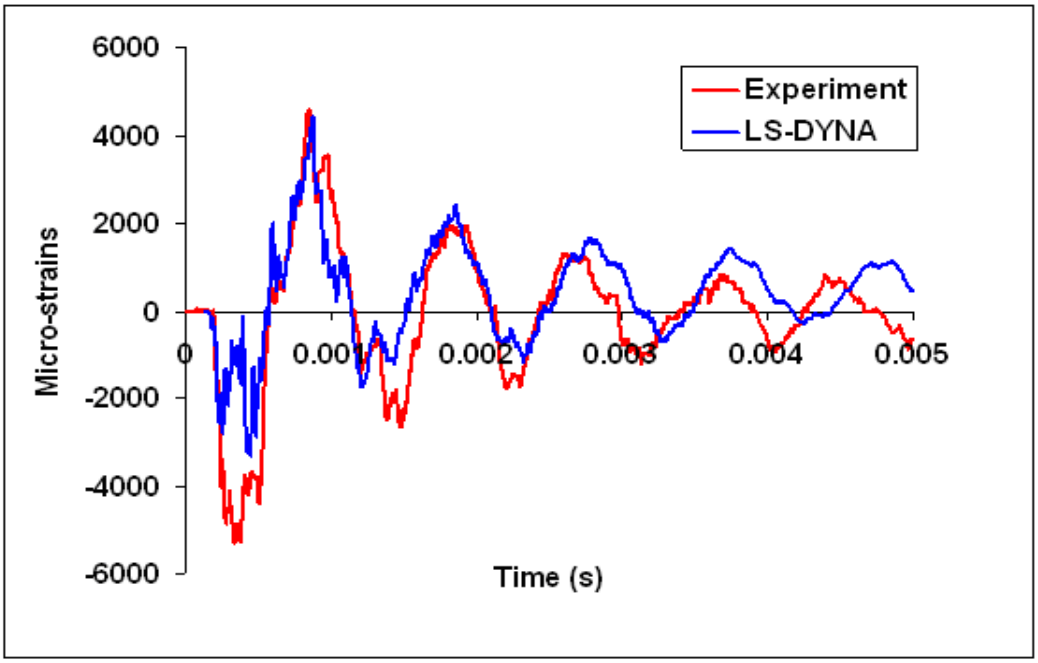

(b)

Fig 9.22 Comparison of LS-DYNA and experimental strain histories for GL/GR/GL at (a) 125 °C (b) – 60 °C

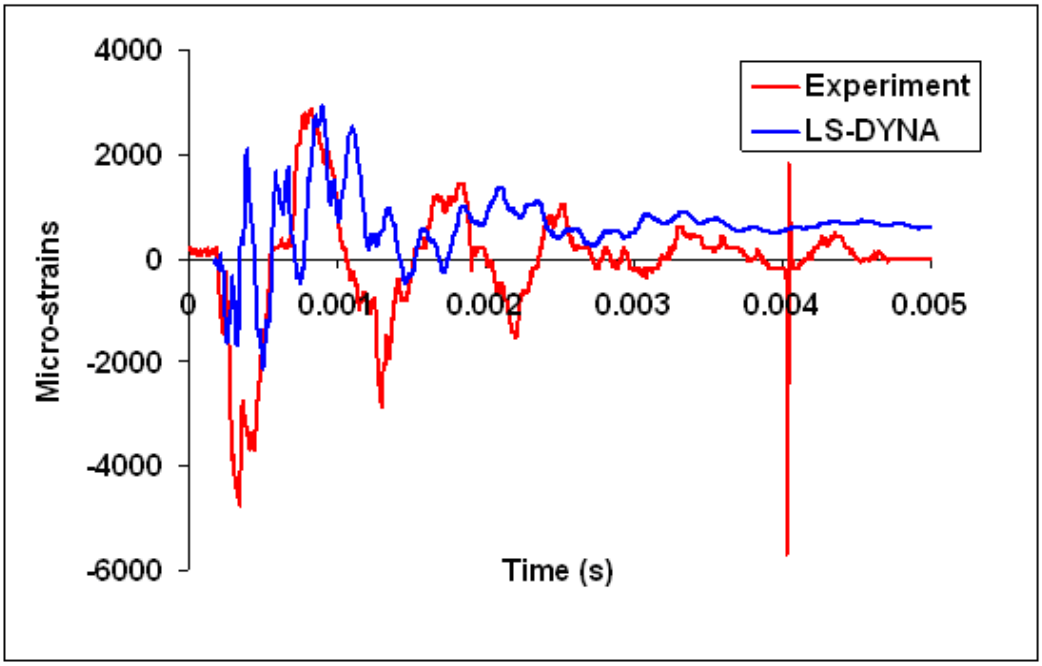

(a)

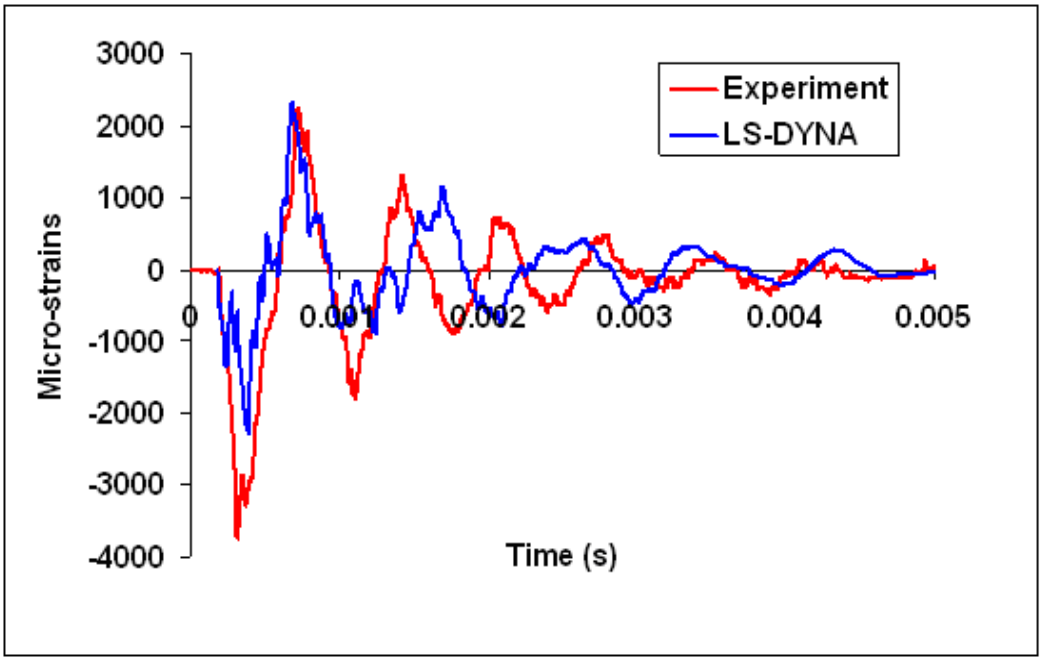

(b)

Fig 9.23 Comparison of LS-DYNA and experimental strain histories for GR/GL/GR at (a) 125 °C (b) – 60 °C

In Figure 9.21, the dynamic strain comparison is shown for the non hybrid GR composite. The results are similar to those of GL.

Figures 9.22-9.23 show the dynamic strain comparison for the hybrid GL/GR/GL and GR/GL/GR composite respectively. Here the results are better matched than those for non hybrid composites in terms of frequency of vibration. It can be seen that the magnitude of the strains for the model is smaller than that obtained experimentally.

(c) Comparison of Force-Time histories

The force time histories could not be captured during experiments. However FE model provides the force-time histories of ballistic tests. Figure 9.24 shows the predicted force-time histories of GR composite impacted at 299 m/s (full penetration) and 275 m/s (partial penetration) for tests conducted at 125 ºC, also GR impacted at 233 m/s for test conducted at − 60 ºC. It is clear that the higher impact velocity produced lower contact time for three cases. The magnitude of the force tends to decrease with a decrease in impact velocity. The predicted force time histories of GL/GR/GL composite are shown in Figure 9.25. Results are shown for GL/GR/GL composite impacted at 325 m/s (full penetration) and 308 m/s (partial penetration) for tests conducted at 125 ºC, also GL/GR/GL impacted at 325 m/s (partial penetration) for test conducted at − 60 ºC. It can be seen that the contact force is lower for low temperatures even though the impact velocity is the same. It also shows that contact time is longer for partial penetration than full penetration.

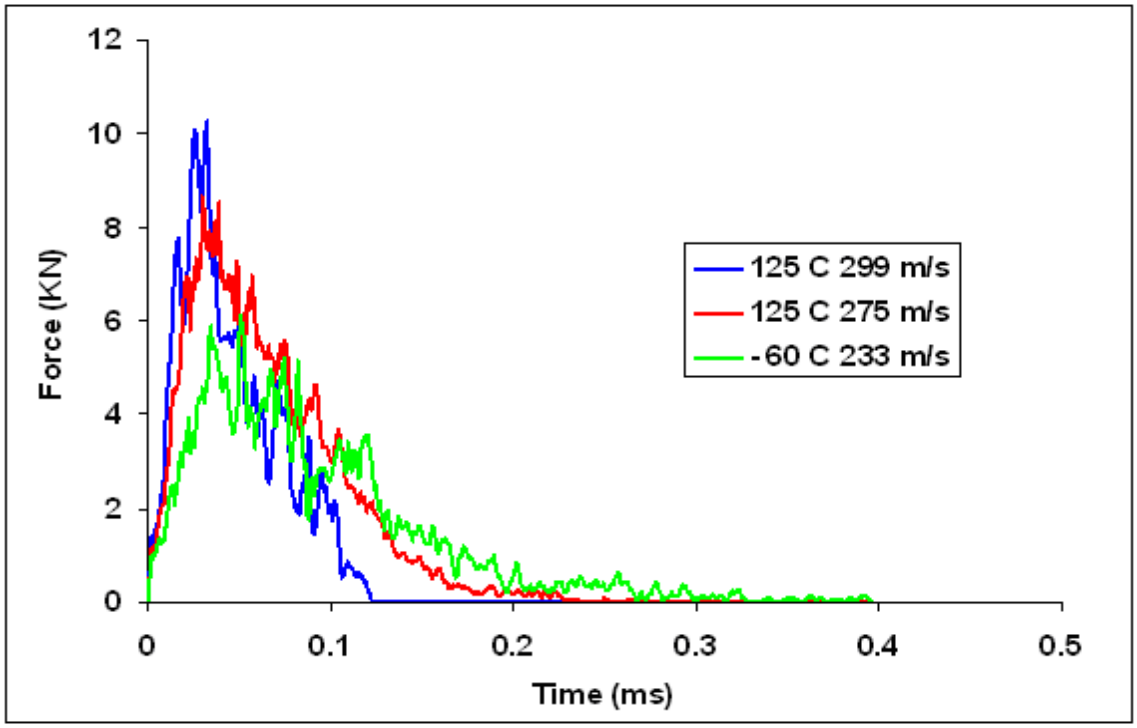

Figure 9.24 Comparison of FE predicted force-time histories of GR composite panel impacted by a 22 caliber copper projectile

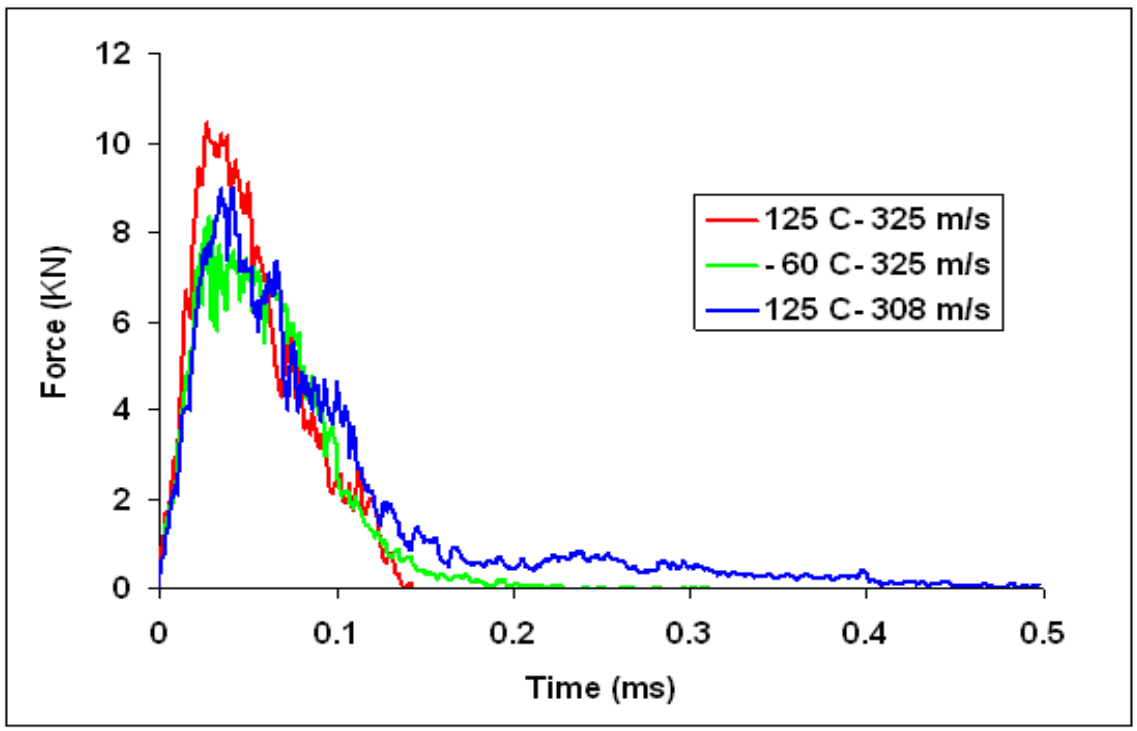

Figure 9.25 Comparison of FE predicted force-time histories of GL/GR/GL composite panel impacted by a 22 caliber copper projectile

During the ballistic impact event, if the projectile partially penetrated, the velocity of the projectile decreased and became zero before traveling the entire thickness of the composite. Thus typical force-time histories of partial penetration tests would have a linear increase at the beginning and return the zero after reaching maximum force. The drops that are observed in the force time histories represent the failure of the composite layers. As soon as a composite layer is damaged, the projectile loses its contact temporarily. Once the following layer is reached, the contact force starts to increase again. The projectile passes through the entire thickness in a very short time in case of full penetration. In the event of much higher impact velocities, the contact between the projectile and the composite would end before the maximum force is reached. Thus, the force produced by full penetration tests will be lower than those produced by partial penetration cases [81]. It can therefore be said that the contact force tend to increase with an increased impact velocity up to the ballistic limit. A further increase in impact velocity after the ballistic limit will cause a reduction in contact force.

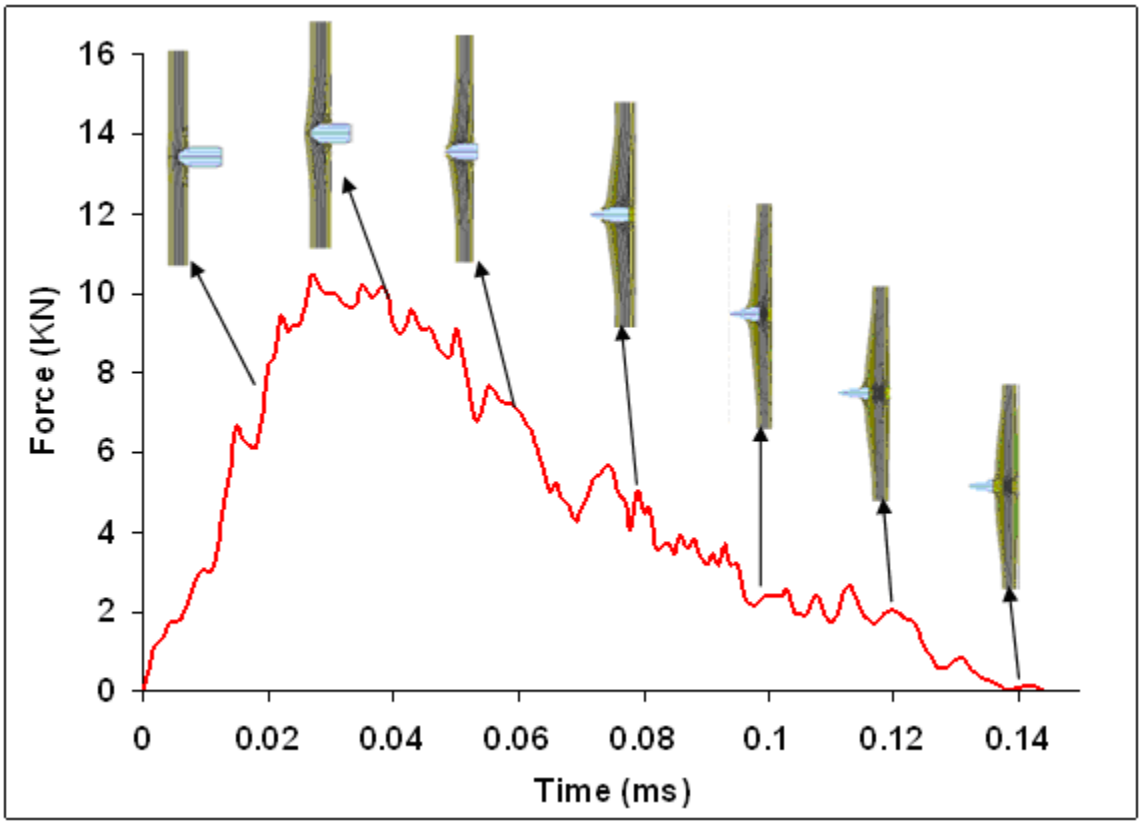

Figure 9.26 Comparison of FE predicted force-histories and damage progression for hybrid GL/GR/GL composite impacted at 325 m/s by a 22 caliber copper projectile

Figure 9.26 shows force time histories and damage progression for hybrid GL/GR/GL composite impacted at 325 m/s by a 22 caliber copper projectile. The damage progression is shown at 0.02 m/s intervals. Figure 9.27 shows the close up view of the damage progression. It can be seen that the major delamination occurs close to the lower surface between the contacts of the GL and GR composite. From the cross-sectional views of the composite, it is also confirmed that the delamination is greater in lower layers.

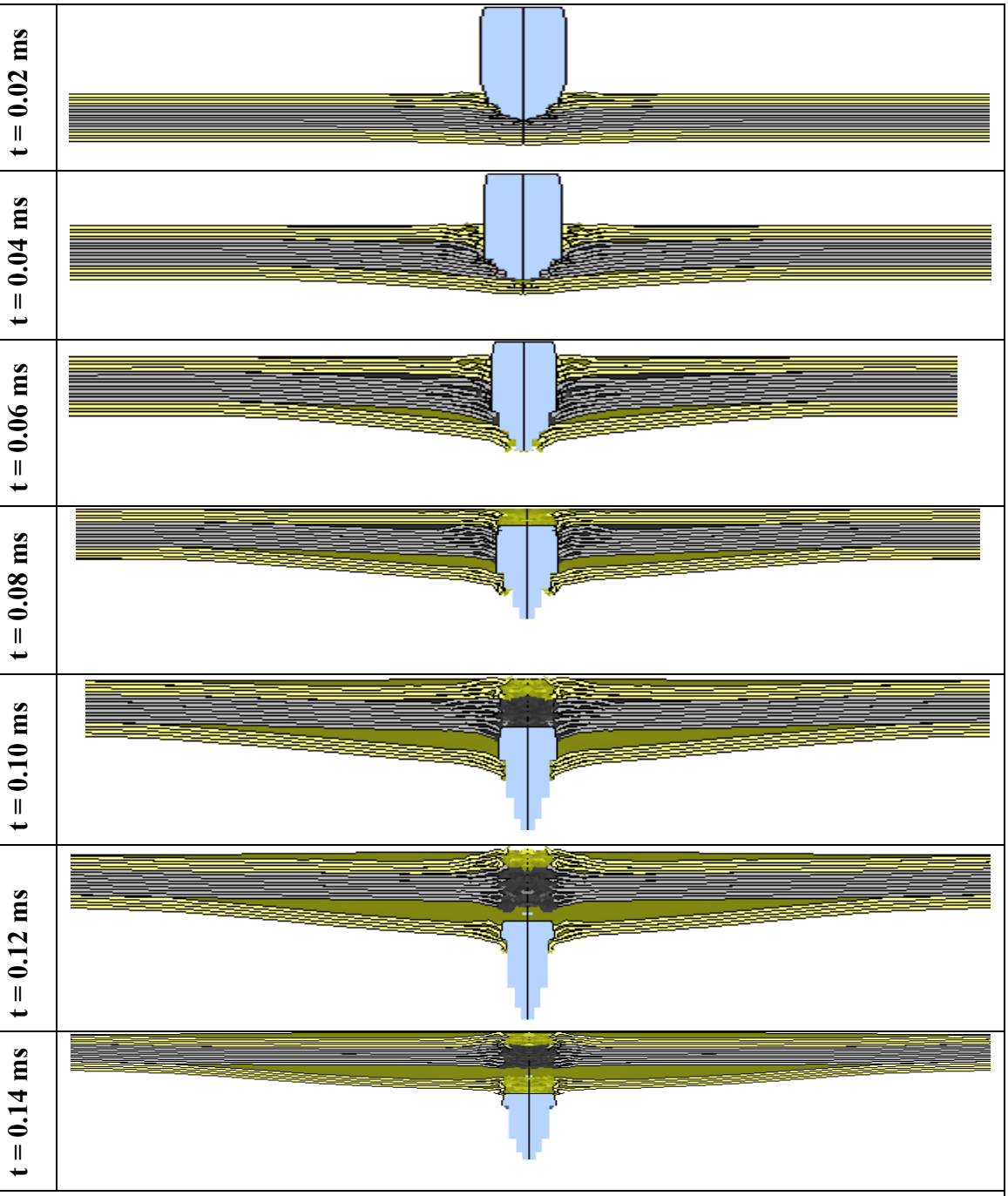

Figure 9.27 Damage progression for hybrid GL/GR/GL composite impacted at 325 m/s by a 22 caliber copper projectile

(d) Comparison of post-impact damage patterns

Figures 9.28 to 9.31 show the comparison of experimentally obtained and FE predicted post impact damage patterns of ballistic impact tests. Each figure shows comparisons

made at 125 ºC and –60 ºC respectively. Figures 9.28 to 9.31 show the comparison for non-hybrid GL impacted at 365 m/s and 404 m/s, hybrid GL/GR/GL impacted at 325 m/s and 345 m/s, hybrid GR/GL/GR impacted at 368 m/s and 312 ms/ and non-hybrid GR impacted at 299 m/s and 256 m/s, respectively. The finite element model successfully predicted the damage observed during the experiments. Significant delamination between dissimilar layers during the ballistic impact tests of hybrid composite was predicted by the finite element model. The broken fibers appeared at the tension side of the experimental pictures for all lay-up sequences, but were not seen in the FE prediction. This is because of the strain based element erosion criterion used in the FE model. The area where broken fibers are seen represents failed material. On the other hand the failed elements are eroded and removed from calculation in the FE model, so they aren't seen in the comparisons.

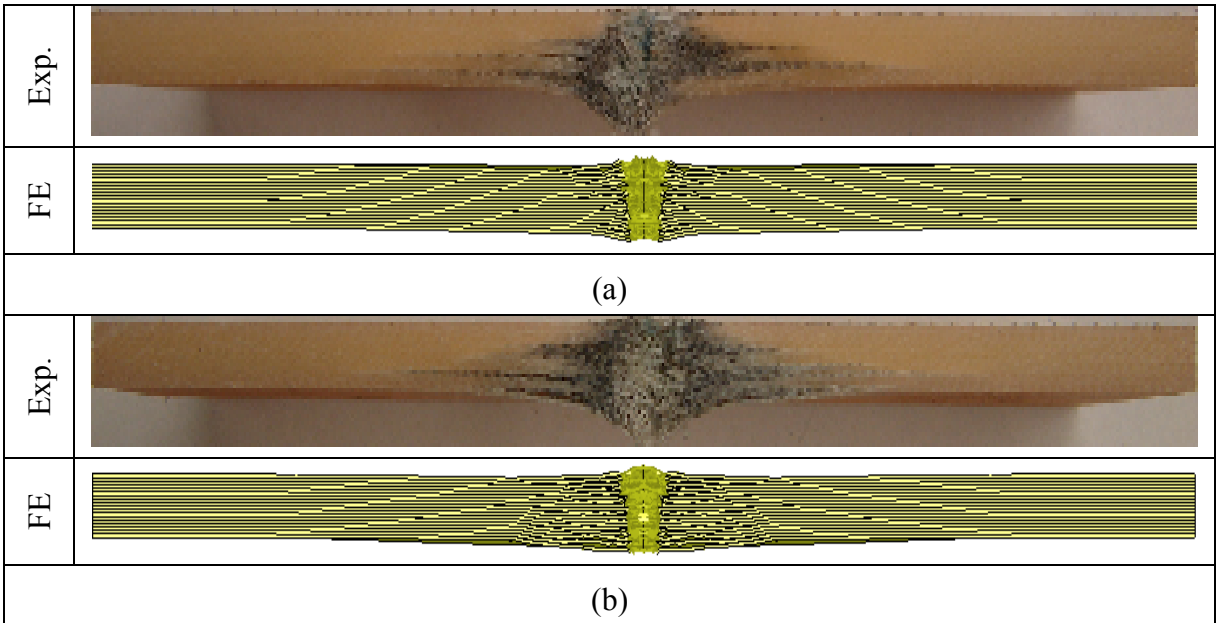

Figure 9.28 Comparisons of post impact damage patterns for non-hybrid GL impacted at (a) 125 ºC and 365 m/s (b) –60 ºC and 404 m/s

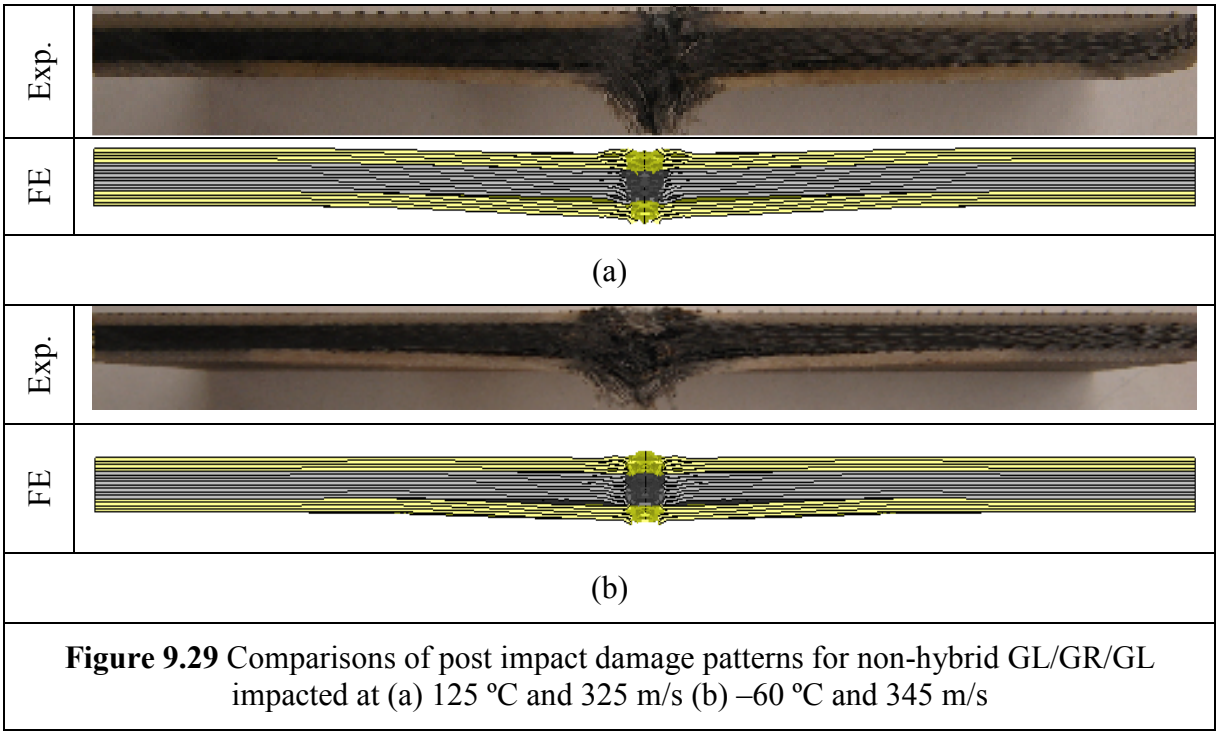

Figure 9.29 Comparisons of post impact damage patterns for non-hybrid GL/GR/GL impacted at (a) 125 ºC and 325 m/s (b) –60 ºC and 345 m/s

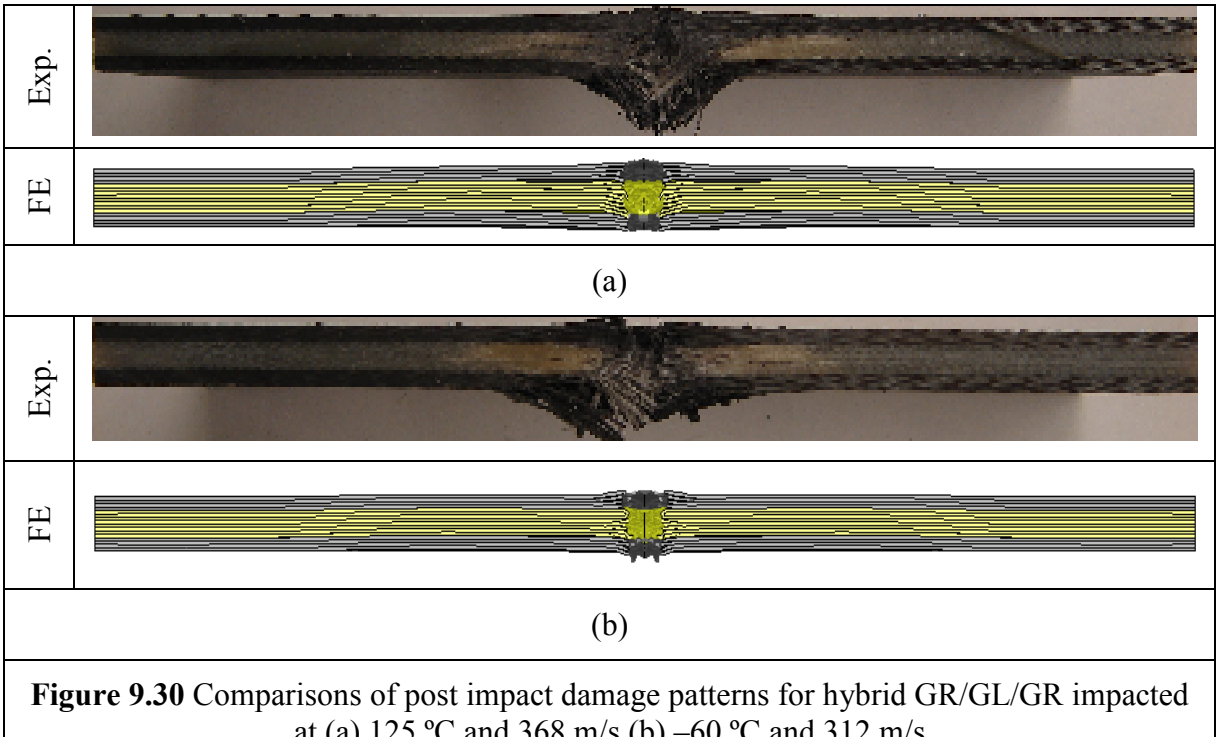

Figure 9.30 Comparisons of post impact damage patterns for hybrid GR/GL/GR impacted at (a) 125 ºC and 368 m/s (b) –60 ºC and 312 m/s

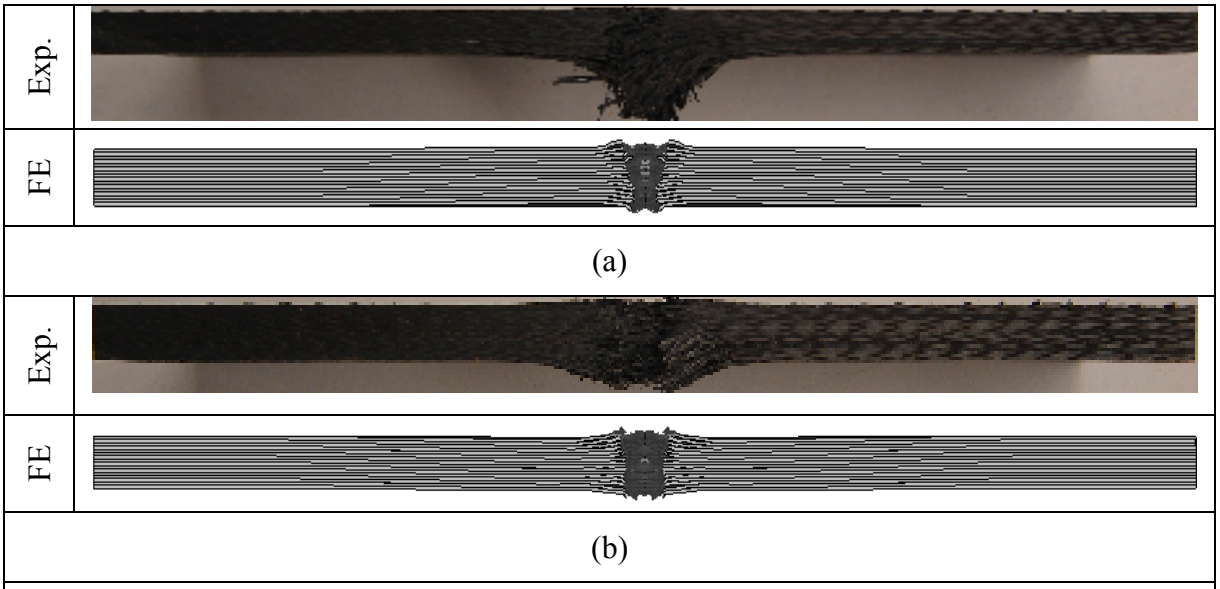

Figure 9.31 Comparisons of post impact damage patterns for hybrid GR impacted at (a) 125 ºC and 299 m/s (b) –60 ºC and 256 m/s

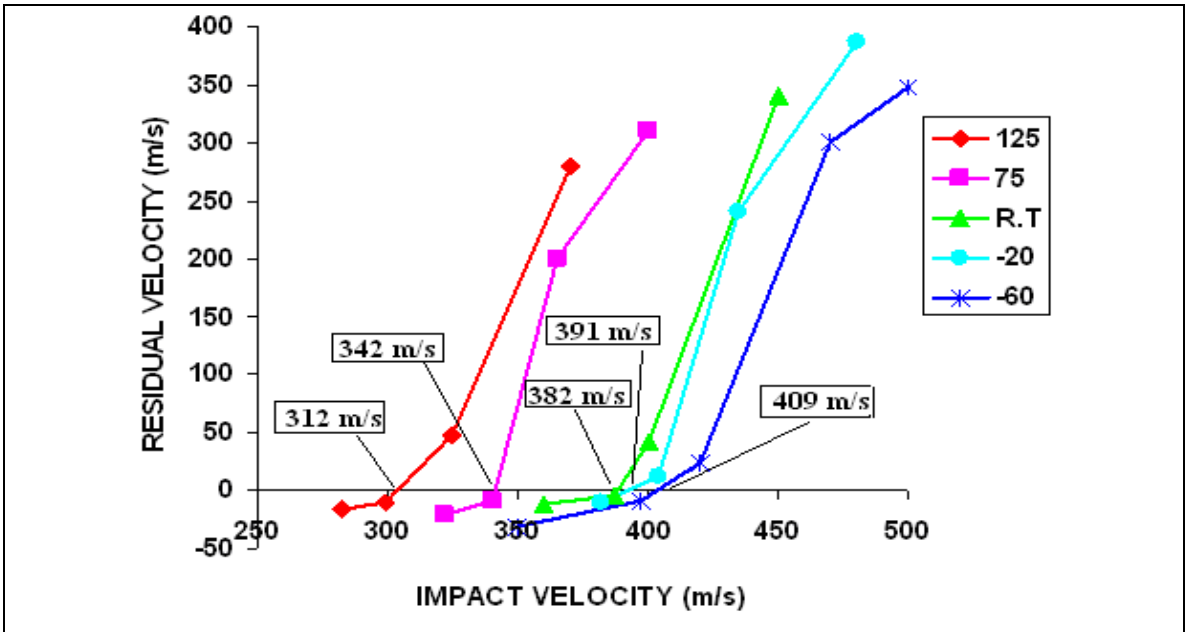

Figure 9.32 FE predicted residual velocity (V_R) and impact velocity (V_I) relations for GL at all test temperatures

Figure 9.32 shows the residual velocity plotted against the impact velocity for GL at all the test temperatures. It is assumed that the point where the curves intersect the x-axis is the ballistic limit of the composite.

9.5 CONCLUSIONS FOR FINITE ELEMENT STUDIES

(a) The FE model incorporated with MAT_22 (Chang-Chang material model) was successfully used to simulate the low velocity and ballistic impact tests.

(b) The validity of the FE model for low velocity impacts was confirmed when after comparison with experimental results such as, force, energy, strain histories and post-impact damage patterns. The experimental and FE predicted results agreed sufficiently for low-velocity impact tests. The model however, could be improved by introducing a material model that accurately captures the actual non-linear behavior of the material.

(c) The validity of the FE model for ballistic impact was confirmed after comparison with experimental results such as strain histories and post-impact damage patterns.

(d) The experimental post impact damage patterns for ballistic tests were in better agreement than those of low velocity impact. This is due to the fact that the behavior of the material is more brittle under high strain rate, and hence the Chang-Chang model is more suited for modeling ballistic impact than low velocity impact.

Chapter 10

10.1 GENERAL CONCLUSIONS

a) Under tensile loading, temperature has an effect on all the composite layups tested. The effect of temperature on the modulus of elasticity was negligible, but was significant on the ultimate stress, Poison's ratio and failure strain

b) Under low velocity impact loading, GL proved to be more impact resistant under all test temperatures, while GR was the least resistant. The impact resistance of the hybrid composites was better than GR's but less than GL's.

c) As temperature increased, the delamination area of the composites decreased.

d) Under ballistic impact, the ballistic limit (V_{50}) for GL was the highest. The ballistic limit (V_{50}) for the GR composite was the worst, while those of the hybrids were somewhere in between of those for GL and GR.

e) The ballistic limits (V_{50}) for the GR and hybrid composites were more stable and less sensitive to a change in the test temperature than that for GL.

f) At very high test temperatures, the impact resistance of the hybrids under ballistic impact becomes better than those of GL.

g) LS-DYNA was successful in predicting the impact behavior of the composites under high and low velocity impacts. However, it predicts the impact behavior of the composite under ballistic impact better than that for low velocity impact.

10.2 MAJOR CONTRIBUTION OF THIS RESEARCH

Based on literature review it was found that limited research and in some cases no research has been done of the temperature effect on the behavior of hybrid composites; specifically the temperature effect on the low velocity impact response and on the ballistic resistance or ballistic limit has not been studied. The major contributions of this research to the scientific community are as follows:

a) The effect of temperature on drop weight impact of hybrid and non hybrid

woven composite materials

b) The effect of temperature on ballistic impact of hybrid and non hybrid woven composite materials with emphasis on the ballistic limit (V_{50}) of the material

c) Development of testing methodologies for ballistic impact at high and low temperatures

d) Development of a finite element model to predict the behavior of hybrid woven composites at high and low temperatures

10.3 FUTURE WORK

Some of the recommended future work can be summarized as follows:

(a) The study of the effect of strain rate on the composite at high and low temperatures

(b) Use of the actual high strain rate material behavior in the FEM model and use of a better material model to predict the material behavior

(c) Development of an analytical model that incorporates the effect of temperature to predict the ballistic limit of the material

10.4 PUBLICATION

- Yougashwar Budhoo, Feridun Delale and Benjamin Liaw, Ramki Iyer, "*Temperature effect on drop-weight impact of hybrid woven composites"*, American Society of Mechanical Engineers (ASME), International Mechanical Engineering Congress and Exposition, November 2010,

10.5 FUTURE PUBLICATIONS

- Yougashwar Budhoo, Feridun Delale and Benjamin Liaw, "*Temperature effect on drop-weight impact of plain weave woven S2-Glass/SC-79 epoxy composites"*, to be published
- Yougashwar Budhoo, Feridun Delale and Benjamin Liaw, "*Temperature effect on ballistic impact of non-hybrid and hybrid woven composites"*, to be published

References

1. Jones M. R., “Mechanics of Composite Materials, Chapter 1.4., Applications of Composite Materials”, Edwards Brothers, Ann Arbor, MI, 1998

2. Naik K. N., “Woven Fabric Composites, Introduction”, Technomic Publishing Company Inc., Pennsylvania, 1994.

3. Chou T.W. and Ko K. F., “Textile structural composites, Introduction to textile structures and their behavior”, Elsevier Science Publishing Company, New York, 1989.

4. Hancox N.L., “Introduction to fiber composite hybrids”, Ch. 1 in Fibre Composite Hybrid Materials, Hancox NL (Ed), Applied Science Publishers, London, 1981.

5. Reyes G. and Kang H., “Mechanical behavior of lightweight thermoplastic fiber–metal laminates”, Journal of Materials Processing Technology, Volume 186, Issues 1-3, 7 May 2007, Pages 284-290.

6. N.K. Naik, P. Yernamma, N.M. Thoram, R. Gadipatri, V.R. Kavala, “High strain rate tensile behavior of woven fabric E-glass/epoxy composite”, Polymer Testing, Volume 29, Issue 1, February 2010, Pages 14-22.

7. Thwe M.M., Liao K., “Effects of environmental aging on the mechanical properties of bamboo-glass fiber reinforced polymer matrix hybrid composites”, Composites: Part A 33 (2002) 43-52.

8. Velmurugan R. and Manikandan V., “Mechanical properties of Palmyra / glass fiber hybrid composites” Composites Part A: Applied Science and Manufacturing, In Press, Accepted Manuscript, Available online 11 July 2007.

9. Paiva C. Z. Júnior, Carvalho L. H., Fonseca V. M., Monteiro S. N. and d’Almeida J. R. M., “Analysis of the tensile strength of polyester/hybrid ramie–cotton fabric composites” Polymer Testing, Volume 23, Issue 2, April 2004, Pages 131-135.

10. Velde K. V. and Kiekens P., “Effect of material and process parameters on the mechanical properties of unidirectional and multidirectional flax/polypropylene composites”, Composite Structures, Volume 62, Issues 3-4, 2003, Pages 443-448.

11. Arbelaiz A., Fernández B., Cantero G., Llano-Ponte R., Valea A. and Mondragon I., “Mechanical properties of flax fiber/polypropylene composites. Influence of fiber/matrix modification and glass fiber hybridization”, Composites Part A: Applied Science and Manufacturing, Volume 36, Issue 12, December 2005, Pages 1637-1644.

12. Scida D., Aboura Z., Benzeggagh M. L. and Bocherens E., “Prediction of the elastic behavior of hybrid and non-hybrid woven composites”, Composites Science and Technology, Volume 57, Issue 12, 16 January 1998, Pages 1727-1740

13. Ganesh V.K. and Naik N.K., “Failure behavior of plain weave fabric laminates under on-axis uniaxial tensile loading: I-Laminate Geometry”. Journal of Composite Material.1996, 30(16), 1748-1778.

14. Ganesh V.K. and Naik N.K., “Failure behavior of plain weave fabric laminates under on-axis uniaxial tensile loading: II-Analytical Geometry”. Journal of Composite Material. Volume 30, Issue 16, 1996, 1779-1782.

15. Ganesh V.K. and Naik N.K., “Failure behavior of plain weave fabric laminates under on-axis uniaxial tensile loading: III-Effect of fabric Geometry”. Journal of Composite Material, Volume 30, Issue 16, 1996, 1823-1856.

16. Ishakawa T. and Chou T.W., “Stiffness and strength behavior of woven fabric composites”. Journal of Material Science. Volume 17, 1982, Pages 3211-3220.

17. Ishakawa T. and Chou T.W., “Elastic behavior of woven hybrid composites”. Journal of Composite Materials, Volume 16, 1982, Pages 2-19.

18. Ishakawa T. and Chou T.W., “One dimensional micromechanical analysis of woven fabric composites”. AIAA J., , Volume 21, Issue 12, 1983, Pages 1714-1721.

19. Ishakawa T. and Chou T.W., “In-plane thermal expansion and thermal bending coefficients of fabric composites”. Journal of Composite Materials. Volume 17, 1983, Pages 92-104.

20. Ishakawa T., Matsushima M., Hyashi Y., and Chou T.W., “Experimental confirmation of the theory of elastic moduli of fabric composites”. Journal of Composite Materials. Volume 19, 1985, Pages 443-458.

21. Peng X.Q. and Cao J., “A continuum mechanics-based non-orthogonal constitutive model for woven composite fabrics”, Composites Part A: Applied Science and Manufacturing, Volume 36, Issue 6, June 2005, Pages 859-874.

22. Huang Z.M. and Ramakrishna S., “Modeling inelastic and strength properties of textile laminates: a unified approach”, Composites Science and Technology, Volume 63, Issues 3-4, February-March 2003, Pages 445-466.

23. Huang Z. M., “The mechanical properties of composites reinforced with woven and braided fabrics”, Composites Science and Technology, Volume 60, Issue 4, 1 March 2000, Pages 479-498.

24. Yu W. R., Pourboghrat F., Chung K., Zampaloni M. and Kang T. J.
“Non-orthogonal constitutive equation for woven fabric reinforced thermoplastic composites”, Composites Part A: Applied Science and Manufacturing, Volume 33, 2002, Pages 1095-1105.

25. E.J. Barbero, P. Lonetti, K.K. Sikkil, “Finite element continuum damage modeling of plain weave reinforced composites”, Composites Part B: Engineering, Volume 37, Issues 2-3, April 2005-March 2006, Pages 137-147

26. Tabiei, Y. Jiang, “Woven fabric composite material model with material nonlinearity for nonlinear finite element simulation”, International Journal of Solids and Structures, Volume 36, 1999, Pages 2757-2771.

27. Aminjikarai B., Tabiei A., “A strain-rate dependent 3-D micromechanical model for finite element simulations of plain weave composite structures Composite Structures”, Volume 81, 2007, Pages 407–418.

28. Tabiei A., Ivanov I., “Materially and geometrically non-linear woven composite micro-mechanical model with failure for finite element simulations”. International Journal of Non-Linear Mechanics, Volume 39, 2004, Pages 175– 188.

29. Ivanov I., Tabiei A., “Three dimensional computational micro-mechanic model for woven fabric composites”, Composite Structures, Volume 54, 2001, Pages 489-496

30. Naik N.K. , Shrirao P., Composite structures under ballistic impact, Composite Structures, Volume 66, 2004, Pages 579–590.

31. Starratt D., Sanders T., Cepus E. , Poursartip A., Vazir R., “An efficient method for continuous measurement of projectile motion in ballistic impact experiments”, International Journal of Impact Engineering, Volume 24,2000, Pages 155-170.

32. Belingardi G., Vadori R., “Low velocity impact tests of laminate glass-fiber-epoxy matrix composite material plates”, International Journal of Impact Engineering, Volume 27, 2002, Pages 213–229

33. Mili F., Necib B., “Impact behavior of cross-ply laminated composite plates under low velocities”, Composite Structures, Volume 51, 2001, Pages 237-244.

34. Robb MD, Arnold WS, Marshall IH. “The damage tolerance of GRP laminates under biaxial pre-stress”. Composite Structures, Volume 32, 1995, Pages 141–149.

35. Caprino G., Spataro G. and Luongo S. D., “Low-velocity impact behavior of fibreglass–aluminium laminates”, Composites Part A: Applied Science and Manufacturing, Volume 35, Issue 5, May 2004, Pages 605-616.

36. Ercan Sevkat, Benjamin Liaw, Feridun Delale, Basavaraju B. Raju,. “Effect of repeated impacts on the response of plain-woven hybrid composites”. Composites Part B: Engineering, In Press, Accepted Manuscript, Available online 10 February 2010

37. Sun CT, Chattopadhyay S., “Dynamic response of anisotropic laminated plates under initial stress to impact of a mass”. Journal of Applied Mechanics, Volume 42,1975, Pages 693–708.

38. Sun CT, Chen JK. “On the impact of initially stressed composite laminates. Journal of Composite Materials”, Volume 19, 1985, Pages 490–504.

39. Whittingham B., Marshall I.H., Mitrevski T., Jones R., “The response of composite structures with pre-stress subject to low velocity impact damage”, Composite Structures, Volume 66,2004, Pages 685–698.

40. Khalili M.R., Malekzadeh K., Mittal R.K., “Effect of physical and geometrical parameters on transverse low-velocity impact response of sandwich panels with a transversely flexible core”., Composite Structures, Volume 77, 2007, Pages 430–443.

41. Shivakumar, K.N., Elber, W., and Illg, W. “Prediction of impact force and duration due to low-velocity impact on circular composite laminates”. J. Applied Mechanics, Volume 52, 1985, Pages 674-680.

42. Abrate, S. “Modeling of impacts on composite structures”. Composite Structures, Volume 51, 2001, Pages 129-138.

43. Abrate, S. “Impact on Composite Structures”. Cambridge University Press, Cambridge, UK, 1998

44. Jime´nez O., Sullcahuaman J.A., Sa´nchez-Soto M., Martinez A.B., “Low energy impact evaluation using non conservative models”, International Journal of Solids and Structures, Volume 42, 2005, Pages 5758–5764.

45. Malekzadeh K., Khalilib M.R., Mittal R.K., “Response of composite sandwich panels with transversely flexible core to low-velocity transverse impact: A new dynamic model” International Journal of Impact Engineering, Volume 34, 2007, Pages 522–543

46. Chun L and Lam K.Y., “Dynamic Response of Fully Clamped laminated composite plates subjected to low-velocity impact of a mass”, International Journal of Solids Structures, Volume 35, No. 11, 1998, Pages 963- 979.

47. Guinarda S., Allix O., D. Degeorgesa G., Vineta A., “A 3D damage analysis of low-velocity impacts on laminated composites”, Composites Science and Technology, Volume 62,2002, Pages 585–589.

48. Li C.F., Hub N., Yina Y.J., Sekinec H., Fukunaga H., “Low-velocity impact-induced damage of continuous fiber-reinforced composite laminates. Part I. An FEM numerical model”, Composites Part A, Volume 33, 2002, Pages 1055–1062.

49. Li C.F., Hub N., Chenga J.G., Fukunagac H., Sekinec H., “Low-velocity impact-induced damage of continuous fiber-reinforced composite laminates. Part II. Verification and numerical investigation”, Composites Part A, Volume 33, 2002, Pages 1063–1072.

50. Pica RDW, Hinton E., "Finite element analysis of geometrically nonlinear plate behavior using a Mindlin formulation", Computer Structures, Volume 11, 1980, Pages 203–15.

51. Besant T., Davies G.A.O., Hitchings D., "Finite element modeling of low velocity impact of composite sandwich panels", Composites A, Volume 32, 2001, Pages 1189-1196.

52. Elder D.J., Thomson R.S., Nguyen M.Q., Scott M.L., "Review of delamination predictive methods for low speed impact of composite laminates", Composite Structures Volume 66,2004, Pages 677–683.

53. Hou J.P., Petrinic N., Ruiz C., "A delamination criterion for laminated composites under low-velocity impact", Composites Science and Technology, Volume 61, 2001, Pages 2069–2074.

54. Naik N. K., Sekher C.Y. and Meduri S., "Damage in woven-fabric composites subjected to low-velocity impact", Composites Science and Technology, Volume 60, Issue 5, April 2000, Pages 731-744.

55. Lee Y.S., Kang K.H. and Park O., "Response of hybrid laminated composite plates under low-velocity impact's, Computers & Structures, Volume 65, Issue 6, December 1997, Pages 965-974.

56. Yang, S. H. and Sun, C. T., "Indentation law for composite laminates". ASTM STP, 1982, 786, 425449.

57. Kim Hyonny, Welch D.A., Kedward K.T., "Experimental investigation of high velocity ice impacts on woven carbon/epoxy composite panels". Composites Part A, Volume 34, 2003, Pages 25–41.

58. Wu E. and Chang L.C., "Woven glass/epoxy laminates subject to projectile impact", International Journal of Impact Engineering, Volume 16, 1995, No. 4, Pages 607-619.

59. Zaretsky E., DeBotton G., M. Perl "The response of a glass fibers reinforced epoxy composite to an impact loading", International Journal of Solids and Structures, Volume 41,2004, Pages 569–584.

60. Cork C.R., Foster P.W., "The ballistic performance of narrow fabrics", International Journal of Impact Engineering, Volume 34, 2007, Pages 495–508.

61. Cheeseman Bryan A., Bogetti T.A. "Ballistic impact into fabric and compliant composite laminates", Composite Structures, Volume 61, 2003, Pages 161–173.

62. Czarnecki G.J., "Estimation of the V_{50} using semi-empirical (1-point) procedures"' Composites Part B, Volume 29B, 1998, Pages 321-329.

63. Naik N.K., Doshi A.V., "Ballistic impact behavior of thick composites: Parametric studies"' Composite Structures, In Press, Corrected Proof, Available online 30 January 2007.

64. Naik N.K., Shrirao P., Reddy B.C.K., "Ballistic impact behavior of woven fabric composites: Formulation"' International Journal of Impact Engineering, Volume 32, 2006, Pages 1521–1552.

65. Naik N.K., Shrirao P., Reddy B.C.K., "Ballistic impact behavior of woven fabric Composites". Parametric studies Materials Science and Engineering A, Volume 412, 2005, Pages 104–116.

66. Billon H.H., Robinson D.J., "Models for the ballistic impact of fabric armor", International Journal of Impact Engineering, Volume 25, 2001, Pages 411-422.

67. Gu. B., "Analytical modeling for the ballistic perforation of planar plain-woven fabric target by projectile"' Composites Part B, Volume 34, 2003, Pages 361–371.

68. Parga-Landa B. and Hernandez-Olivares F., "An analytical model to predict impact behavior of soft armors", Int. J. Impact Engineering, Volume 16, No. 3, 1995, Pages 455-466.

69. Nadler B, Steigmann D.J., "A model for frictional slip in woven fabrics", C. R. Mecanique, Volume 331, 2003, Pages 797–804.

70. Puente L. J., Zaera R., Navarro C., "An analytical model for high velocity impacts on thin CFRPs woven laminated plates". International Journal of Solids and Structures, Volume 44, 2007, Pages 2837–2851.

71. Morye S.S., Hine P.J., Duckett R.A., Carr D.J., Ward I.M., "Modeling of the energy absorption by polymer composites upon ballistic impact". Composites Science and Technology, Volume 60, 2000, Pages 2631-2642.

72. Ercan Sevkat, Benjamin Liaw, Feridun Delale, Basavaraju B. Raju,. "A combined experimental and numerical approach to study ballistic impact response of S2-glass fiber/toughened epoxy composite beams". Composites Science and Technology, Volume 69, Issues 7-8, June 2009, Pages 965-982

73. Rabb R. J. and Fahrenthold E.P., "Numerical simulation of oblique impact on orbital debris shielding", International Journal of Impact Engineering, Volume 23, 1999, Pages 735-744.

74. Walter, M.E., and Ravichandran G., "Experimental simulation of matrix cracking and debonding in a model brittle matrix composite". Exp. Mech., Volume 37(2), 1997, Pages 126–131.

75. Patricia P Parlevliet, Harald E.N. Bersee and Adriaan Beukers, "Residual stresses in thermoplastic composites- A study of the literature-Part 1: Formation of residual stresses", Applied Science and Manufacturing, Volume. 37, 2006, Issue 11, Pages 1847-1857

76. Patricia P Parlevliet, Harald E.N. Bersee and Adriaan Beukers,. "Residual stresses in thermoplastic composites- A study of the literature-Part 11: Experimental techniques", Volume. 37, 2006, Issue 11, Pages 1847-1857

77. Patricia P Parlevliet, Harald E.N. Bersee and Adriaan Beukers,. "Residual stresses in thermoplastic composites- A study of the literature-Part 111: Effects of residual stresses", Volume. 37, 2006, Issue 11, Pages 1847-1857

78. Bosze E.J., Alawar A., Bertschger O., Tsai Y. and Nutt S.R., "High-temperature strength and storage modulus in unidirectional hybrid composites", Composites Science and Technology, Volume 66, Issue 13, October 2006, Pages 1963-1969.

79. Dlouhy I., Chlup Z., Boccaccini D. N., Atiq S. and Boccaccini A. R., "Fracture behavior of hybrid glass matrix composites: thermal ageing effects", Composites Part A: Applied Science and Manufacturing, Volume 34, Issue 12, December 2003, Pages 1177-1185.

80. Schmitt-Thomas Kh.G., Yang Z.G. and Malke R., "Failure behavior and performance analysis of hybrid-fiber reinforced PAEK composites at high temperature", Composites Science and Technology, Volume 58, Issue 9, September 1997, Pages 1509-1518.

81. Lipetzky P., Dvorak G.J. and Stoloff N.S., "Tensile properties of a SiC/SiC composite". Materials Science and Engineering A, Volume 216, Issues 1-2, 15 October 1996, Pages 11-19.

82. Liaw, B. M., Cheung, C. K., Delale, F., Walser, A. D. and Raju, B. B., "Tension-Induced Damage in S2 Glass/Toughened Epoxy Composites at Room and Elevated Temperatures," Proceedings of 13th Annual ESD Advanced Composites Conference, September. 28-29, 1998, Detroit, Michigan.

83. Hirai Y., Hiroyuki Hand Jang-Kyo K., "Impact response of woven glass-fabric composites—II. Effect of temperature". Composites Science and Technology, Volume 58, Issue 1, January 1998, Pages 119-128.

84. Levin K., “Effect of low velocity impact on compression strength of quasi-isotropic laminate”. In: Proceedings of American society for composites: 1st technical conference. Technomic, Lancaster, PA, 1986. Pages 313–25.

85. Khojin A. S., Bashirzadeh R., Mahinfalah M. and Jazar R. N., “The role of temperature on impact properties of Kevlar/fiberglass composite laminates” Composites Part B: Engineering, Volume 37, Issues 7-8, October-December 2006, Pages 593-602.

86. Gómez-del Río T., Zaera R., Barbero E. and Navarro C., “Damage in CFRPs due to low velocity impact at low temperature”. Composites Part B: Engineering, Volume 36, Issue 1, January 2005, Pages 41-50.

87. Go´mez-del Rý´o T., Zaera R., Barbero E., Navarro C., “Damage in CFRPs due to low velocity impact at low temperature”. Composites Part B, Volume 36, 2005, Pages 41–50.

88. Gustin J, Joneson A, Mahinfalah M, Stone J., “Low velocity impact of combination Kevlar/fiber carbon sandwich composite”. Journal of Composite Structures, Volume 69(4), 2005, Pages 396–406.

89. Khojin A.S., Mahinfalah M., Bashirzadeh R. and Freeman B., “Temperature effects on Kevlar/hybrid and carbon fiber composite sandwiches under impact loading”. Composite Structures, Volume 78, Issue 2, April 2007, Pages 197-206

90. Schultz, J. M. and Friedrich, K., “Effect of temperature and strain rate on the strength of a PET/glass fiber composite”. Journal of Material Science, Volume 19, 1984, Pages 2246-2258.

91. Dutta PK., “Low temperature compressive strength of glass fiber reinforced polymer composites”. J Offshore Mech Arctic Eng., Volume 116, 1994, Pages 167–172.

92. Kwang-Hee I, Cheon-Seok C, Sun-Kyu K, In-Young Y., “Effects of temperature on impacts damages in cfrp composite laminates”. Composites Part B, Volume 32, 2001, Pages 669–82.

93. Zimmerman RS, Adams DF., “Impact performance of various fiber reinforced composites as a function of temperature”. In: Proceeding of 32nd International SAMPE symposium, Anaheim, CA; Pages 1461–71, 1987

94. Lo´pez-Puente J, Zaera R, Navarro C., “The effect of low temperatures on the intermediate and high velocity impact response of CFRPs”. Composites Part B, Volume 33, 2002, Pages 559–66.

95. Gillespie Jr JW, Gama BA, Cichanowski CE, Xiao JR. 'Interlaminar shear strength of plain weave S2-glass/SC79 composites subjected to out-of-plane high strain rate compressive loadings". Composite Science and Technology, Volume 65, 2005, Pages 1891–908

96. "Hexcel technical fabrics handbook", reinforcements for composites, March 2009.

97. Cox BN, Flanagan G. "Handbook of analytical methods for textile composites", NASA CR 4750, March 1997.

98. Ishikawa, T. and T.W. Chou, "In-plane thermal expansion and thermal bending coefficients of Fabric composites, "Journal of Composite Materials, Volume 17, Pages 72-104, 1983

99. Vishay Micro-measurements, Tech Notes TN-513-1, "Measurement of thermal expansion coefficient using strain gages", 2007

100. Vishay Micro-measurements, Tech Notes TN-504-1, "Strain gages thermal output and gage factor variation with temperature", 2007

101. Naik N. K., Shrirao. P and Reddy B.C.K, "Ballistic impact behavior of woven fabric composites: Formulation", International Journal of Impact Engineering, Volume 32: 2006; Pages 1521-1552

102. Garcia-Castillo, S.K., Sanchez-Saez, S., Lopez-Puente, J., Barbero, E. and Navarro, C., "Impact behavior of preloaded glass/polyester woven plates", Composite Science and Technology, Volume 69: 2009; Pages 711-717

103. Morye, S.S., Hine, P.J., Duckett, R.A., Carr. D.J., and Ward, I.M., "Modeling of the energy absorption by polymer composites upon ballistic impact", Composite Science and Technology, Volume 60: 2000; Pages 2631-2642

104. Cheeseman, B.A., and Bogeti, T.A., "Ballistic impact into fabric and compliant composite laminates", Composite Structures, Volume 61: 2003; Pages 161-173

105. Lee S-W.R., Sun, C.T., "A quasi static penetration model for composite laminates", Journal of Composite Materials, Volume 27: 1993; Pages 251-271

106. Ellis R.L., "Ballistic impact resistance of graphite epoxy composites with shape memory alloy and extended chain polyethylene spectra hybrid components. Masters of Science thesis, Mechanical Engineering Department, Virginia Polytechnic Institute and State University, Blacksburg, Virginia, 2006